

# The Messenger



No. 164 – June 2016

Solar activity and instrument data quality  
VISIR Upgrade Science Verification  
XXL Survey: First results  
LEGA-C Survey: First data release





# Adaptive Optics Facility Status Report: When First Light Is Produced Rather Than Captured

Robin Arsenault<sup>1</sup>  
 Pierre-Yves Madec<sup>1</sup>  
 Elise Vernet<sup>1</sup>  
 Wolfgang Hackenberg<sup>1</sup>  
 Domenico Bonaccini Calia<sup>1</sup>  
 Paolo La Penna<sup>1</sup>  
 Jérôme Paufique<sup>1</sup>  
 Harald Kuntschner<sup>1</sup>  
 Jean-Francois Pirard<sup>1</sup>  
 Marc Sarazin<sup>1</sup>  
 Pierre Haguenaer<sup>1</sup>  
 Norbert Hubin<sup>1</sup>  
 Ignacio Vera<sup>1</sup>

<sup>1</sup> ESO

First light for the 4 Laser Guide Star Facility (4LGSF) took place in Paranal on 26 April 2016 with four laser units in operation for the first time. A combined test with the first laser guide star unit and the Ground Layer Adaptive optics Assisted by Lasers (GRAAL) instrument in October 2015 demonstrated the whole acquisition sequence of the Adaptive Optics Facility (AOF). Many tools that will support the operation of the AOF for science observations have meanwhile been implemented. GALACSI was granted Provisional Acceptance in Europe in April 2016, completing the system tests and qualification in Garching of the adaptive optics modules GRAAL and GALACSI (Ground Atmospheric Layer Adaptive Optics for Spectroscopic Imaging), their real-time computers and the deformable secondary mirror (DSM). Results of tests both in the laboratory and on sky are presented. The installation of the DSM and GALACSI will be completed by early 2017, to be followed by commissioning of all AOF systems.

#### ESO Project Team:

P. Duhoux, J.-L. Lizon, S. Guisard, P. Lilley, L. Petazzi, P. Hammersley, I. Guidolin, L. Kern, T. Pfommer, C. Dupuy, R. Guzman, J. Quentin, M. Quattri, R. Holzlöhner, D. Popovic, M. Comin, S. McClay, S. Lewis, F. Gago, J. Kolb, A. Jost, J. Argomedo, S. Tordo, R. Donaldson, R. Conzelmann, M. Lelouarn, R. Siebenmorgen, M. Downing, J. Reyes, M. Suarez Valles, S. Ströbele, S. Oberti, P. Gutierrez Cheetam, M. Kiekebusch, C. Soenke, E. Aller-Carpentier, P. Jolley, J. Vernet, A. Manescau-Hernandez, L. Mehrgan, G. Calderone, A. van Kesteren, G. Chiozzi, H. Sommers, D. Dorigo, T. Bierwirth, J.-P. Kirchbauer, S. Huber, G. Fischer, A. Haimerl, S. Lévêque, P. Amico, G. Hubert, S. Brillant, P. Baksai, J. C. Palacio, I. Munoz, E. Fuenteseca

#### Chronicle of recent AOF activities

The Adaptive Optics Facility (Arsenault et al., 2010; 2014) is a long-term project on the Very Large Telescope, Unit 4 (UT4) to provide the adaptive optics systems for the two UT4 instruments MUSE (the Multi Unit Spectroscopic Explorer), fed by GALACSI, and the High Acuity Wide field K-band Imager (HAWK-I), fed by GRAAL with a four sodium laser guide star system. After years of planning, construction and testing, with the completion of reviews for Provisional Acceptance Europe (PAE) of AOF modules in the course of 2015, activities are now shifting to Paranal.

The first laser guide star unit (LGSU#1) was installed and tested on UT4 in 2015, with first light in April 2015, and the three other units were then completed. The LGSU#1 commissioning was completed in August 2015 and the unit showed excellent performance. It confirmed the good design choices and validated all the interfaces with UT4. PAE for the 4LGSF system was granted at the end of 2015 and in January 2016 the three remaining LGSUs were re-integrated in Paranal and installed on UT4. On 26 April 2016 first light for the 4LGSF took place (see cover image and Release eso1613) and the commissioning of the 4LGSF in stand-alone mode could begin.

In the meantime, a two-year-long system testing phase was concluded in Garching (February 2016). The adaptive optics (AO) modules GRAAL and GALACSI were

mounted in that order on the ASSIST (Adaptive Secondary Setup and Instrument Simulator) test bench and tested in realistic conditions. GRAAL tests were completed in early 2015 and GRAAL's PAE was granted in April 2015. Then the system was prepared for shipment and re-integrated in Paranal in June. This provided a unique opportunity in October 2015 to undertake a combined commissioning run with LGSU#1 and GRAAL, allowing many aspects of the acquisition sequence of the AOF on the telescope to be debugged and tested under real conditions. This evaluation was very instructive and useful to the project and again validated many design choices.

Then the GALACSI module was installed on ASSIST and tests continued. By autumn 2015, the tests in the MUSE wide-field mode configuration were completed and a start could be made with tests of the MUSE narrow-field mode. These were completed in February 2016 and the PAE for GALACSI was granted in April.

In parallel, many tools required to optimise the operation of the AOF have been developed, ranging from new versions of the GuideCam tool and the observing tool to the delivery of the laser traffic control software and the complete refurbishment of the astronomical site monitor. Most of these tools are now operational. The commissioning period of the AOF itself will ensure a final integration of these tools into the operational scheme of the AOF. All these tests have

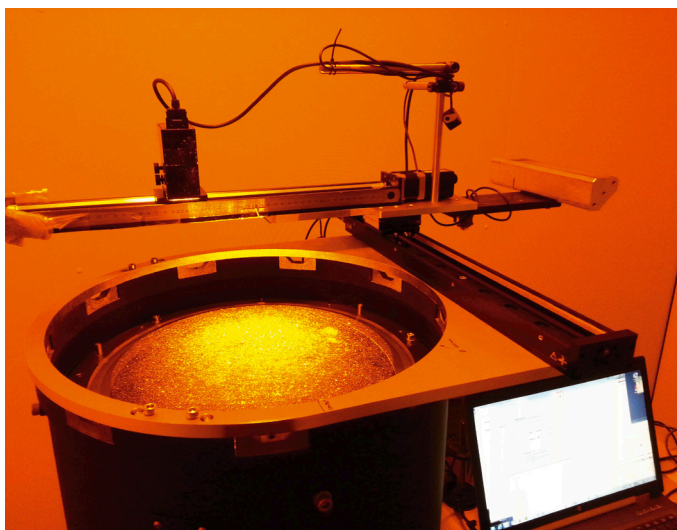
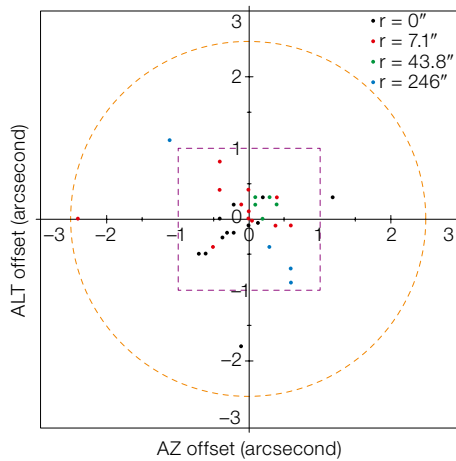


Figure 1. Characterisation of the beam profile from the optical tube assembly shown in the Garching cold chamber, after integration with the beam control diagnostic system and the laser.



**Figure 2.** Accuracy of the pointing of the laser guide stars (LGSU#1). The red circle is the requirement. The final performance is better than the requirements by a factor of two, ensuring a short acquisition time for the AOF and a small overhead with respect to observation without laser guide star. Symbol colour indicates pointing angle from telescope optical axis.

demonstrated full compliance of the AOF systems with their specification and the desired performance has been reached and clearly demonstrated.

Throughout the AOF review process, and the system testing and installations in Paranal, the project has placed strong emphasis on training our Chilean colleagues. Many trips and exchanges took place between Garching and Paranal. This spirit of collaboration and enthusiasm will no doubt ensure that the astronomical community receives expert support for the AOF systems and effective maintenance and optimisation of its performance will take place.

#### 4LGSF highlights

The 4LGSF subsystem of the AOF has demanded a substantial effort in terms of manpower, finance and contract supervision. The engineering systems expertise within the AOF/4LGSF project has ensured an efficient overview of the numerous state-of-the-art components composing this facility (Hackenberg et al., 2014).

There are five key specifications of the lasers that represented real challenges in the early years of the AOF project. These were:

1. High power output: 22 watt;

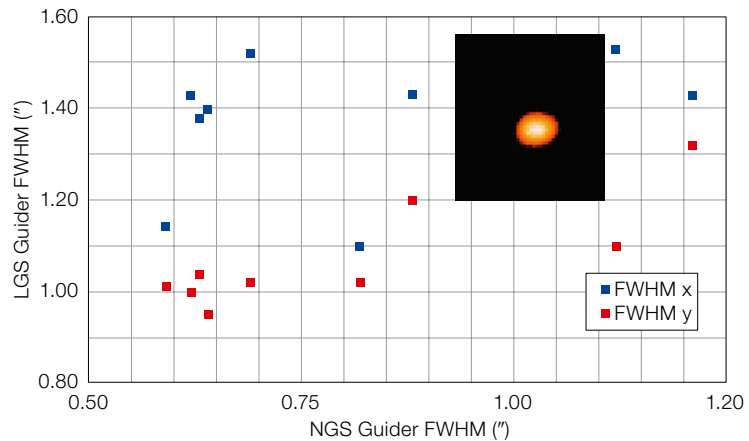


**Figure 3.** The laser guide star spot size versus the natural guide star (NGS) image full width half maximum (FWHM) measured by the telescope guider. The two values of FWHM are plotted separately.

2. Pointing accuracy of the laser spot: < 5 arcseconds peak-to-valley;
3. Laser spot size: < 1.35 arcseconds for 1-arcsecond seeing ( $30^\circ$  from zenith);
4. Return flux of  $5 \times 10^6$  photons  $\text{m}^{-2} \text{sec}^{-1}$  at the UT4 Nasmyth focus (for average sodium density of  $4 \times 10^{13} \text{m}^{-2}$ );
5. Reliability and robustness.

The power figure was reached early in the development phase and did not represent a major issue for the TOPTICA/MPB consortium in charge of delivering the five laser units (four plus one spare). The robust and simple laser design ensured the stable behaviour of the laser output power during its development and all the test phases in Garching, and today at the telescope. The most impressive demonstration was the reception of the first laser unit in Garching; after unloading from the truck transport (TOPTICA headquarters are 35 kilometres from Garching), rolling off into the ESO laboratory, making the connections and switching on, the power meter unflinchingly showed a remarkable and stable dead-on 22-watt output! This speaks for the laser's robustness, which was always considered an important feature for a system that was to be operated in an observatory environment. Also the numerous systems in operation on the AOF require a long mean time between failure in order to fulfil the requirement of high night-time availability.

The pointing accuracy was also a difficult requirement; one must remember that the operational optical quality for all 4LGSF optics is in the diffraction regime. This demands high optical quality from the components, careful alignment, stable

and rigid systems to maintain alignment and careful engineering to control the pointing. The system met the specification in the laboratory in Garching with no margin. At this stage the project decided to implement a laser pointing camera (Bonaccini Calia et al., 2014), which would relieve this specification somewhat. The laser pointing camera is a small unit mounted on the telescope top ring that identifies the laser star, determines its position with respect to the telescope axis and updates the laser pointing if it is too far off. This system was delivered by the Rome Observatory and its implementation has been very successful (see Figure 2).

The laser spot size is also within specification and is evidence for the stable and excellent image quality of both the laser beam control diagnostic system and the optical telescope assembly. Figure 1 shows the characterisation of the beam profile in the Garching cold chamber after integration with the beam control diagnostic system and the laser.

In early 2008, when the laser call for tender was launched, the interaction between the laser beam and the atomic fine structure of the sodium atoms was not so well understood, strange as this may seem in hindsight. Coordinated efforts between the ESO laser and atomic physics community helped to improve this situation (Holzlöhner et al., 2008; 2010; 2012). These efforts have been largely successful as the spectral format prescribed has delivered the desired outcome. It was decided to specify to the laser supplier to inject 20 watts into the main Na  $D_{2a}$  line and 10% of this power

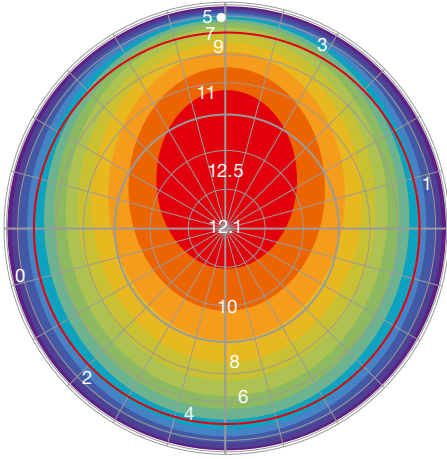


Figure 4. Simulation of the expected return flux (for a simulated laser flux of 16 watt) plotted over the sky. The variation across the hemisphere is due to the interaction between the beam polarisation and the Earth's magnetic field; the maximum occurs towards the south magnetic pole. Measured values range between about 10 and  $20 \times 10^6$  photon  $m^{-2} s^{-1}$  (laser is actually 22 watt not 16) and follow well the distribution simulated across the hemisphere.

in the Na  $D_{2b}$  line. This should prevent the sodium atoms from recombining in a state where the main Na  $D_{2a}$  laser line can no longer excite the atoms. The result is an improved return flux.

The first on-sky results of return flux are very encouraging, but the final assessment will only be made after a complete year of monitoring to cover the full range of seasonal variations of the density of the atmospheric sodium layer (Figure 4).

#### GRAAL-LGSU#1 combined tests

The GRAAL module (Arsenault et al., 2014; Paufique et al., 2012) serves the HAWK-I imager and provides a ground layer correction over the  $7.5 \times 7.5$  arc-minute field of view of HAWK-I. It also provides an option called maintenance and commissioning mode, featuring on-axis natural guide star adaptive optics. This mode allows the 1170 degrees of freedom of the DSM to be fully exploited and aims at testing and validating the correction capability of the mirror.

The installation of GRAAL on UT4 took place in June 2015 (Figure 6) and the combined commissioning with LGSU#1 in October 2015. Obviously, no adaptive optics verification could be done in Octo-

ber 2015 without the DSM. However, many loops and offload schemes could be tested and the LGSU#1 could be acquired on one wavefront sensor and the tip-tilt star selection tested. This allowed many steps to be executed under real conditions and offered reassurance as to the estimated acquisition overhead, which had already been tested on ASSIST in Garching. With all the loops closing (except the main adaptive optics loop with the DSM), the overhead was always found to be less than four minutes (requirement five minutes). The jitter loop on one laser was closed on this occasion: the jitter mirror in the LGSU#1 was controlled by the GRAAL laser guide star wavefront sensor to reduce the tip-tilt of the laser spot caused by telescope shake.

The pupil alignment on the wavefront sensor was, however, found to become decentered by more than we had predicted. This misalignment arises from a combination of factors including telescope misalignment, but also from the co-rotator (inside GRAAL) and the Nasmyth co-rotator. However, simulations and tests on ASSIST (with GALACSI, see Figure 7) convinced us that this could be handled by the scheme of regular command matrix updates.

The GuideCam tool was used for tip-tilt star selection, and the laser traffic control software proved very useful to predict and prevent laser collisions with other telescope beams. The most frequent collisions were experienced with the Visible and Infrared Survey Telescope for Astronomy (VISTA), the VLT Survey Telescope (VST) and the Auxiliary Telescopes (ATs).

#### GALACSI performance

As for the GRAAL module, the tests of the GALACSI module (La Penna et al., 2014) on ASSIST clearly demonstrated that it fulfils the system specifications. The performance requirements for the GALACSI wide-field mode is to increase the received energy per pixel by a factor of two, over the  $60 \times 60$  arcsecond MUSE field of view at 750 nm wavelength and for 1.1-arcsecond seeing. This is defined for a given atmospheric refractive index structure parameter ( $C_n^2$ ) distribution. This parameterisation was assumed

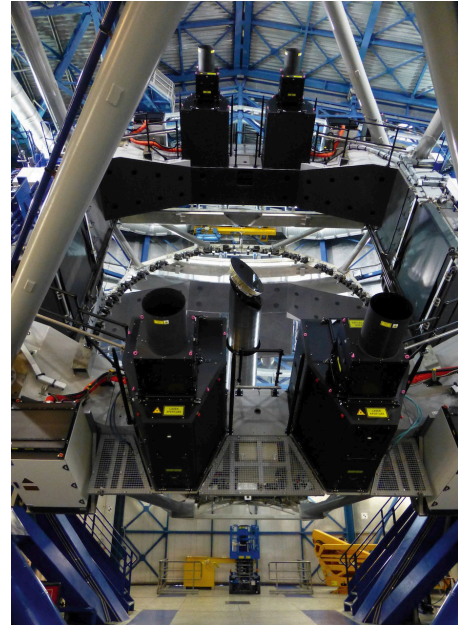


Figure 5. The four laser guide star units mounted on the UT4 centrepiece with their respective laser and instrument control cabinets.

early on in the GALACSI system simulations and the design concept was expected to provide the desired correction. This can clearly be seen in Figure 8.

The ASSIST test bench comprises only three discrete phase screens to simulate the continuous distribution of turbulence in the atmosphere. This number of phase screens and their relative importance are not fully representative of the specified  $C_n^2$  profile. However, when the ASSIST distribution was simulated, we could reproduce the measured values of ensquared energy (dashed line on Figure 8) well. This convinced us that on sky with the specified  $C_n^2$  profile, the GALACSI module would provide the required correction. With the specified atmosphere, simulations predict a factor of two in improvement in ensquared energy (EE) with 55% turbulence in the first 500 metres above ground.

These tests were carried out relatively quickly as they implemented a similar algorithm to the GRAAL ground layer adaptive optics correction (Arsenault et al., 2013) and little surprise was expected. However, the GALACSI-MUSE narrow-field mode involved a new, complex algorithm for laser tomography. The complete



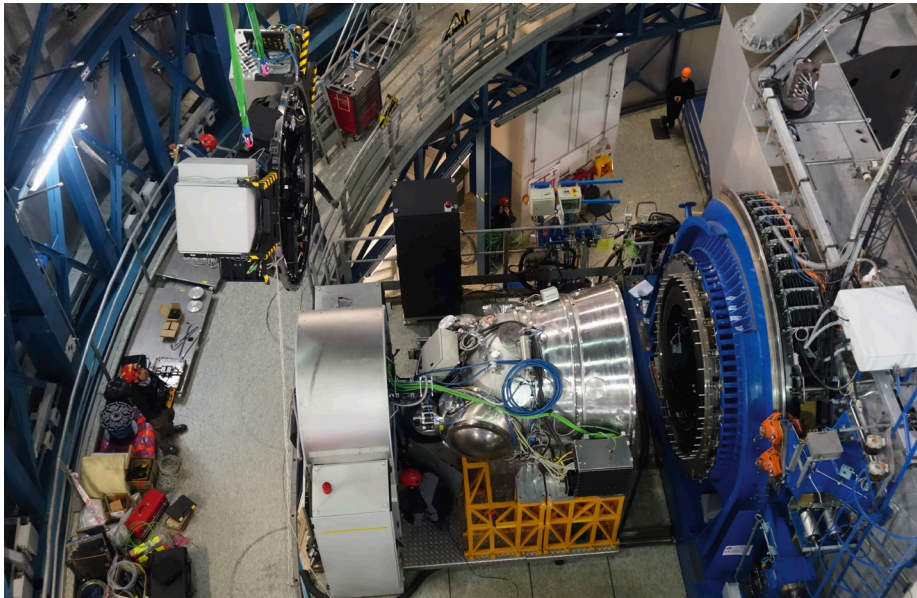


Figure 6. The GRAAL module being handled above the Nasmyth A platform of UT4 (top left of picture) before being sandwiched between HAWK-I and the Nasmyth flange.

definition of the command matrix for this algorithm was defined by the ESO Adaptive Optics Group and performed beyond expectations. The main difficulty arose with the measurement of the Strehl ratio values in the visible. The specification called for a Strehl ratio of 5% (goal 10%) at 650 nm in a 5-arcsecond field of view and for 0.6-arcsecond seeing. One should not be misled by such “low” values of the Strehl ratio! This is a true challenge for adaptive optics due to the short wave-

length (visible, 650 nm); it corresponds to a 77% Strehl ratio at 2.2  $\mu\text{m}$  and starts to approach planet-finder performance if the goal value is considered (82% Strehl ratio at 2.2  $\mu\text{m}$ ).

Despite the challenges, the image improvement is indeed spectacular (see Figure 9) and measurements of the Strehl ratio confirm this impression. The tests performed on ASSIST also revealed a very robust algorithm. The correction also worked well in worse seeing conditions (using the 1.1-arcsecond seeing simulation) and was found to be stable. Besides, the correction appeared to be robust enough that the control matrix does not

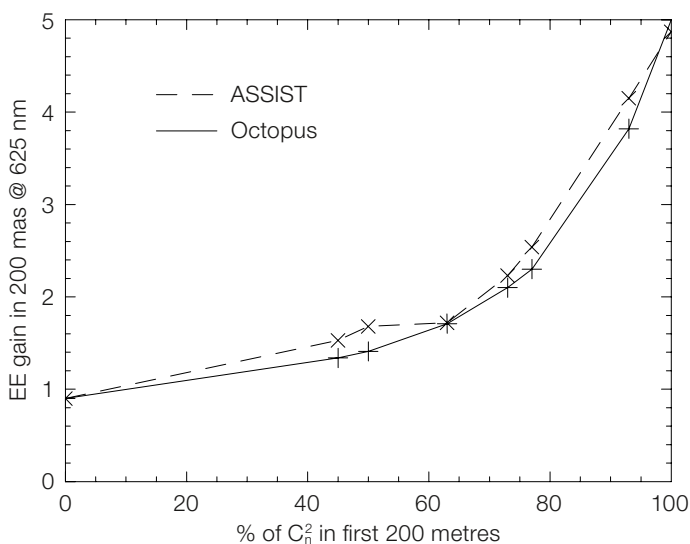


Figure 8. The evolution of the correction on ASSIST at 625 nm as a function of the fraction of turbulence in the ground layer (first 200 metres). The improvement starts getting substantial when more than 60% of the turbulence lies below 200 metres altitude. Good agreement is seen between the simulation (solid line, Octopus) and the ASSIST measurements.

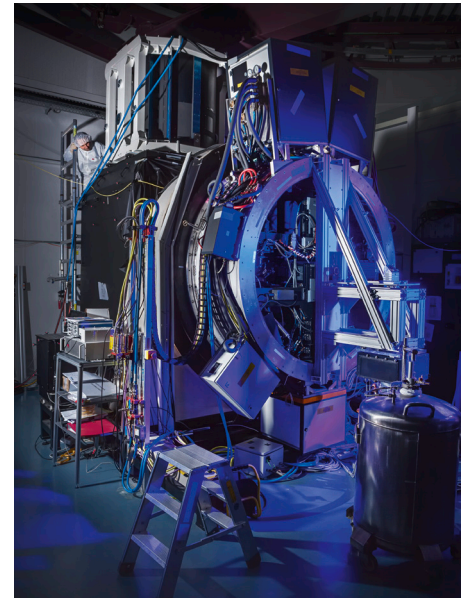


Figure 7. The GALACSI module mounted on the ASSIST test bench. A special rig has been produced to interface the IRLS (InfraRed Low Order Sensor) used for tip-tilt and focus sensing with the MUSE narrow-field mode.

have to be modified when the turbulence profile evolves, which will certainly simplify operations.

### Benefits of the system tests

The choices for the design and construction of the ASSIST test bench (Stuik et al., 2012) were initially guided by the need to provide Microgate and ADS (the two companies in charge of delivering the new secondary mirror unit to ESO) with a tool allowing the final optical calibration of the DSM (Arsenault et al., 2013; Manetti et al., 2014 and Briguglio et al., 2014). At the end of the manufacturing process, each DSM capacitive sensor has to be optically calibrated, and the optical shell flattened to within 7.5 nm root mean square error. This requires an interferometric setup. Due to the convex shape of the DSM, this set-up ended up in a cumbersome 2 x 2 x 3 metre tower made of a 1.7-metre diameter aspherical primary mirror and a much smaller aspherical secondary mirror (see Figure 10).

It was thus decided to add, at the input of this tower, a simple source simulator and turbulence generator, and to design



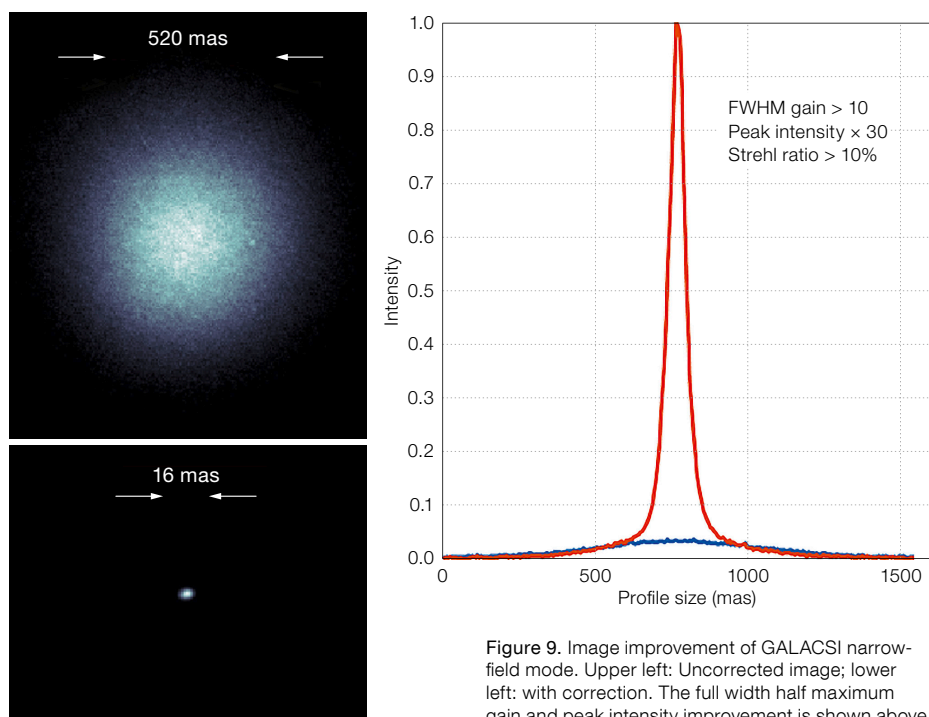


Figure 9. Image improvement of GALACSI narrow-field mode. Upper left: Uncorrected image; lower left: with correction. The full width half maximum gain and peak intensity improvement is shown above.

a VLT focus simulator to be located at the output of ASSIST. The complete ASSIST would then not only be able to achieve the last step of the DSM optical calibration but also to fully characterise GRAAL and GALACSI before going to Paranal. The nice optical design was provided by Bernard Delabre, and NOVA (University of Leiden) supplied the system and covered most of the costs and effort.

More than four months were necessary to complete the critical optical calibration of the DSM. During the two years of tests on ASSIST, several “birth defects” in the subsystems have been identified and corrected. Four months were spent on fixing two major failures of the new secondary mirror unit, time much more fruitfully and efficiently spent in the laboratory than on the telescope!

The ASSIST setup with the VLT control model allowed a configuration that was very close to that of the final telescope to be achieved. Therefore, substantial progress could be made on template coding and testing and on the software infrastructure. The complete acquisition sequence could be tested and optimised. Finally, ASSIST has offered a comfortable work environment with calibrated atmospheric

turbulence, a situation much more stable and reproducible than on the telescope.

The AOF staff who have operated the system for these past two years in the laboratory have gained a superb knowledge and understanding of the system. No doubt unknowns, new issues and problems will surface once the system is operating on UT4, but the experience gained in Garching will prove invaluable in solving these efficiently. A number of Paranal staff have travelled to Garching and have been using the system to prepare them for the future operation and maintenance work at the observatory.

#### AOF operation tools and infrastructure

At the instigation of the AOF Scientist, many tools were put in place to optimise the AOF’s operation. Many of them have been mentioned already. The GuideCam tool has been developed for GRAAL/HAWK-I to allow tip-tilt natural guide star selection. A similar version with some additional functionalities is being developed for GALACSI/MUSE as well.

The laser traffic control system (Amico et al., 2105) is a piece of software used to

predict optical collisions between the powerful laser beams of the 4LGSF and the lines of sight of other telescopes on the mountain. It has been in operation for two observing periods and we have received very positive feedback from Science Operations in Paranal. A web interface displays the situation of all the telescopes on Cerro Paranal and predicts any collision with the AOF lasers. Priority rules are implemented and recommendations are made to the telescope operator. Alarms are triggered when a collision is imminent. The observing tool has also been updated by implementing a query system to the laser traffic control system to check whether an observing block risks a collision. This will serve observers during the night and help in the preparation and scheduling of observing blocks.

The AOF observing mode to select will depend on atmospheric conditions. To this end the astronomical site monitor went through three major improvements:

1. New atmospheric tools have been implemented; a multi-aperture scintillation sensor and a differential image motion monitor have been installed on a higher structure (7 metres above ground) so that they are less sensitive to the near-ground surface layer, which can cause a systematically more pessimistic reading of the seeing than the telescope guider. A new SLOpe Detection And Ranging instrument (SLODAR) has also been Paranalised and integrated into the astronomical site monitor infrastructure.
2. The database to store the readings of these new tools has been upgraded to include additional parameters. This database is also automatically replicated in Garching.
3. Finally, a new display tool has been developed and implemented. The standard setup has been chosen to faithfully replicate the previous look and feel, so that many users may not yet have noticed the difference. But this new display tool is very powerful and allows any user, through a login, to define his/her own preferred setting and parameters.

The astronomical site monitor will provide the turbulence distribution in the atmosphere, which will be a critical criterion for



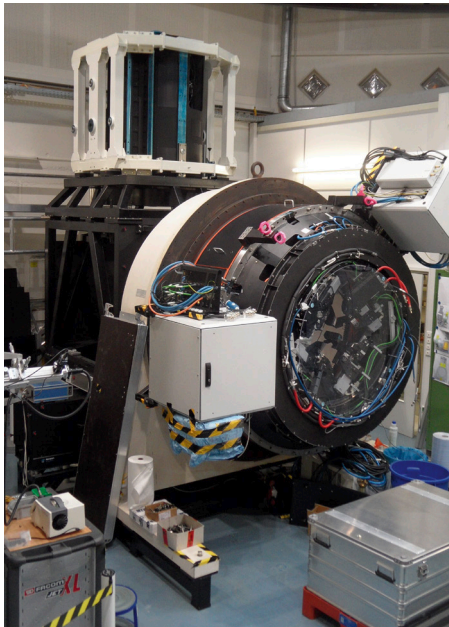


Figure 10. The GRAAL module on ASSIST with the DSM at the top during system tests in Garching.

observation mode scheduling (Kuntschner et al., 2012). The simple rule is:

- Good seeing 0.6 arcseconds and better implies GALACSI laser tomography adaptive optics and MUSE narrow-field mode;
- Worse seeing  $\sim 1$  arcsecond and strong ground layer, 70 % below 500 metres, implies GALACSI ground larger adaptive optics and MUSE wide-field mode;
- Even worse seeing  $\sim 1$  arcsecond and strong and very low ground layer (below 300 metres) implies GRAAL/HAWK-I;
- In all other conditions, seeing-limited operation (about 30 % of the time).

### Science outlook

It is planned to first use the AOF in MUSE wide-field mode for science from mid-2017 onward. Other modes such as the narrow-field mode of MUSE and HAWK-I ground layer adaptive optics will follow in 2018. With the adaptive secondary mirror, all foci at UT4 can be provided with turbulence-corrected images, without the addition of adaptive modules and supplementary optics in front of the instruments. The concept is more far-reaching than only a deformable secondary mirror, since the instrument park is optimised to benefit from this upgrade. In 2020 a

new instrument at the Cassegrain focus will follow (ERIS — Enhanced Resolution Imager and Spectrograph), which combines the use of the near-infrared integral field unit SINFONI and a diffraction-limited camera sensitive up to  $5 \mu\text{m}$ . All UT4 instruments can make use of natural guide stars as well as up to four laser guide stars for wavefront sensing.

For MUSE's wide-field mode, the adaptive optics module GALACSI will concentrate the energy of the point spread function across the field of view, enabling more occasions with excellent seeing conditions in regular observing time to be available. MUSE's narrow-field mode opens up a new domain with Strehl conditions of  $> 5\%$  in the visible (650 nm), which facilitates science cases for very crowded field integral field spectroscopy, such as for the centres of galaxies and globular clusters.

HAWK-I with GRAAL is expected to provide about a factor of two improvement in the occurrence of good  $J$ -,  $H$ - and  $K$ -band images ( $< 0.4$  arcseconds). Improvement is also expected for all seeing conditions, promising almost space-based observatory quality images in the near-infrared.

### Next phases and milestones

Two main systems remain to be installed on the telescope. In October 2016 there will be a UT4 shutdown until December to install the new secondary mirror unit with the deformable secondary mirror. Then, the telescope will be re-validated in non-adaptive optics mode. In early January 2017, the GRAAL maintenance and commissioning mode will be used to validate the adaptive optics correction capability of the DSM, while GALACSI will be re-integrated and installed on UT4. This operation should be completed by March 2017.

The AOF team will then conduct regular commissioning runs throughout 2017 with the goal of delivering the GALACSI-MUSE wide-field mode for Observing Period 100. After this the project will focus on commissioning the GRAAL ground layer adaptive optics and GALACSI laser tomography adaptive optics modes.

### Conclusions

The AOF has completed its activities in Garching and now the focus is shifting ever more to Paranal, completing the stand-alone 4LGSF commissioning and then moving on to the installation of the deformable secondary mirror on UT4 in the fourth quarter of this year. With this facility in place commissioning of GALACSI in wide-field mode can start, yielding the first science by mid-2017. HAWK-I/GRAAL narrow-field mode and MUSE's ground layer adaptive optics will follow in 2018. The suite of instruments is accompanied by a full set of operation tools and an upgrade of the astronomical site monitor, which will all support efficient operation of the AOF. The current progress and laboratory measurements within specification of the adaptive optics models for HAWK-I and MUSE establish high expectations for the onset of science observations from mid-2017.

### Acknowledgements

The AOF project started at ESO in 2006; we thus celebrate its tenth anniversary this year! We are very grateful to all the team members who have been dedicated to this project since its beginning and for their hard work even in the difficult times of technical failures and challenges. Also, a great many people have contributed to the AOF for temporary support activities, or a review board panel; they are also warmly thanked for their contributions. We also very much appreciate all the functional managers and group leaders who have been helping to solve resource issues and conflicts during this long effort. The AOF has also greatly benefited from the expert support of its industrial partners, and we wish to thank here especially Microgate, ADS Intl., TOPTICA, MPB and SAFRAN Reosc.

### References

- Amico, P. et al. 2015, *The Messenger*, 162, 19
- Arsenault, R. et al. 2010, *The Messenger*, 142, 12
- Arsenault, R. et al. 2013, *The Messenger*, 151, 14
- Arsenault, R. et al. 2013, in *AO4ELT Conference – Adaptive Optics for Extremely Large Telescopes*, Florence, Italy, May 2013
- Arsenault, R. et al. 2014, *The Messenger*, 156, 2
- Arsenault, R. et al. 2014, *Proc. SPIE*, 9148
- Bonaccini Calia, D. et al. 2014, *Proc. SPIE*, 9148
- Briguglio, R. et al. 2014, *Proc. SPIE*, 9148
- Hackenberg, W. et al. 2014, *Proc. SPIE*, 9148
- Holzlohner, R. et al. 2008, *Proc. SPIE*, 7015
- Holzlohner, R. et al. 2010, *A&A*, 510, A20
- Holzlohner, R. et al. 2012, *Proc. SPIE*, 8447
- Kuntschner, H. et al. 2012, *Proc. SPIE*, 8448
- La Penna, P. et al. 2014, *Proc. SPIE*, 9148
- Manetti, M. et al. 2014, *Proc. SPIE*, 9148
- Paufique, J. et al. 2012, *Proc. SPIE*, 8447
- Stuik, R. et al. 2012, *Proc. SPIE*, 8447



# A Fruitful Collaboration between ESO and the Max Planck Computing and Data Facility

Nathalie Fourniol<sup>1</sup>  
Stefano Zampieri<sup>1</sup>  
Manuel Panea<sup>2</sup>

<sup>1</sup> ESO  
<sup>2</sup> Max Planck Computing and Data Facility, Garching, Germany

The ESO Science Archive Facility (SAF), contains all La Silla Paranal Observatory raw data, as well as, more recently introduced, processed data created at ESO with state-of-the-art pipelines or returned by the astronomical community. The SAF has been established for over 20 years and its current holding exceeds 700 terabytes. An overview of the content of the SAF and the preservation of its content is provided. The latest development to ensure the preservation of the SAF data, provision of an independent backup copy of the whole SAF at the Max Planck Computing and Data Facility in Garching, is described.

## The ESO Science Archive Facility

The SAF is the unique access point to ESO data via services that are increasingly used by the community. The ESO SAF currently contains about 700 TB of ESO data in the form of more than 40 million distinct files. About twice this amount of data is actually stored, as a second copy of all archived files is present in the system. The data from over 20 individual instruments, spread among the three ESO sites — namely Paranal, La Silla, and APEX — are transferred continuously via the network from Chile to Garching. Ninety per cent of the files reach Garching in less than 15 minutes. Once saved in the SAF, these data are then published, in the sense that authorised users can download them. Projections show that with the arrival of the next few instruments, which will generate large amounts of data, the SAF will reach its first petabyte in 2018.

The SAF is the one and only access point to all La Silla Paranal Observatory raw data and to processed data thereof. Figure 1 shows the current web interface to the SAF and its collections<sup>1</sup>. As well as raw data from the observatory, data

Category	Access Point	Data collection	Data Type	Instruments
LPO Raw Data	Raw data query form (all instruments) Instrument specific query forms Direct retrieval of raw data by file name	All ESO raw data	Various	Many La Silla Paranal instruments
LPO Data Products	Phase 3 main query form Phase 3 imaging query form Phase 3 spectral query form Phase 3 VIRCAI-specific query form <i>(Description of reduced data products types)</i>	Phase 3 Data Products (ESO public surveys; ESO pipeline-reduced products; Large programs: GOODS, zCOSMOS, etc.)	Currently, Imaging and Spectroscopy	Various Pipeline products for UVES, XSHOOTER, HARPS, and more to come.
	Catalogue Facility query interface	Phase 3 Catalogues [ESO User Portal authentication required also when browsing]	Catalogues	Various
	FEROS and HARPS-Polarimetry pipeline processed data query form	FEROS and HARPS-Polarimetry pipeline processed data	Spectroscopy	FEROS, HARPS-Polarimetry, HARPS reduced calibrations (other HARPS see Phase3 above)
	Other Advanced Data Products (available only as downloadable packages, no query form)	Various (30 Doradus, Corot, GaBoDs, etc.)	Spectroscopy Imaging Flux maps	FEROS WFI APEX
	Science Verification, Commissioning, EIS, etc. (no query form)	Full list of available data packages	Various	Many
APEX Quick Look Products	APEX query form	APEX	Heterodyne, Bolometer	APEX-2A, LABOCA, SABOCA, SHeFI

products are generated either by the community (Arnaboldi et al., 2014) or produced in-house (Romaniello et al., 2016a). Recent analysis on downloads of these data products as well as the raw data have shown that the SAF is a very popular science resource in itself, aggregating a new astronomical community and attracting new registrations to the user portal at a rate of a couple per day (Romaniello et al., 2016b).

In order for this mine of scientific data to be available to users, the archived data need to be preserved. The SAF content resides in a data centre at ESO where machines run continuously (Figure 2). The ESO archive system is based on software developed at ESO called NGAS (Next Generation Archive System; Wicenc et al., 2007), also used by the ALMA Science Archive<sup>2</sup>. The system uses the RAID5 technology, which ensures data redundancy. The second copy in the system, produced for any newly archived data within the hour, provides additional redundancy.

But this of course is not enough. To ensure data preservation and availability, one must also plan against major disaster or long-lasting disruption, while hoping to never experience such an event. That is where the collaboration between ESO

Figure 1. The ESO Science Archive Facility homepage.

and the Max Planck Computing and Data Facility comes in, where a backup copy of all ESO data now resides.

## The Max Planck Computing and Data Facility

The Max Planck Computing and Data Facility (MPCDF, formerly known as Rechenzentrum Garching [RZG]) is the main computing centre of the Max Planck Society. The MPCDF provides computing and data management services for all Max Planck Institutes across Germany in many fields of science, including materials and life sciences, theoretical chemistry, polymer research, astrophysics, plasma physics and others.

Apart from several mid-range Linux computer clusters, the MPCDF operates a supercomputer, currently an IBM iDataPlex system with Intel Ivy Bridge processors and Nvidia K20X GPUs. In total there are about 83 000 cores with a main memory of 280 terabytes and a peak performance of about 2.8 petaflop s<sup>-1</sup>, making it one of the fastest computers in Germany. In close collaboration with scientists, the MPCDF also develops and

optimises algorithms and programs for high performance computing.

The MPCDF data science team supports the development and deployment of data management solutions for big data projects. Large amounts of experimental data and data from supercomputer simulations are managed and stored in three tape libraries in two different locations, with a total capacity of about 40 000 tapes. One of the libraries is shown in Figure 3. The combined amount of backup and archive data stored at the MPCDF currently totals over 50 petabytes, with a current growth rate of almost 1.5 petabytes per month.

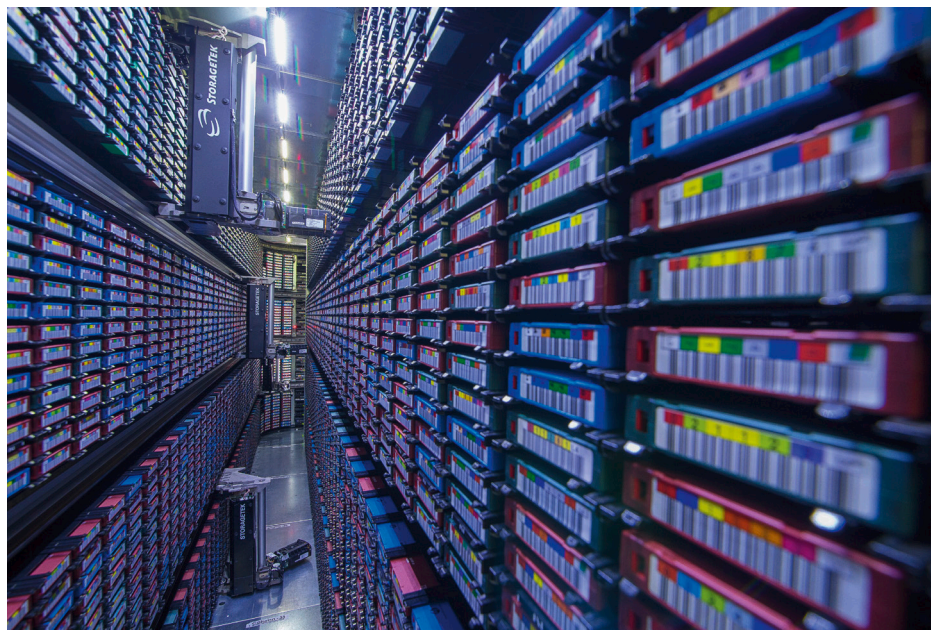
An important requirement of some of the stored data is its long-term availability. This is especially true for the humanities because of the irreproducibility of the data, for example, scans of valuable documents from the Max Planck Institute for Art History or recordings of endangered human languages from the Max Planck Institute for Psycholinguistics. Through redundancy at the logical and at the physical level, the storage of data for a period of time that surpasses the typical life-cycle of the hardware and software components employed can be guaranteed, with the goal of keeping the data forever. Some of the data still stored at MPCDF originated in the early 1980s, almost 40 years ago.

### Implementation of a collaboration

The possibility of storing a backup copy of the ESO archive at the MPCDF was first discussed between ESO and the MPCDF in November 2012. The agreement signed thereafter by both parties stipulated that the MPCDF offered to save a backup copy in their tape library of all ESO's archived data. ESO developed in-house an automatic procedure for transferring the data to the MPCDF. The replication of archived data then started on 7 May 2015 and, as planned, it took eight months to handle the backlog (at that point in time 690 terabytes of data were replicated). As of 20 January 2016, the backlog has been cleared, and the replication process is now operational, meaning that all newly archived data are backed up in near real time at



Figure 2. An image of the ESO Data Centre where the SAF content resides.



the MPCDF. This process has been working non-stop and flawlessly since then.

Figure 3. One of the tape libraries at Max Planck Computing and Data Facility (MPCDF) on the Garching Research Campus.

### Acknowledgements

Our first thank-you goes to Felix Stoehr, who first established a contact between ESO and MPCDF colleagues, which then triggered the discussions and the eventual collaboration. We also want to thank Nicolas Rosse, Laura Mascetti and Michael Boelter for their dedication in helping to test the process and then running it in operation. Maurice Klein Gebbinck is also to be thanked for testing the replication procedure.

Finally, this article is an opportunity for ESO to say a big thank you to the MPCDF for this very fruitful and successful collaboration, which is also, and not least, of long-term benefit to all of the SAF users.

### References

- Arnaboldi, M. et al. 2014, *The Messenger*, 156, 24
- Romaniello, M. et al. 2016a, in prep.
- Romaniello, M. et al. 2016b, *The Messenger*, 163, 5
- Wicencec, A. et al. 2007, *The Messenger*, 129, 27

### Links

- <sup>1</sup> ESO SAF: <http://archive.eso.org/>
- <sup>2</sup> ALMA Science Archive: <http://almascience.eso.org/alma-data/archive>



# Solar Activity-driven Variability of Instrumental Data Quality

Christophe Martayan<sup>1</sup>  
Alain Smette<sup>1</sup>  
Reinhard Hanuschik<sup>1</sup>  
Pierre van Der Heyden<sup>1</sup>  
Steffen Mieske<sup>1</sup>

<sup>1</sup> ESO

The unexplained variability of the data quality from Very Large Telescope instruments and the frequency of power cuts have been investigated. Origins for the variability in ambient temperature variations, software, data reduction pipelines and internal to hardware could be discarded. The most probable cause appears to be correlated with the evolution of the cosmic ray rate, and also with solar and terrestrial geomagnetic activity. We report on the consequences of such variability and describe how the observatory infrastructure, instruments and data are affected.

## Context

With the improvement over time of detector stability and the increase in frequency and level of instrument health monitoring, any deviations in quality control parameters due to larger than normal changes in ambient conditions (for example, temperature and air pressure) are now easier to detect. Sometimes, unusual glitches are registered. Once hardware and software problems have been discarded as the probable cause, a few events still remain unexplained. Such problems can have real consequences for data quality.

The primary cause for such variability lies in the Sun–Earth relationship. The solar maximum occurred around 2012–2014, although this cycle (24) is characterised by a low level of activity. Solar activity and geomagnetic changes induced by the

Sun lead to a number of consequences on Earth as listed in Table 1.

There are five classes of geomagnetic storm, from G1 (minor, ~ 1500 per solar cycle of 11 years) to G5 (extreme, 0 to 4 per solar cycle), as classified by the US National Oceanic and Atmospheric Service (NOAA<sup>1</sup>). The consequences of geomagnetic storms can range from the appearance of aurorae and disturbances to migration patterns, to complete black-out of the electrical systems on Earth and failure of satellite electronics. The largest recorded geomagnetic super-storm (combination of consecutive severe to extreme storms) that hit the Earth occurred in 1859 (the Carrington event<sup>2</sup>) with aurorae down to sub-equatorial regions, although they are usually limited to the polar circles. The terrestrial apparent magnetic field inverted and some induced currents caused the telegraph to fail and to deliver electric shocks to operators. More recently, in 1989, a power blackout occurred in Canada and northern USA due to strong induced currents generated by another storm, but three times weaker than the 1859 one.

Northern Chile lies in the South Atlantic Geomagnetic Anomaly, where the magnetic field is much lower than everywhere else on Earth<sup>3</sup>. As a consequence, the geomagnetosphere is less effective in protecting this region from the effects of cosmic rays and particles coming from the Sun. Most satellites crossing this region are set in safe mode to protect them from the higher cosmic ray and particle flux. In addition, it is known that at a defined latitude, higher altitude regions receive more cosmic rays. The increase is also larger for latitudes ranging from the equator to  $\pm 30^\circ$ , including all ESO observatories; the NOAA World Magnetic Model gives details<sup>4</sup>. Therefore, it is pertinent to ask whether some or all of the types of activity listed in Table 1 have an impact on the measured instrument vari-

ability and data quality, as well as in the dependability of the observatory infrastructure.

There are very few cosmic ray/neutron monitoring stations in the southern hemisphere. They represent less than 20 % of the worldwide network covered by the Neutron Monitor DataBase<sup>5</sup>. In addition, there are no neutron monitoring stations in South America and Africa and others are located in regions with a stronger magnetic field. As a consequence we have compared the measurements from the monitoring stations in the Kerguelen Islands (southern Indian Ocean, latitude  $-49^\circ$ ) and Terre Adélie (continental Antarctica) with our data.

## Cosmic ray monitoring during the minor geomagnetic storm 4–5 September 2015

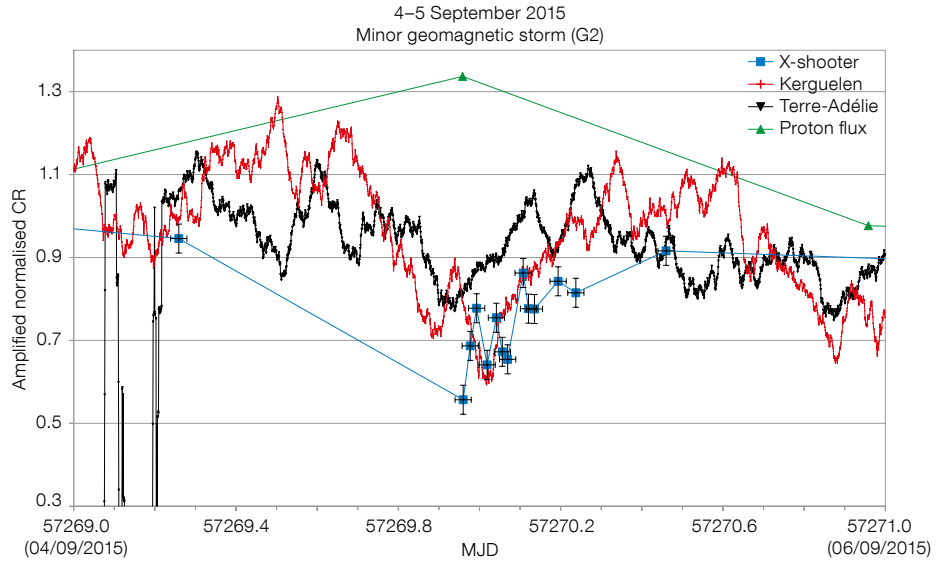
The monitoring of the health of the instruments at Paranal Observatory is carried out daily during morning calibrations. Various parameters<sup>6</sup> are obtained concerning the detectors, such as the bias and dark levels, readout noise, etc. However, X-shooter (Vernet et al., 2011) is the only instrument to specifically monitor the number of transient events, from the detector dark exposures with the near-infrared arm. The level of the dark current is partially caused by radioactive decay within the instrument itself. However, the main cause of variability for the darks is caused by the impact of particles originating outside the observatory, such as “real” cosmic rays. Unfortunately, as for other instruments, the monitoring is only carried out once a day, leading to a low temporal sampling.

However, during the night 4–5 September 2015, regular sequences of three 5-minute darks were specifically executed to determine whether the dark cosmic ray rate and readout noise (RON) levels were affected together. Figure 1 shows

Table 1. Solar and geomagnetic activity and their consequences.

Type of solar/geomagnetic activity	Consequences on Earth	Consequences on data and instrument
Solar flare — radiation/proton storm (RS)	Aurora, airglow	Increase/decrease in flux of cosmic rays
Coronal mass ejection (CME)	Radio burst and blackout	Instrumental parameter level variability
Fast dense coronal solar wind (SW)	Geomagnetic storms	Electronics failure
Magnetic fluctuations (MF)	Variation of Earth’s apparent magnetic field including its axis	Power loss
Co-rotating interaction region (CIRC)	Induced Foucault currents, Forbush effect	

**Figure 1.** Relative evolution of the cosmic ray rate during the minor geomagnetic storm of 4–5 September 2015. The x-axis gives the Modified Julian Day (time) and the y-axis corresponds to the relative CR rates. The X-shooter (blue squares), Kerguelen Islands (red), Terre-Adélie (black) CR rates all show first a decrease then a return to the normal level once the solar wind intensity is back to normal (Forbush effect). The density of protons carried out by the fast dense solar wind, which causes the storm, is shown in green.



the comparison of the time evolution of the relative cosmic ray rate measured by X-shooter (blue squares) vs. the CR rates from the Kerguelen Islands and Terre-Adélie stations (red and black curves respectively, hereafter KERG and TERA). At the beginning of this minor geomagnetic storm (G1 level), all the curves show a dip. This paradoxical behaviour is called the Forbush effect (Forbush, 1937; 1938). The solar magnetic loops, often extended by the solar matter beyond the Earth, act like a shield, deviating the cosmic rays. As these are mostly of extra-Solar System origin, this effect causes a decrease in the CR rate. However, in this event, a fast, dense solar wind brought protons (green curve in Figure 1) that reached the Earth, generating the geomagnetic storm.

A linear regression between the X-shooter CR rate and those of KERG and TERA indicates a strong correlation, with a Pearson coefficient larger than 4–5 $\sigma$ .

The follow-up of this event with X-shooter illustrated its capability to serve as a CR rate-monitoring instrument. This monitoring can be carried out at almost no cost during the day and at night, when the instrument is not being used for calibrations or scientific observations, without disturbing operations.

**Impact of solar and geomagnetic activity on X-shooter dark exposures**

One can also ask whether the instruments and their subsystems can be

affected by other geomagnetic and/or solar events besides cosmic rays. Before investigating this question a few considerations are necessary. Firstly, it should be noted that the dark current rate of the X-shooter near-infrared arm shows a reproducible and slow increase over several months following each thermal cycle that is not understood. The same behaviour is also noticeable in other near-infrared instruments like the High Acuity Wide field K-band Imager (HAWK-I). Therefore, in order to better assess the impact of the local variations related to astronomical events in the X-shooter dark

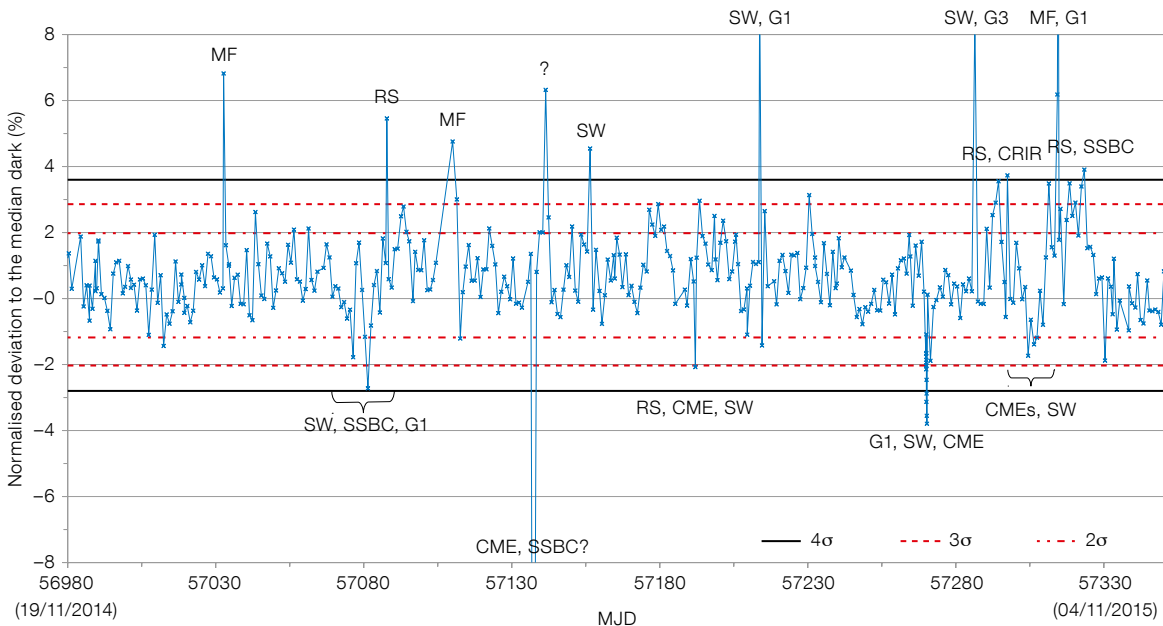


**Figure 2.** X-shooter normalised near-infrared detector dark level after removal of the long-term trend (blue points and line). The 2, 3 and 4 $\sigma$  standard deviations are shown with horizontal lines. The events at more than 3 $\sigma$  are annotated with a possible explanation: CME: coronal mass ejection; CRIR: co-rotating interaction region; Gx: geomagnetic storm of class x (1 to 5); MF: magnetic fluctuation; RS: radiation and proton storm; SSBC: solar sector boundary crossing; SW: fast dense solar coronal wind.

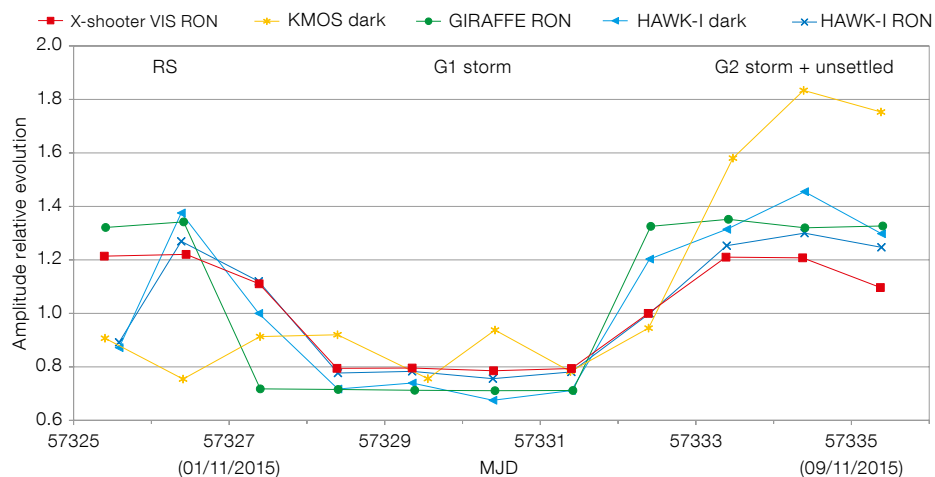


**Figure 3.** Temporal evolution of a few instrumental parameters (X-shooter VIS readout noise, KMOS median dark, GIRAFFE readout noise, HAWK-I median dark and readout noise) which correlate, over the period 30 October to 12 November 2015.

level, this slow long-term trend was removed. Secondly, the median and standard deviation ( $\sigma$ ) of the dark rate are computed and frames showing absolute deviations larger than  $3\sigma$  are visually examined. The dark level and its glitches over the period 19 November 2014 to 29 November 2015 are shown in Figure 2. At the epochs of the noted events indicated on Figure 2, all instrumental and pipeline problems, as well as variations in ambient temperature, can be discarded as the probable cause. Manual inspection of the individual frames showed confirmatory evidence of frames deviating from the normal.

We found that 94% of the deviating X-shooter dark levels can be matched to specific geomagnetic or solar activity, as recorded<sup>7</sup>. Only one event in this one-year period remains unexplained. The probability of a random temporal coincidence between dark glitches and solar events would be 1% (for example, non-random correlation of more than  $3\sigma$ ). Sometimes, aurorae and geomagnetic storms can happen even without obvious registered phenomena. Often, events like a CME apparently decrease the dark level (even if it is difficult to explain). Others, such as the magnetic fluctuation of the geomagnetosphere (crack), or recoupling with the solar magnetosphere, usually lead to an increase in the dark level. In some cases, it is difficult to conclude whether there is a positive or negative effect of the solar event on the data quality, as the dark level can increase or decrease. This is especially true if there is a combination of events including CME, SW, etc.

However, as already mentioned, the temporal sampling of X-shooter near-infrared darks is usually too low, meaning that the calibrations must be taken at the time of the event in order to record it. The duration of the events range from a few minutes to several days. In most cases, because no calibrations were taken during the event, the sampled dark curve remains unaffected, while it would have



probably shown a glitch at the time of the event occurrence. Despite this limitation, one can recognise an event representing the Forbush effect, as shown in Figure 1, visible in Figure 2 at MJD  $\sim$  57 270. During this event, there is a moderate to strong ( $2.5\text{--}3\sigma$ ) correlation of the near-infrared dark level, and also of the X-shooter ultra-violet–blue (UVB) and visible (VIS) detector bias levels and the UVB and VIS readout noise, with the Kerguelen/Terre Adélie and X-shooter near-infrared CR rates.

#### Impact of solar and geomagnetic activity on the Paranal instruments and data quality

Since X-shooter darks show a response to solar and geomagnetic activity, it is justifiable to ask whether other Paranal instruments might react as well. Two strong limitations are apparent: the first is the infrequent temporal sampling, the second the lack of simultaneity of the calibration for a particular instrument with the reference data of X-shooter dark/CR and the Kerguelen/Terre Adélie CR record. Despite these difficulties, we chose the time interval from 30 October

to 12 November 2015. During this period, several CMEs and geomagnetic storms G1 to G2 occurred, but there was also a quiet time.

Over this period, a search for a correlation between various detector parameters and the X-shooter or Kerguelen/Terre Adélie CR rates was carried out. On average, three parameters (among them bad pixel number, pattern noise, bias or dark level, readout noise) per instrument were examined. The instruments that were tested are: FORS2, KMOS, GIRAFFE, X-shooter (UVB/VIS arms), VISIR, SINFONI, HAWK-I, VIRCAM and OMEGACAM. They were chosen because at least one is located at each of the VLT Unit Telescopes and the VLT survey telescopes. As an example, a comparison of the temporal relative evolution of a few parameters from four instruments showing a similar trend is displayed in Figure 3.

Linear regressions between the chosen instrumental parameters and the CR values were carried out. The regression and Pearson coefficients were computed. To define whether the instrumental quantity correlates with the CR, values of the Pearson coefficient of more than  $2\sigma$  and

**Table 2.** Correlation of instrument parameter values with evolution of the X-shooter or KERG/TERA CR rates.

Type of CR monitoring	Fraction of instrument parameters with correlation $> 2\sigma$ (%)	Fraction of instruments with correlation at:	
		$\geq 2\sigma$	$\geq 3\sigma$
X-shooter	54	6/9	2/9
KERG/TERA	60	6/9	3/9

$3\sigma$  were considered. During the events, instrumental parameter variations of less than 1% (no change) to 155% were found. The main results are given in Table 2.

Slightly more than half of the tested parameters per instrument apparently vary with the CR evolution as indicated by the percentages in Table 2 column 2. Not only is the number of bad pixels affected, but also the dark/bias level and/or the readout noise. In Table 2 columns 3 and 4, the correlation of the parameter variation with the CR evolution is given. It is better than  $2\sigma$  in two thirds of the instruments and better than  $3\sigma$  in the remaining one third of the cases. These results indicate that all the tested instruments seem to be impacted in some way by geomagnetic and solar activity. It is also worth mentioning that some simultaneous disturbance in several instruments located on different telescopes occurred, pointing to a common origin. Other more sophisticated statistical methods seem to confirm the correlations.

The temporal coverage and the samples used are still quite small. Ideally, obtaining better sampling would improve the significance, but this is difficult to reconcile with normal Paranal operations. However, geomagnetic activity cannot be blamed for all variations or glitches that occur. In all cases, severely affected calibrations are stored in the archive (but are not generally available) and the calibration data are retaken. Such events can occur during both daytime and nighttime but monitoring activity is generally confined to the daytime, so occurrences at night may be missed. However, one might take advantage of the Forbush effect (decrease in cosmic rays) to observe faint objects and avoid the magnetic fluctuation events (increase in readout noise) as often as possible.

#### Other impacts on the observatory infrastructure

Beyond the effect on the data quality and health of Paranal instruments, solar and geomagnetic activity can also disturb operations in another way. Severe/extreme storms are known to generate possible widespread voltage control

problems and some protective systems will mistakenly trip out key assets from the grid, inducing pipeline currents, etc., according to NOAA<sup>1</sup>. In particular, the solstice G4+G4 superstorm (22–23 June 2015) and the Halloween G5+G5 superstorm (29–30 October 2003) generated power cuts in Sweden, possibly also in Argentina, induced currents in various countries, aurorae in tropical areas, magnetic declination fluctuations reaching 20 degrees, etc.

At Paranal, power cuts occurred in some areas at the times of these storms, damaging hardware, including on the telescope platform and systems under stabilised current control. No other specific reason could be found for these power cuts. Generally, the main electrical systems destroyed during these powerful geomagnetic storms are the transformers, breakers, etc. This is exactly what happened at Paranal. A correlation between power cuts and superstorms corresponds to a random probability of  $\sim 0.0005\%$ , which is highly unlikely. In addition to monitoring solar and geomagnetic activity, preventive and corrective actions to be taken when a new superstorm occurs have been defined.

#### Prospects

Paranal instruments, being highly sensitive, are affected by external disturbances, such as solar and geomagnetic events. In some cases, the data quality benefits from them, but not always and it could be strongly and negatively impacted. When several solar events occur simultaneously, their consequences on the day-to-day functioning of the observatory, the instrument health and data quality are difficult to predict. X-shooter appears to be able to follow, with adequate temporal sampling, the evolution of the cosmic ray rate and some of the solar and geomagnetic events. Such monitoring could be harnessed to provide added value to the community.

The Sun should now evolve towards the quiet phase of its unusual cycle number 24 and that will help in improving the stability of the instruments and their data. Fortunately, because the South Atlantic Magnetic Anomaly is drifting eastwards

with time, in almost a century Chile should be free from its effects.

#### Acknowledgements

Kerguelen Islands and Terre Adélie neutron monitor data were kindly provided by the French Polar Institute (IPEV, Brest) and by the Paris Observatory.

The results presented in this paper rely on data collected at the Argentine Islands (Akademik Vernadsky base), Antarctic; Isla de Pascua Mataverí (Easter Island), Chile; Trelew, Argentina; and Port-aux-Français, Kerguelen Islands, France. We thank the National Antarctic Scientific Center of Ukraine (NASC), the Dirección Meteorológica de Chile (DMC), the Institut de Physique du Globe de Paris (IPGP), Universidad Nacional de La Plata (UNLP), Royal Meteorological Institute of Belgium (RMIB) and the École et Observatoire des Sciences de la Terre (EOST), for supporting their operation and INTERMAGNET<sup>8</sup> for promoting high standards of magnetic observatory practice.

#### References

- Forbush, S. E. 1937, PhRv, 51, 1108
- Forbush, S. E. 1938, PhRv, 54, 975
- Vernet, J. et al. 2011, A&A, 536A, 105

#### Links

- <sup>1</sup> NOAA Space Weather Scales: [http://www.swpc.noaa.gov/sites/default/files/images/NOAA\\_scales.pdf](http://www.swpc.noaa.gov/sites/default/files/images/NOAA_scales.pdf)
- <sup>2</sup> Super solar flares and the Carrington event: [http://science.nasa.gov/science-news/science-at-nasa/2008/06may\\_carringtonflare/](http://science.nasa.gov/science-news/science-at-nasa/2008/06may_carringtonflare/)
- <sup>3</sup> Chulliat, A. S. et al., 2014. doi: 10.7289/V5TH8JNW
- <sup>4</sup> World Magnetic Model: [https://www.ngdc.noaa.gov/geomag/WMM/data/WMM2015/WMM2015\\_F\\_MERC.pdf](https://www.ngdc.noaa.gov/geomag/WMM/data/WMM2015/WMM2015_F_MERC.pdf)
- <sup>5</sup> Neutron Monitor DataBase: <http://www.nmdb.eu/>
- <sup>6</sup> ESO Quality control and data processing group: <http://www.eso.org/observing/dfo/quality/>
- <sup>7</sup> Log of space weather: <http://www.spaceweather.com/>
- <sup>8</sup> INTERMAGNET: <http://www.intermagnet.org>



# Science Verification for the VISIR Upgrade

Daniel Asmus<sup>1</sup>  
 Mario van den Ancker<sup>1</sup>  
 Valentin Ivanov<sup>1</sup>  
 Hans-Ulli Käufel<sup>1</sup>  
 Florian Kerber<sup>1</sup>  
 Bruno Leibundgut<sup>1</sup>  
 Andrea Mehner<sup>1</sup>  
 Yazan Momany<sup>2</sup>  
 Eric Pantin<sup>3</sup>  
 Konrad R. W. Tristram<sup>1</sup>

<sup>1</sup> ESO

<sup>2</sup> INAF – Osservatorio Astronomico di Padova, Italy

<sup>3</sup> Laboratoire AIM, CEA/DSM – CNRS – Université Paris Diderot, IRFU/SAP, Gif sur Yvette, France

The Very Large Telescope spectrometer and imager for the mid-infrared (VISIR) was upgraded in 2015 with new detectors and several new modes were added. Science Verification (SV) is carried out for new ESO instruments as well as for substantial upgrades to existing instruments. Sparse aperture masking and coronagraphy in the mid infrared have now been added to VISIR's capabilities and during SV these new observational modes, together with the recommissioned burst mode, were used to demonstrate the observational capabilities of the instrument. The SV process for VISIR is briefly described and some results from the successful observations are presented. All SV data are publicly available.

The VISIR upgrade project (Käufel et al., 2015) replaced the *N*-band low-resolution grating by a prism, the old detectors by new AQUARIUS (1024 × 1024 pixel) detectors, and added to the high spatial resolution capabilities by deploying coronagraphic and sparse aperture masking modes. In addition, support is now provided for monitoring of the precipitable water vapour integrated column through the atmosphere to enable the best mid-infrared observing conditions to be selected. The VISIR burst mode, which enables very high time resolution sampling, was recommissioned shortly before the Science Verification run.

## Proposal solicitation and submission

The call for VISIR upgrade Science Verification proposals was issued<sup>1</sup> on 15 November 2015 and advertised through the ESO Science Newsletter<sup>2</sup> on 18 November. Thirty-five proposals had been received by the deadline on 15 December 2015. The VISIR upgrade SV team evaluated all the proposals. Two SV proposals that requested the same targets and observing modes as Period 97 programmes were rejected. A few other programmes requesting instrument modes that were not part of the upgrade were also rejected. The cut-off line was defined at 44 hours of allocated time, which meant that 22 programmes could receive an allocation. All PIs were informed of the outcome of the selection on 27 January 2016 and the Phase 2 material was submitted by all successful PIs by 12 February 2016.

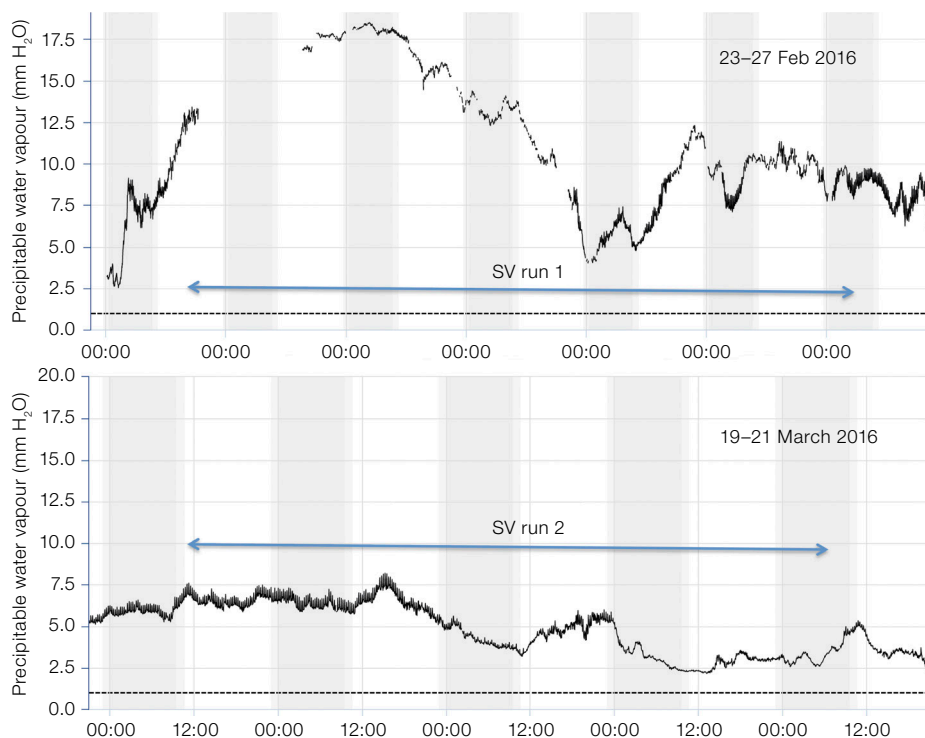
A wide range of science topics were allocated time. They included the imaging of Solar System objects (including the companions of asteroids), exoplanetary systems, protoplanetary and debris discs around young stars, the environments of evolved stars and nearby active galactic nuclei (AGN).

## Observations

The VISIR upgrade Science Verification took place on VLT Unit Telescope 3 in February and March 2016. Originally, the nights from 23 to 27 February 2016 were scheduled, but as these SV nights were very strongly affected by adverse atmospheric conditions, three half nights from 19 to 21 March were added. The 22 observing programmes selected required a total of 43.6 hours of telescope time. Of these programmes, 12 were fully completed and another six received partial data. Only four programmes could not be observed at all. The instrument worked without major fault and no substantial loss for technical reasons was recorded.

The conditions during the first run of SV nights were extremely poor. Out of the four nights 1.5 nights were lost to bad weather with the telescopes closed. The remaining time suffered from high humidity in the atmosphere above Paranal. During the 2.7 nights when the telescope was open, the precipitable water vapour, as measured by the dedicated LHATPRO

Figure 1. The precipitable water vapour record from the LHATPRO radiometer over the two runs of VISIR SV in February and March 2016.



radiometer installed on Paranal as part of the VISIR upgrade project (Kerber et al., 2015) never dropped below 4 mm, with an average around 10 mm. Figure 1 (upper panel) shows the log of the precipitable water vapour measurements spanning the time of the SV observations. For comparison, median precipitable water vapour conditions on Paranal are around 2.4 mm (Kerber et al., 2014). Technically, most of the SV run was unsuitable for mid-infrared observations.

Given this unsuccessful run, ESO allocated another three half nights between 19 and 21 March 2016 to recover some of the SV observations. This second run was much more successful (see Figure 1, lower panel) and yielded data for a majority of the SV programmes. These data are of excellent quality and in almost all cases we were able to obtain unique high-contrast observations. All new VISIR modes were used during SV and worked as expected. A few minor technical problems were uncovered, which were remedied for regular operations, starting with Period 97 (1 April–30 September 2016).

### Archive and data processing

All raw data have been archived and are publicly available. The automatic data processing and transfer worked well, considering the high data rates produced by the new modes of VISIR, especially the burst mode, which yields up to 200 GB/hour worth of data.

The VISIR upgrade SV web page<sup>3</sup> contains direct links to the raw data. A new version of the VISIR data reduction pipeline was released and now supports basic reduction for all the new modes tested during SV, except for sparse aperture masking. The pipeline can be accessed through the SV upgrade web page<sup>3</sup> or via the VLT pipelines page<sup>4</sup>.

### A few first results

VISIR observations of Jupiter were obtained in burst mode. Figure 2 shows the southern hemisphere of Jupiter in the *M*-band (4.8  $\mu\text{m}$ ). This is the first *M*-band image of Jupiter's springtime hemisphere from an 8-metre-class tele-

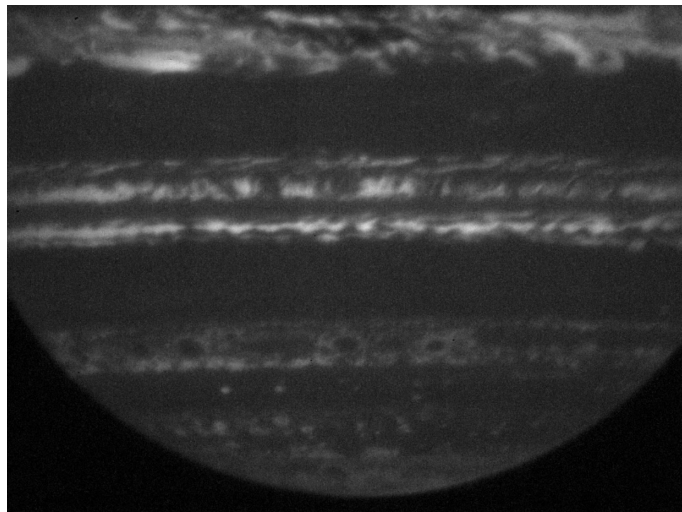


Figure 2. The southern hemisphere of Jupiter imaged with VISIR in the *M*-band utilising burst mode.

scope, allowing us to probe deeper into Jupiter's atmosphere than was possible with any other instrument. The VISIR images will also be used by the proposing team to select regions of interest for closer scrutiny by the *Juno* mission once it arrives at Jupiter in late 2016.

The sparse aperture masking mode was used to image the massive young stellar object NGC 3603 IRS9A, complementing VLT NAOS–CONICA sparse aperture masking data in the *K*<sub>s</sub>- and *L*-bands (Sanchez-Bermudez et al., 2016).

Figure 3 shows the interferograms at 10.5  $\mu\text{m}$  of NGC 3603 IRS9A (left upper) and the calibrator star HD 96918 (left lower). The fuzzier appearance of NGC 3603 IRS9A with respect to the calibrator star demonstrates that the science target is clearly resolved at the baselines corresponding to the sub-apertures of the sparse aperture mask. The right panels show the spatial Fourier transform of the interferogram which can, in a second processing step, be converted to visibility. In comparison to the calibrator, the disappearance of visibility at the highest

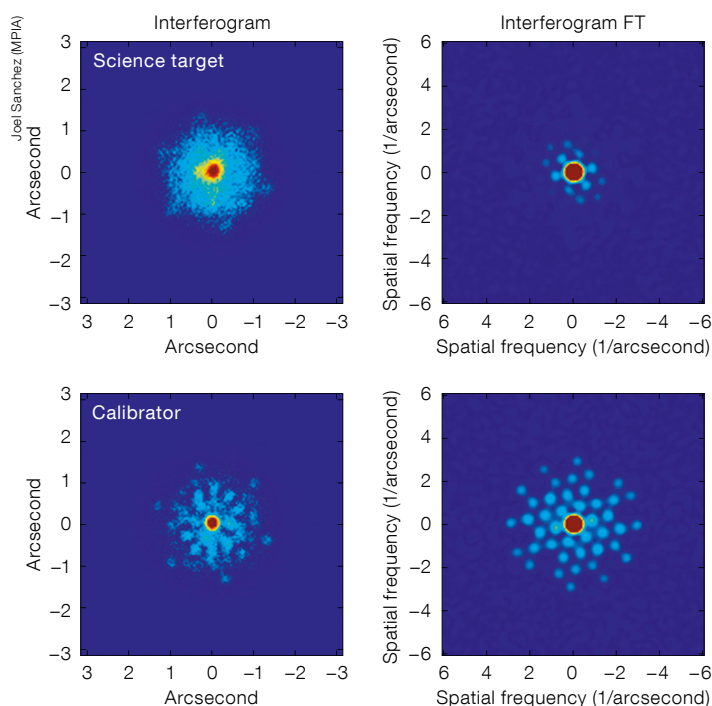


Figure 3. Interferograms at 10.5  $\mu\text{m}$  from VISIR sparse aperture masking of NGC 3603 IRS9A (left upper) and the calibrator star HD 96918 (left lower). The right-hand panels show the Fourier transform (FT) of the interferograms of both target (upper) and calibrator (lower), where the asymmetry of the envelope of NGC 3603 IRS9A is apparent.



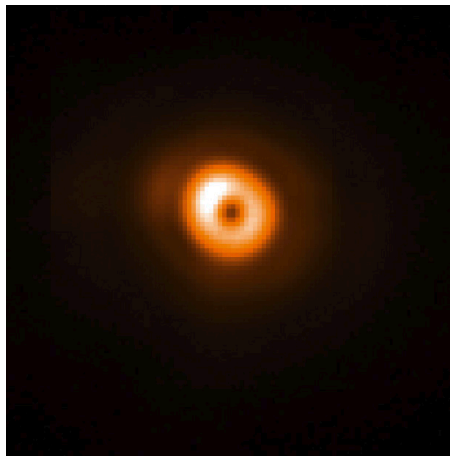


Figure 4. The mid-infrared extended dust emission around the Wolf-Rayet star WR104 is revealed by the VISIR coronagraphic annular groove mask.

spatial frequency is a measure of the spatial extent of the object. The goal of the observations is to constrain the position angle of the presumed bipolar cavities and the morphology of the outer envelope surrounding the central source. A preliminary analysis shows that the target has an angular size of at least  $\sim 450$  milliarcseconds, which is consistent with the size of the  $11.7 \mu\text{m}$  envelope reported by Vehoff et al. (2010) and by Sanchez-Bermudez et al. (2016) at lower wavelengths. With an angular resolution of  $\lambda/2D$ , where  $D$  is the maximum diameter of the sparse aperture mask, and a robust calibration in the closure phases, the new sparse aperture masking mode of VISIR is the only technique that enables the different contributions to the NGC 3603 IRS9A morphology at the half-arcsecond angular scale to be disentangled in the mid infrared.

The Wolf-Rayet star WR104 is carbon-rich and classified as a late WC-type. It shows an inner structure indicative of a binary system and an infrared excess presumably arising from warm and hot dust components. WR104 was observed at  $12.4 \mu\text{m}$  with the new annular groove phase mask coronagraph to detect the extended dust surrounding the central star. Figure 4 shows the outer structure with the central star light blocked behind the coronagraphic mask. An attenuation of the light of the central star by a factor of 42 is achieved by the coronagraph.

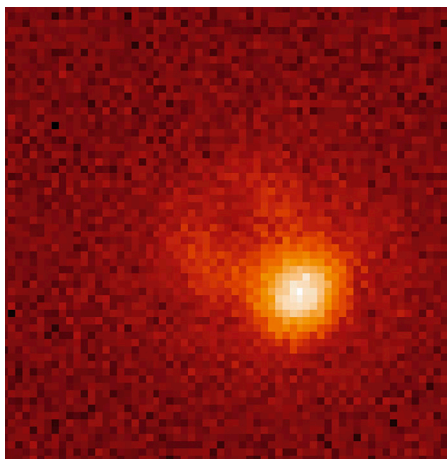
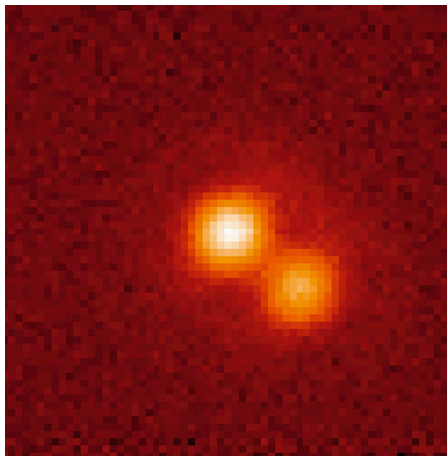


Figure 5. Demonstration of the AGPM coronagraph on the visual binary star  $\eta$  Oph (HR 6378) with the broad  $12.4 \mu\text{m}$  filter. The upper image shows the binary without the annular groove phase mask, and the lower image with the coronagraph occulting the left-hand star.

A further example of an observation with the coronagraphic annular groove mask is shown in Figure 5. This observation shows the binary star  $\eta$  Oph (HR 6378) with and without the mask inserted. In the right image with the mask inserted, the cancellation of the star beneath the mask is excellent. These observations were taken during commissioning of the annular groove phase mask in January 2016.

Circinus is one of the nearest galaxies to the Milky Way with an active nucleus. It is hidden behind the Galactic Plane and oriented almost edge-on, so that its nucleus can be observed best in the infrared. The goal of the VISIR burst mode observations was to investigate a possible emission of dust outside the

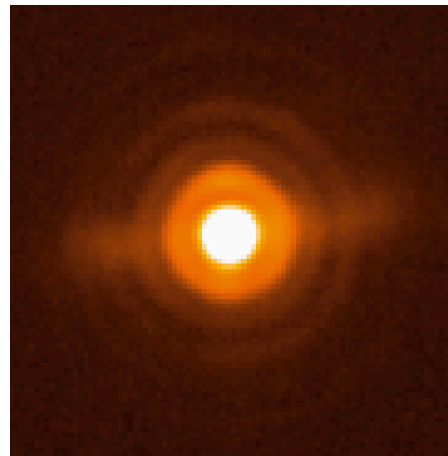


Figure 6. VISIR burst mode image of the close vicinity of the Circinus AGN taken with the PAH2\_2 narrow filter.

AGN torus and situated in the polar region, on scales of a few parsec from the centre. The image shown in Figure 6 was obtained using the PAH2\_2 filter at  $\sim 12 \mu\text{m}$ . It is dominated by the bright central point-like source, which is responsible for the Airy rings, illustrating the superb image quality that VISIR reaches in burst mode. The unresolved emission comes from warm dust surrounding the AGN. Owing to the excellent image quality, an extended, bar-like structure becomes nicely visible. This emission traces dust along the edge of the ionisation cone on scales of tens of parsecs, well outside the expected AGN torus.


#### References

- Käufel, H. U. et al. 2015, *The Messenger*, 159, 15
- Kerber, F. et al. 2014, *MNRAS*, 439, 247
- Kerber, F., Querel, R. R. & Neureiter, B. 2015, *J. Phys., Conf. Ser.*, 595, 012017
- Sanchez-Bermudez, J. et al. 2016, *A&A*, 588, A117
- Vehoff, S. et al. 2010, *A&A*, 520, 78

#### Links

- <sup>1</sup> Call for VISIR upgrade SV proposals: <http://www.eso.org/sci/publications/announcements/sciann15081.html>
- <sup>2</sup> ESO Science Newsletter November 2015: <http://www.eso.org/sci/publications/newsletter/nov2015.html>
- <sup>3</sup> VISIR upgrade SV page: <http://www.eso.org/sci/activities/vltsv/visir-upgrade.html>
- <sup>4</sup> VLT instrument pipelines: <http://www.eso.org/sci/software/pipelines/>





FORS2 image of the Galactic star-forming region RCW 34 (also catalogued as Gum 19). This colour composite, formed from images in broadband filters (*B*, *V*, *R*) and a narrowband  $H\alpha$  filter, emphasises the diffuse emission ionised by the central O-type star. This young region also has many low-mass stars in the process of emerging from the parental molecular cloud. See Release eso1521 for details.



# A Stellar Census in NGC 6397 with MUSE

Sebastian Kamann<sup>1</sup>  
 Tim-Oliver Husser<sup>1</sup>  
 Martin Wendt<sup>2,3</sup>  
 Roland Bacon<sup>4</sup>  
 Jarle Brinchmann<sup>5,6</sup>  
 Stefan Dreizler<sup>1</sup>  
 Eric Emsellem<sup>7,4</sup>  
 Davor Krajnović<sup>3</sup>  
 Ana Monreal-Ibero<sup>8</sup>  
 Martin M. Roth<sup>3</sup>  
 Peter M. Weilbacher<sup>3</sup>  
 Lutz Wisotzki<sup>3</sup>

<sup>1</sup> Institut für Astrophysik, Universität Göttingen, Germany

<sup>2</sup> Institut für Physik und Astronomie, Universität Potsdam, Germany

<sup>3</sup> Leibniz-Institut für Astrophysik (AIP), Potsdam, Germany

<sup>4</sup> CRAL, Observatoire de Lyon, Saint-Genis Laval, France

<sup>5</sup> Sterrewacht Leiden, Universiteit Leiden, the Netherlands

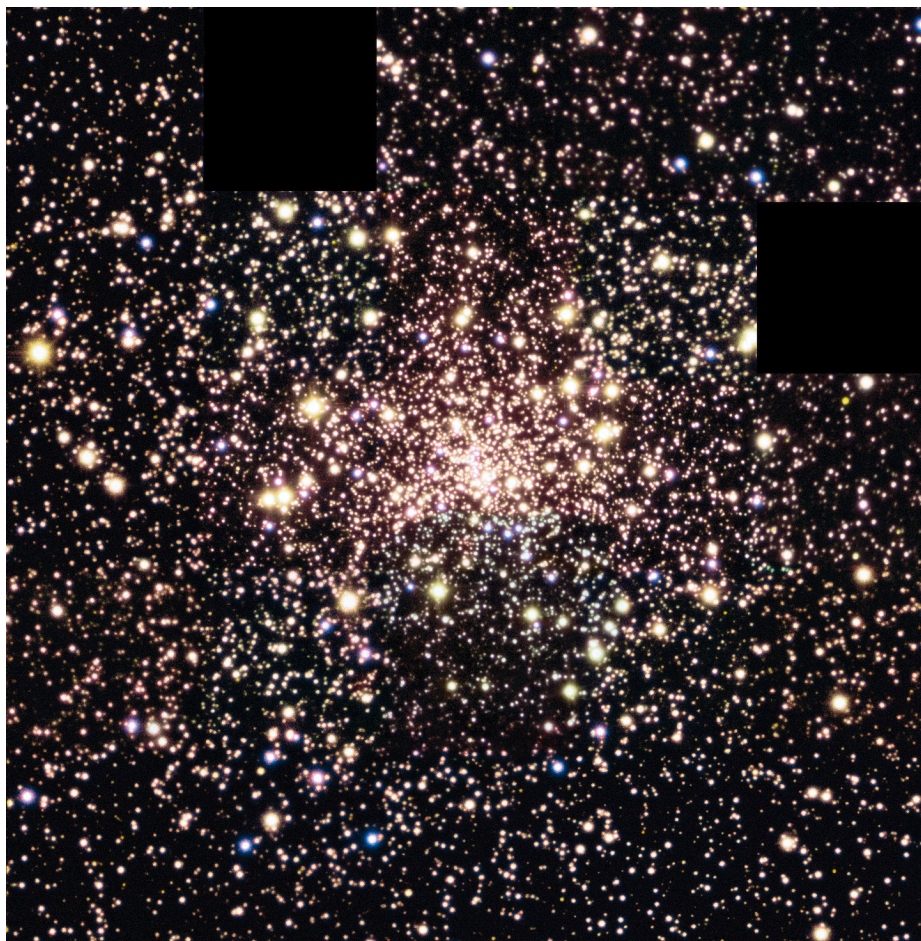
<sup>6</sup> Instituto de Astrofísica e Ciências do Espaço, Universidade do Porto, Portugal

<sup>7</sup> ESO

<sup>8</sup> GEPI, Observatoire de Paris, PSL Research University, CNRS, Université Paris Diderot, Sorbonne Paris Cité, Meudon, France

The new and powerful integral-field spectrograph on the VLT, the Multi-Unit Spectroscopic Explorer (MUSE), was designed to search for distant galaxies to an unprecedented depth, but it is also capable of opening new science windows on the Galaxy. To demonstrate this capability, the globular cluster NGC 6397 was observed during the commissioning of MUSE in August 2014. We outline how the analysis of this unique dataset allowed us to assemble the largest spectroscopic sample of stars in a globular cluster to date. We also highlight the scientific applications that benefit from such MUSE data.

MUSE (Bacon et al., 2012) is an optical integral-field spectrograph that observes a continuous field of view of 1 by 1 arcminute on the sky, sampled at a spatial resolution of 0.2 arcseconds. The instrument splits the field of view into 24 slices, each feeding a different spectrograph.



The spectrographs operate at a medium resolution,  $R$ , of 1700–3500, which allows for the inclusion of a large wavelength range, 4800 Å to 9300 Å, in a single exposure. The data reduction process which transforms the 24 raw CCD images into a three-dimensional datacube is quite complex and summarised in Weilbacher et al. (2012). A fully reduced cube contains about  $300 \times 300$  spaxels (spatial elements), which each consist of about 3600 spectral elements.

MUSE's design as a true spectrophotometric instrument with the capability to observe several thousand stars simultaneously makes it a very powerful tool for the investigation of stellar fields. There are two reasons for the large multiplexing factor. First, the number of spaxels is much higher than for any other existing integral-field spectrograph. Second, the continuous spatial coverage at a sampling below the atmospheric seeing allows techniques to disentangle the light

Figure 1.  $VRI$  colour image created from the MUSE mosaic of NGC 6397. The image is  $5 \times 5$  arcminutes in size and consists of 23 individual MUSE pointings. The images have been corrected for varying background levels.

contributions of blended stars to be used. Such techniques are of crucial importance, especially in crowded stellar fields such as the central regions of globular clusters, and will be described in more detail below.

The globular cluster NGC 6397 is, at a distance of  $\sim 2.3$  kpc, one of the closest Galactic globular clusters. It has a mass of about  $10^5 M_{\odot}$  and its metallicity of  $[Fe/H] = -2$  is low, even when compared to other Galactic globular clusters (Harris et al., 1996). The central  $5 \times 5$  arcminute region of NGC 6397 was observed during the third MUSE commissioning run (see Bacon et al., 2014) by means of a mosaic of 23 pointings (with two outer pointings missing due to constraints on the commissioning activities). The total mapped

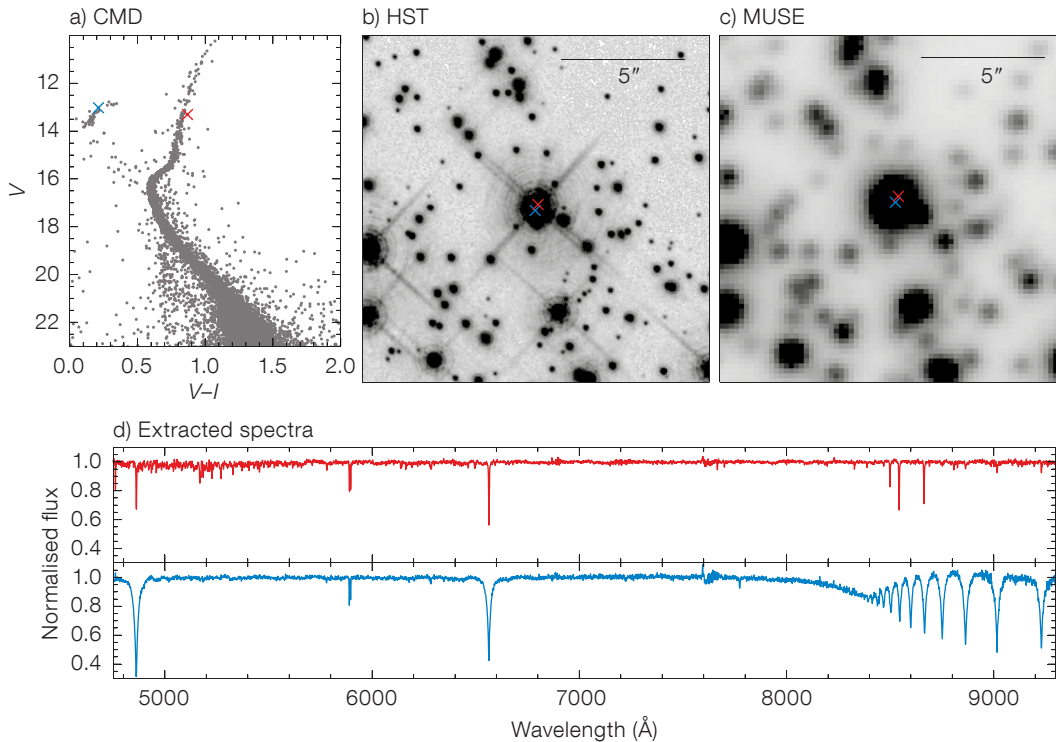


**Figure 2.** Example of the successful extraction of stellar spectra from MUSE data. Panel (a) shows a colour–magnitude diagram of NGC 6397 plotted with Hubble Space Telescope (HST) photometry from Anderson et al. (2008). As can be seen in panels (b) and (c), the two stars highlighted in red and blue appear strongly blended in the MUSE data and even in an HST image. Nevertheless, the extracted spectrum of the blue star shows the broad Paschen bands that are characteristic of hot horizontal branch stars and the red star shows the strong calcium triplet typical for spectra of red giant stars.

area is shown as a colour image made from the MUSE data in Figure 1. The observations of the central  $3 \times 3$  pointings benefited from very good seeing ( $\sim 0.6$  arcseconds), whereas the seeing was higher ( $\sim 1.0$  arcsecond) during the observations of the outer fields. Further details about the data collection and processing are presented in Husser et al. (2016).

### Extraction of spectra

Figure 1 gives a good impression of the typical stellar crowding in the central regions of globular clusters, which can pose a severe limitation for spectroscopic observations. For example, in a multi-object spectrograph, a fibre is placed on the image of every star of interest. However, near the centre of a globular cluster every such fibre will also collect a fraction of light from the star’s close neighbours, leading to a contamination of the observed spectrum. In Kamann et al. (2013), we introduced the concept of crowded-field 3D spectroscopy to overcome this issue. It represents a continuation of optimal extraction algorithms developed for imaging data (such as DAOPHOT, Stetson [1987]) into the

domain of integral-field spectroscopy and uses the point spread function (PSF) of the observations to deblend the spectra of nearby stars. We designed the software package PampelMuse, which we successfully used to analyse the MUSE data of NGC 6397, around this concept. Figure 2 shows that even for stars separated by only 0.2 arcseconds, i.e., about one third of the width of the seeing, uncontaminated spectra can be extracted.

As described in detail in Husser et al. (2016), we could extract 18 932 spectra for 12 307 stars from the full MUSE mosaic of NGC 6397, making this the largest spectroscopic sample obtained so far in any globular cluster. The spectra cover a large range of spectral types and reach down to a magnitude of about  $V = 19$ , several magnitudes below the main sequence turn-off of NGC 6397. The spectra are made available online<sup>1</sup>.

### Spectral analysis

The analysis of the extracted spectra is a multi-step process that starts with estimating stellar parameters from photometry obtained with the Hubble Space Telescope (see small inset in Figure 4).

We compare the brightness and colour of each observed star with an isochrone that matches the colour–magnitude diagram (CMD) of the cluster, yielding an effective temperature and a surface gravity. Using these parameters, a synthetic spectrum is created and used as a template for a cross correlation with the observation in order to derive a radial velocity.

The actual analysis is performed via a Levenberg–Marquardt optimisation that finds the best matching template in a grid of synthetic stellar spectra, using the previously determined values as initial guesses. As a result, we obtain stellar parameters like effective temperature, metallicity and  $\alpha$ -element abundance, as well as a radial velocity. The surface gravity is currently fixed to the one derived from photometry.

A basic principle for all our analyses is never to alter the observed spectra, since every operation, such as re-binning or normalisation, would also result in a loss of information. Instead, we leave the observed spectrum untouched and only change the model spectra. So, for instance, we never remove the continuum flux from the observed spectrum, but try



to find a polynomial that, when multiplied by the model, best matches the observation. Furthermore, instead of removing the telluric absorption lines by means of observations of a telluric standard star, we try to model them. Abundances of water and molecular oxygen are free parameters in the optimisation as well as a line shift and broadening for the telluric spectrum. This approach improves the quality of the derived parameters significantly.

An example of an analysed spectrum is shown in Figure 3. The observed spectrum in black is overplotted with the model spectrum in red that has been found to best match the observation. The residuals are plotted in blue below.

Results for the globular cluster NGC 6397 as a whole are shown in Figure 4 in the form of an Hertzsprung–Russell diagram (HRD), plotting the luminosity as a function of effective temperature. For the luminosity, we derived V-band magnitudes from the spectra and applied a bolometric correction based on the fitted stellar parameters. All the stars are colour-coded with their corresponding metallicity from the analysis. While the variation of the metallicity along the main sequence is presumably due to low signal-to-noise ratio (S/N) in this part of the HRD, the trend on the giant branch may indeed be real, as it has been observed before by other groups and instruments. For instance, Korn et al. (2007) interpreted this variation as the result of atomic diffusion in the stellar atmosphere. The results for NGC 6397 are discussed in detail in Husser et al. (2016).

While the results for single stars are already of good quality, they cannot compete with those from high-resolution spectroscopy. But the greatest strength of our MUSE observations lies in the unprecedented amount of data. Instead of measuring, for instance, the metallicity in a few high-resolution spectra, we can provide a mean value and spread for the metallicity for thousands of stars, either for the whole cluster or limited to a small region in the CMD. Furthermore, the large number of spectra allows us to improve the S/N, especially on the main sequence, by co-adding spectra, either from multiple visits to the same star or from neighbouring stars in the CMD.

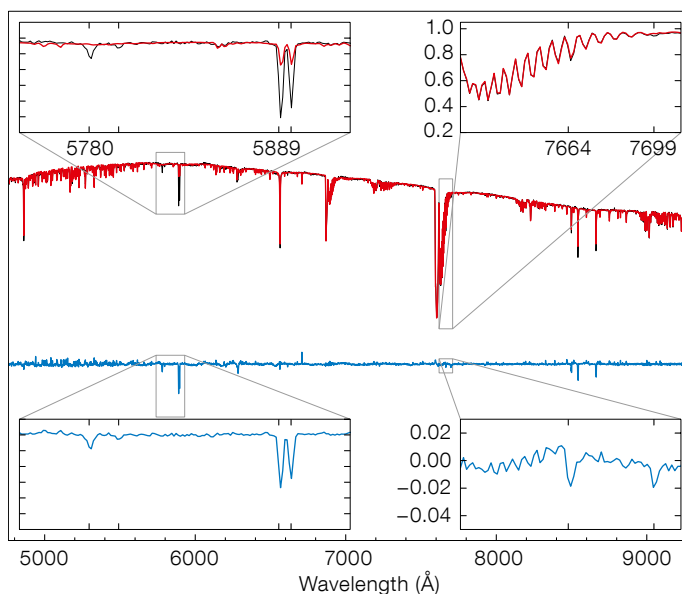


**Figure 3.** Steps in the data processing. In black the PSF-extracted spectrum of one of the brightest stars is shown. The red line shows the best fit, including a telluric absorption correction. In blue, the fitting residuals are displayed to scale with the data and fit. The small inserts zoom into spectral regions of interest for ISM analyses. The left panels show the prominent NaD doublet as well as diffuse interstellar bands at 5780 and 5797 Å. On the right-hand side, the insets illustrate the success of the telluric fit where the weak K I doublet lines clearly stand out. The zoom for the residuals is scaled by a factor of ten.

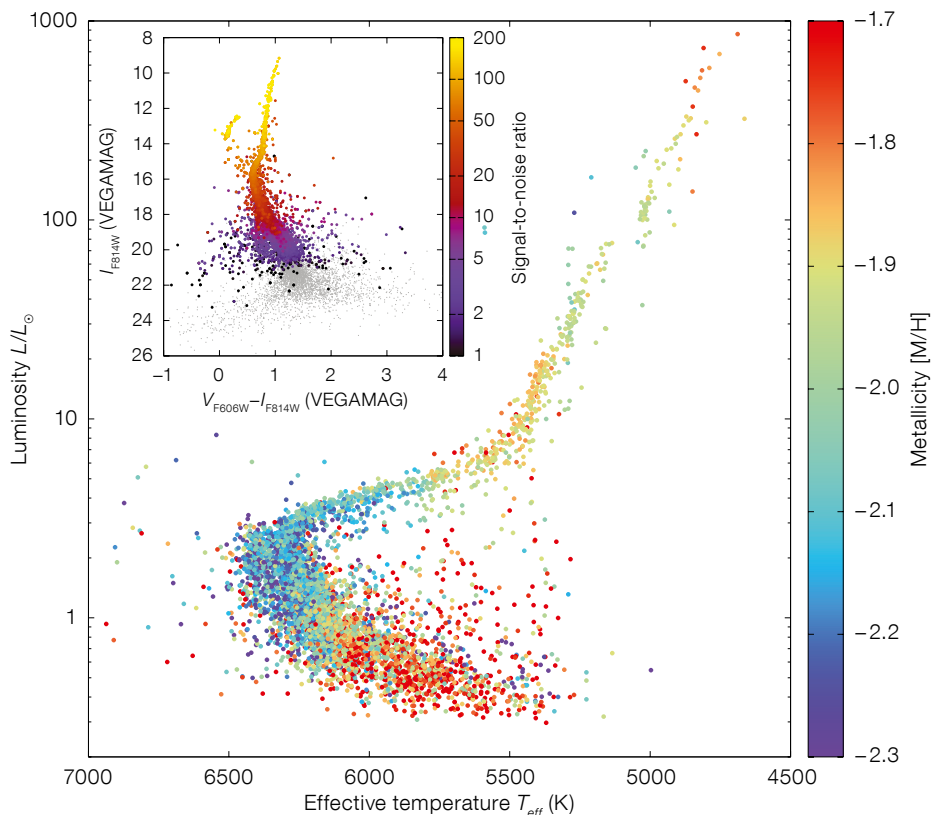


**Figure 4.** The small inset shows the colour–magnitude diagram of NGC 6397. All the stars observed with MUSE are colour-coded with the signal-to-noise ratios of their respective spectra. The large plot shows the Hertzsprung–Russell diagram using the stellar parameters from the analysis. Here the colour indicates the derived metallicity of each star.

## Cluster dynamics

With a mass of around  $10^5 M_A$ , NGC 6397 is only moderately massive when compared to other globular clusters in the Milky Way. For example, Omega Centauri is more than ten times as massive as NGC 6397. A consequence is that the internal dynamics of NGC 6397 are dominated by low velocities — the central dispersion is expected to be as low as  $5 \text{ km s}^{-1}$ . This poses a severe challenge for spectroscopic studies with the low spectral resolution offered by MUSE, because they must achieve an accuracy in radial velocity that is higher than the intrinsic cluster dispersion. From the analysis of telluric absorption bands in the extracted spectra, we could show in Kamann et al. (2016) that the internal accuracy of MUSE is stable at a level of  $1 \text{ km s}^{-1}$ , both across the field of view and over the course of a night. Given the complexity of MUSE, this is a remarkable result that confirms the high stability of the instrument and the excellent quality of the data reduction pipeline.

With respect to the cluster dynamics, the central region is the most interesting one. For example, there is an ongoing debate about the presence of massive black holes, weighing about  $10^2$ – $10^5 M_A$ , in the centres of globular clusters (see, e.g., van der Marel et al. [2010] and Noyola et al. [2010]). However, a common problem of spectroscopic studies is that they can only target isolated stars, where contamination from nearby sources is negligible. Thanks to the spatial coverage of MUSE and our deblending algorithm, we are able to overcome this problem.

Figure 5 shows that our measurements extend much further into the centre than previous radial velocity studies of NGC 6397, allowing us, for the first time, to constrain the presence of a massive black hole in this cluster. To do so, we compared our measurements to dynamical models, some of which are depicted in Figure 5. We found that the velocity dispersion in the centre is higher than what would be expected from the gravitational potential of the bright stars alone. A black hole with a mass of about  $600 M_A$  would be an intriguing explanation for this discrepancy. However, it is not the only possible explanation. Alternatively, a cen-

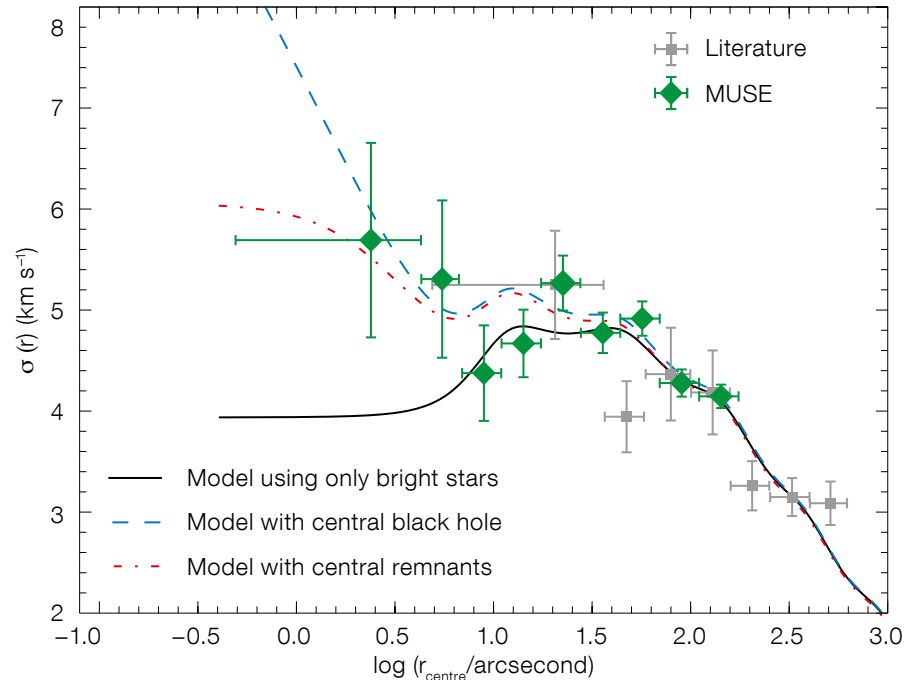


Figure 5. Velocity dispersion of NGC 6397 as a function of distance to the cluster centre as measured by MUSE (green diamonds) and from a compilation of literature studies (grey squares). The different lines show the expected velocity dispersion curves based

on the gravitational potential of the bright stars alone (black solid line), with the addition of a black hole with  $600 M_A$  (blue dashed line), and with the addition of a central accumulation of stellar remnants with a similar mass (red dash-dotted line).

tral accumulation of stellar remnants (such as neutron stars or stellar-mass black holes), which may form as a consequence of mass segregation in the cluster, could also explain our measurements. Further details about our analysis and possible ways to distinguish between the two alternatives in the future can be found in Kamann et al. (2016).

The diagnostic power of the MUSE data is not limited to the search for massive black holes. Thanks to the large stellar sample, we can also look at the cluster dynamics in a two-dimensional way. In doing this, we identified a small rotational component, with a projected amplitude of about  $1 \text{ km s}^{-1}$  around the centre. In addition, we could investigate whether the stellar dynamics change depending on the masses of the investigated stars. Such a dependency can be caused by relaxation processes inside the cluster. Gravitational encounters between member stars will on average accelerate the less massive stars and decelerate the more massive stars, ultimately leading to mass segregation. The investigation

of this phenomenon requires the observation of many stars along the main sequence, because giant stars all have more or less similar masses, and is therefore extremely challenging. In the MUSE data, we found a marginal trend for more massive stars to have a lower central velocity dispersion. Further studies are required to settle this issue, but the commissioning data of NGC 6397 already show the potential of MUSE in this respect.

## Interstellar medium

The template matching of the individual stellar spectra and the comprehensive sky model fits are quite successful. In fact, they are robust to such an extent that we can carry out further studies on the fitting of the residuals themselves, which still feature absorption lines and bands of the interstellar medium (see Figure 3). This is a field of research for which MUSE was not even designed. This study provides a unique insight into small scale structures in the interstellar

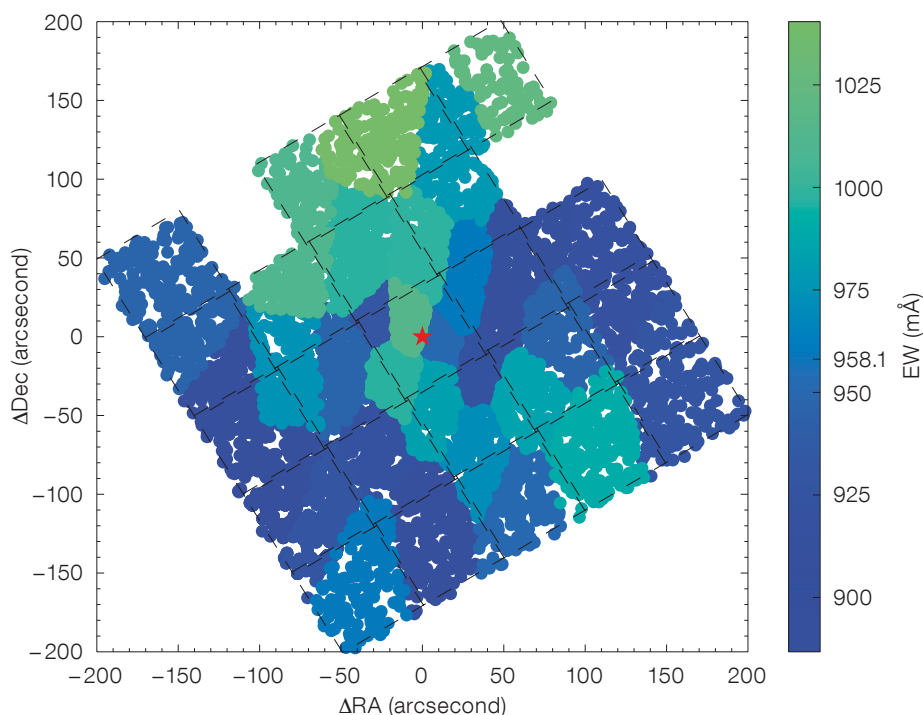


**Figure 6.** Equivalent width map of the NaD doublet. All residual spectra were combined into Voronoi tessellated bins. The colour bar shows the equivalent width range as well as the average value for this species. The uncertainty per bin is of the order of 8 mÅ.

medium (ISM) that could not be traced or spatially resolved with individual isolated spectra.

To reach a higher S/N, we computed the error-weighted average of  $\sim 300$  residual spectra to form several composite spectra of similar S/N. The accuracy of the telluric and stellar fits is very high. The inset in Figure 3 shows both doublet lines of the weak interstellar K I. While K I 7664 Å sits directly on a strong telluric band, K I 7699 Å is hardly affected by skylines at all. Their independently fitted ratio remains very stable and provides great confidence in the applied method. In fact, we can even utilise that ratio as a diagnostic tool to trace optical thickness. Since we know that we can successfully subtract stellar features as well as sky lines, we continued to systematically analyse other weak ISM features, such as a number of diffuse interstellar bands that we observe in the broad wavelength range of the MUSE spectrograph. This analysis will be described in a third follow-up paper on these observations by Wendt et al.

Other, stronger ISM lines even had to be considered during the template matching itself. A particular challenge is the NaD doublet. Here, we expect at least three unresolved contributors: the stellar component, NaD in the Earth's atmosphere, as well as the ISM component(s) along the line of sight. The first two contributions are subtracted. Figure 6 shows the equivalent width of the remaining (interstellar) contributions in the 31 Voronoi tessellated bins (spaxel spectra co-added to increase the S/N). The colours reflect the measured total equivalent width of the NaD doublet for each composite spectrum per bin with an average of about 960 mÅ, and the MUSE pointings are indicated as black dashed lines; a red star marks the centre of the globular cluster. The mapping reveals a compelling small-scale structure in interstellar NaD that is neither correlated with the pointings, nor the number of stars per



bin, i.e., with the cluster itself. At the distance of 100 pc for the edge of the Local Bubble, the linear projection for typical scale sizes is in the order of a milliparsec. This illustrates how MUSE is uniquely able to provide an overview of the small-scale structures of the ISM.

### Prospects

The example of NGC 6397 has shown the huge potential of MUSE for the investigation of crowded stellar fields. The unprecedented number of stars for which spectra can be acquired simultaneously enables completely new science cases. We are currently conducting a large survey of 25 Galactic globular clusters with the aim of obtaining multi-epoch spectroscopy for several thousand stars per cluster. In addition to detailed investigations of stellar parameters, the central dynamics and the ISM, this survey will also reveal clues about the properties of binary stars in the clusters.

Following the installation of the Ground Atmospheric Layer Adaptive Optics for Spectroscopic Imaging (GALACSI) system (see Ströbele et al., 2012), MUSE observations at a significantly higher spa-

tial resolution will soon be possible. In crowded stellar fields, this improvement will even further increase the number of accessible stars. As such fields are not specific to globular clusters, but are also found in the Galactic Bulge or nearby galaxies, we believe that there are huge prospects for MUSE observations similar to those that we have presented for NGC 6397.

### References

- Anderson, J. et al. 2008, *AJ*, 135, 2055
- Bacon, R. et al. 2012, *The Messenger*, 147, 4
- Bacon, R. et al. 2014, *The Messenger*, 157, 13
- Harris, W. E. et al. 1996, *AJ*, 112, 1487
- Husser, T.-O. et al. 2016, *A&A*, 588, 148
- Kamann, S. et al. 2013, *A&A*, 549, 71
- Kamann, S. et al. 2016, *A&A*, 588, 149
- Korn, A. J. et al. 2007, *ApJ*, 671, 402
- Noyola, E. et al. 2010, *ApJ*, 719, 60
- Stetson, P. B. 1987, *PASP*, 99, 191
- Ströbele, S. et al. 2012, *Proc. SPIE*, 8447, 844737
- van der Marel, R. et al. 2010, *ApJ*, 710, 1063
- Weilbacher, P. M. et al. 2012, *Proc. SPIE*, 8451, 84510B

### Links

- <sup>1</sup> Online access to extracted spectra: <http://muse-vlt.eu/science/globular-cluster-ngc-6397/>

# Pulsating Hot Subdwarfs in Omega Centauri

Suzanna K. Randall<sup>1</sup>  
 Annalisa Calamida<sup>2</sup>  
 Gilles Fontaine<sup>3</sup>  
 Matteo Monelli<sup>4</sup>  
 Giuseppe Bono<sup>5,6</sup>  
 Maria Luisa Alonso<sup>7</sup>  
 Valérie Van Grootel<sup>8</sup>  
 Pierre Brassard<sup>3</sup>  
 Pierre Chayer<sup>2</sup>  
 Marcio Catelan<sup>7</sup>  
 Stuart Littlefair<sup>9</sup>  
 Vik S. Dhillon<sup>9,4</sup>  
 Tom R. Marsh<sup>10</sup>

<sup>1</sup> ESO

<sup>2</sup> Space Telescope Science Institute, Baltimore, USA

<sup>3</sup> Département de Physique, Université de Montréal, Canada

<sup>4</sup> Instituto de Astrofísica de Canarias, Tenerife, Spain

<sup>5</sup> Università di Roma "Tor Vergata", Department of Physics, Rome, Italy

<sup>6</sup> INAF – Osservatorio Astronomico di Roma, Monte Porzio Catone, Italy

<sup>7</sup> Pontificia Universidad Católica de Chile, Santiago, Chile

<sup>8</sup> Institut d'Astrophysique et de Géophysique de l'Université de Liège, Belgium

<sup>9</sup> Department of Physics and Astronomy, University of Sheffield, United Kingdom

<sup>10</sup> Department of Physics, University of Warwick, Coventry, United Kingdom

We recently discovered the first globular cluster hot subdwarf pulsators in Omega Centauri ( $\omega$  Cen). These stars were initially thought to belong to the class of rapidly pulsating subdwarf B stars, which are well established among the field star population and have become showcases for asteroseismology. However, our spectroscopic analysis revealed the  $\omega$  Cen variables to be significantly hotter than expected, indicating that they form a new class of subdwarf O pulsators clustered around 50 000 K, not known among the field star population. Non-adiabatic pulsation modelling suggests that the driver for the pulsations occurs via the same iron opacity mechanism that is at work in the rapidly pulsating subdwarf B stars.

The formation and evolution of hot subdwarf B- and O-type stars (sdB and sdO) stars is one of the remaining mysteries in stellar evolution theory. While it is commonly accepted that the cooler sdB stars ( $T_{\text{eff}} \sim 20\,000\text{--}40\,000$  K) are compact and evolved extreme horizontal branch (EHB) stars that have lost too much of their hydrogen envelope near the tip of the red giant branch (RGB) to sustain hydrogen-shell burning on the asymptotic giant branch (AGB) after core helium ignition, the details of their evolution, in particular the dramatic mass loss, remain unclear. The hotter sdO stars ( $T_{\text{eff}} \sim 40\,000\text{--}80\,000$  K) are even more challenging to understand, likely comprising a mixed bag of post-EHB, post-RGB and post-AGB stars.

One of the most promising ways of testing different evolutionary scenarios is by inferring fundamental properties, such as the total stellar mass or the thickness of the remaining hydrogen envelope, from asteroseismological analysis of pulsating hot subdwarfs. This has been done with particular success for the rapidly pulsating subdwarf B (sdBV<sub>r</sub>) stars (Fontaine et al., 2012). These are a well-

established class of pulsator found in a narrow instability strip between  $\sim 29\,000$  and  $36\,000$  K, characterised by multi-periodic luminosity variations on a short timescale of 100–200 s. The observed variations can be explained very nicely in terms of non-radial pressure mode instabilities driven by an opacity mechanism associated with a local overabundance of iron in the driving region.

Although hot subdwarfs are known in large numbers both among the Galactic field population and in globular clusters (where they are identified as EHB or blue hook stars), the exploitation of their pulsations has traditionally been limited to the field star population for the simple reason that, until recently, no hot subdwarf pulsators had been found in a globular cluster.

[A search for hot subdwarf pulsators in  \$\omega\$  Cen](#)

Like so many observational astronomy discoveries, the identification of the first hot subdwarf pulsator candidate in a globular cluster was serendipitous. We

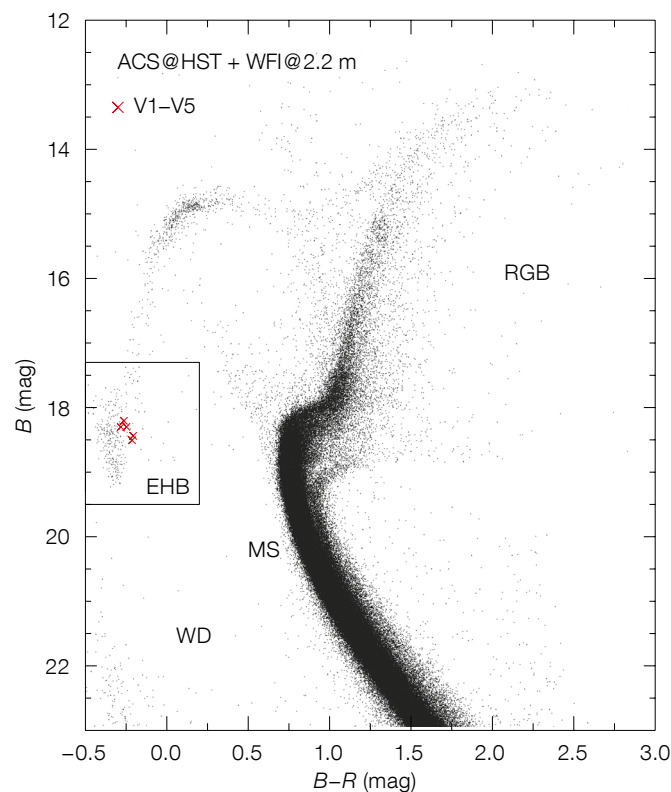


Figure 1. Colour-magnitude diagram of  $\omega$  Cen based on the merged HST ACS/WFI catalogue. The box shows the colour-magnitude cuts applied for our selection of EHB star candidates, and the five rapid sdO pulsators are indicated by red crosses.

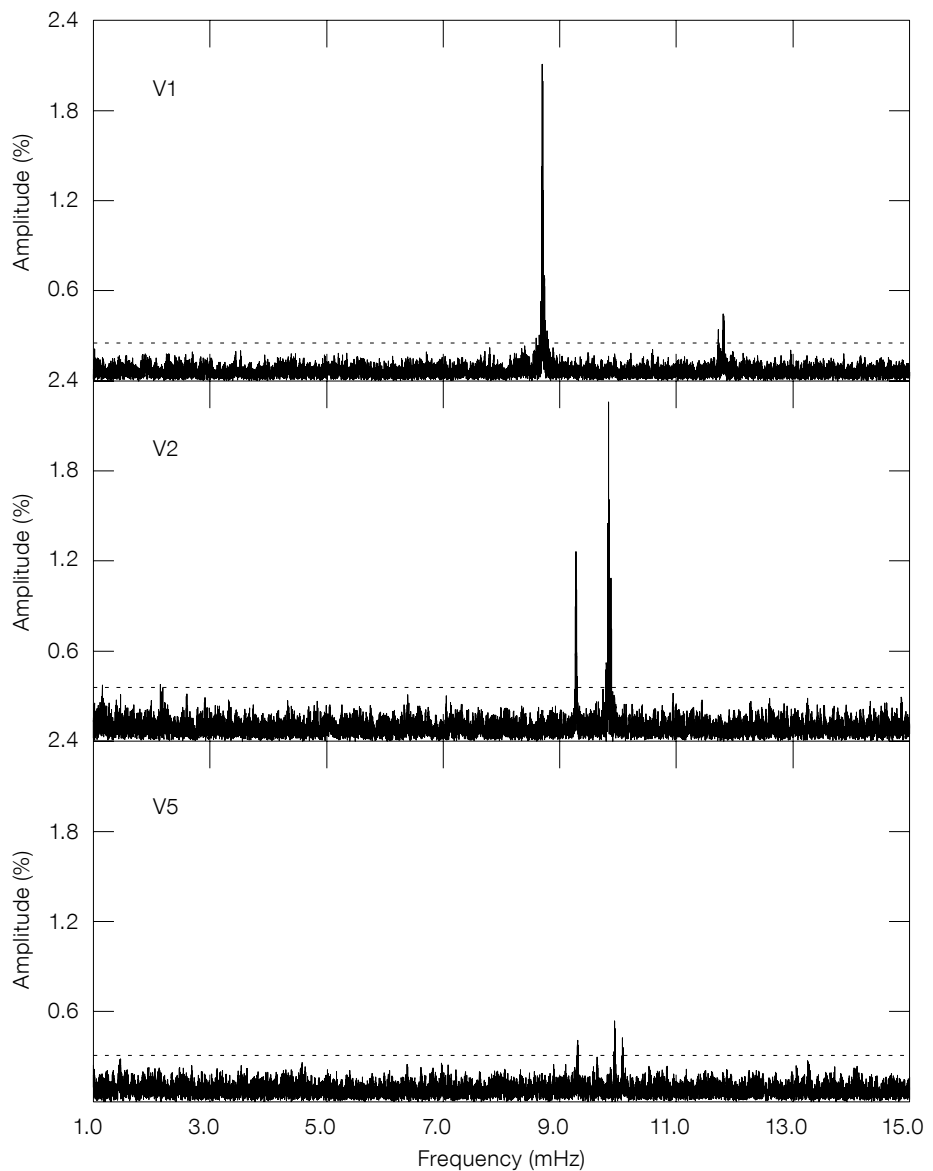


were obtaining time-series photometry with the Superb Seeing Imager 2 (SUSI2) on the New Technology Telescope (NTT) for an unrelated observing programme and chose a more or less random field in  $\omega$  Cen as a backup target at the end of the night. Since at that point the hunt for sdBVr stars in bright nearby globular clusters had been going on for some time without success, we could hardly believe it when our analysis of this short two-hour dataset revealed a 115-second periodicity in a star for which the colour magnitudes were consistent with a hot subdwarf.

This initial discovery paved the way for an extensive follow-up survey with two main observational components: time-series photometry obtained with EFOSC2 and ULTRACAM at the NTT, and multi-object spectroscopy gathered using FOCal Reducer/low dispersion Spectrograph (FORSS2) at the Very Large Telescope (VLT). More details can be found in Randall et al. (2016).

The time-series photometry amounts to nearly 100 hours of fast-cadence ( $\sim 10$  s) monitoring of some 300 stars scattered across off-centre fields in  $\omega$  Cen and identified as EHB candidates based on a colour–magnitude cut in a merged Hubble Space Telescope Advanced Camera for Surveys (ACS) Wide Field Imager (WFI) catalogue (Castellani et al., 2007). The corresponding colour–magnitude diagram of  $\omega$  Cen as well as the colour–magnitude ranges used for our EHB target selection are shown in Figure 1. It appears that this simple selection method is quite reliable, since from our spectroscopic sample of 60 stars only two turned out to not be hot subdwarfs.

From the photometry we were able to not only confirm the variability of the pulsator candidate identified with SUSI2, but also discovered an additional four pulsating EHB candidates, bringing the total number to five (denoted V1–V5 in the order that they were discovered). The pulsational properties of the variables are quite similar, each star showing two to three well-separated oscillations in the 85–125 s range with amplitudes up to  $\sim 2.5\%$  of their mean brightness. Figure 2 shows examples of the Fourier amplitude spectra obtained, the pulsations being clearly



visible above the  $3.7\sigma$  detection threshold imposed. It is worth noting that the highest amplitude peaks show fine frequency structure corresponding roughly to the resolution of the dataset, which are attributed to significant amplitude variations of the pulsations. Such amplitude variations are well documented for the field sdBV<sub>r</sub> stars and are therefore not unexpected.

#### Surprising results from spectroscopy

Given our knowledge of hot subdwarf pulsators in the field and the pulsational properties observed for the  $\omega$  Cen variables, we quite naturally assumed we had

Figure 2. Fourier amplitude spectra for three of the  $\omega$  Cen variables based on the combined ULTRACAM *u*: light curves. The horizontal dashed line indicates the  $3.7\sigma$  detection threshold imposed.

found the long-sought-after globular cluster counterparts to the sdBV<sub>r</sub> stars. However, the spectroscopic data of the new variables painted a different, even more intriguing picture: rather than the expected temperatures around 30 000 K, our atmospheric analysis yielded significantly higher values around 50 000 K, implying that these stars are in fact a new type of sdO pulsator never observed among the field star population!

Figure 3. Location in  $T_{\text{eff}} - \log g$  space of the  $\omega$  Cen variables compared to the different types of field hot subdwarf pulsators known. The reference to the discovery paper is indicated for each.

This can be fully appreciated from Figure 3, where we show the location of the  $\omega$  Cen pulsators compared to the known field hot subdwarf pulsators. Only the previously mentioned sdBV<sub>r</sub> pulsators and the one lone field sdOV star show periods on short timescales comparable to the  $\omega$  Cen variables, while the other types of pulsator oscillate on longer timescales of one to several hours. None of the field star variables falls in the  $\sim 48\,000 - 52\,000$  K range where the  $\omega$  Cen pulsators are found. Conversely, we did not identify any counterparts to the field star variables in  $\omega$  Cen, although this is quite possibly due to the limitations of our dataset both in terms of quality and sample size.

The empirical  $\omega$  Cen instability strip derived from our survey is shown in Figure 4. Here we have included only the 26 targets for which we have both high quality light curves from photometry as well as reliable atmospheric parameters from spectroscopy. Apart from a clear bias towards the pulsators, which were specifically included in the spectroscopic sample, there should be no additional selection effects beyond the colour-magnitude cuts described earlier. From the plot it is not entirely clear whether all stars falling within the instability strip pulsate, or whether non-variable stars co-exist in the same region of  $T_{\text{eff}} - \log g$  space, as is the case for the sdBV<sub>r</sub> pulsators in the field.

### Pulsation calculations

Keeping in mind their very similar pulsation properties and relative proximity in atmospheric parameter space, it seemed likely that the pulsation driving mechanism active in the  $\omega$  Cen variables is the same opacity mechanism that explains the sdBV<sub>r</sub> instability strip so well. Therefore, we extended our existing stellar envelope models to higher temperatures, encompassing the entire range where hot subdwarfs are found. These so-called Montréal second-generation models incorporate traces of iron that are levitating

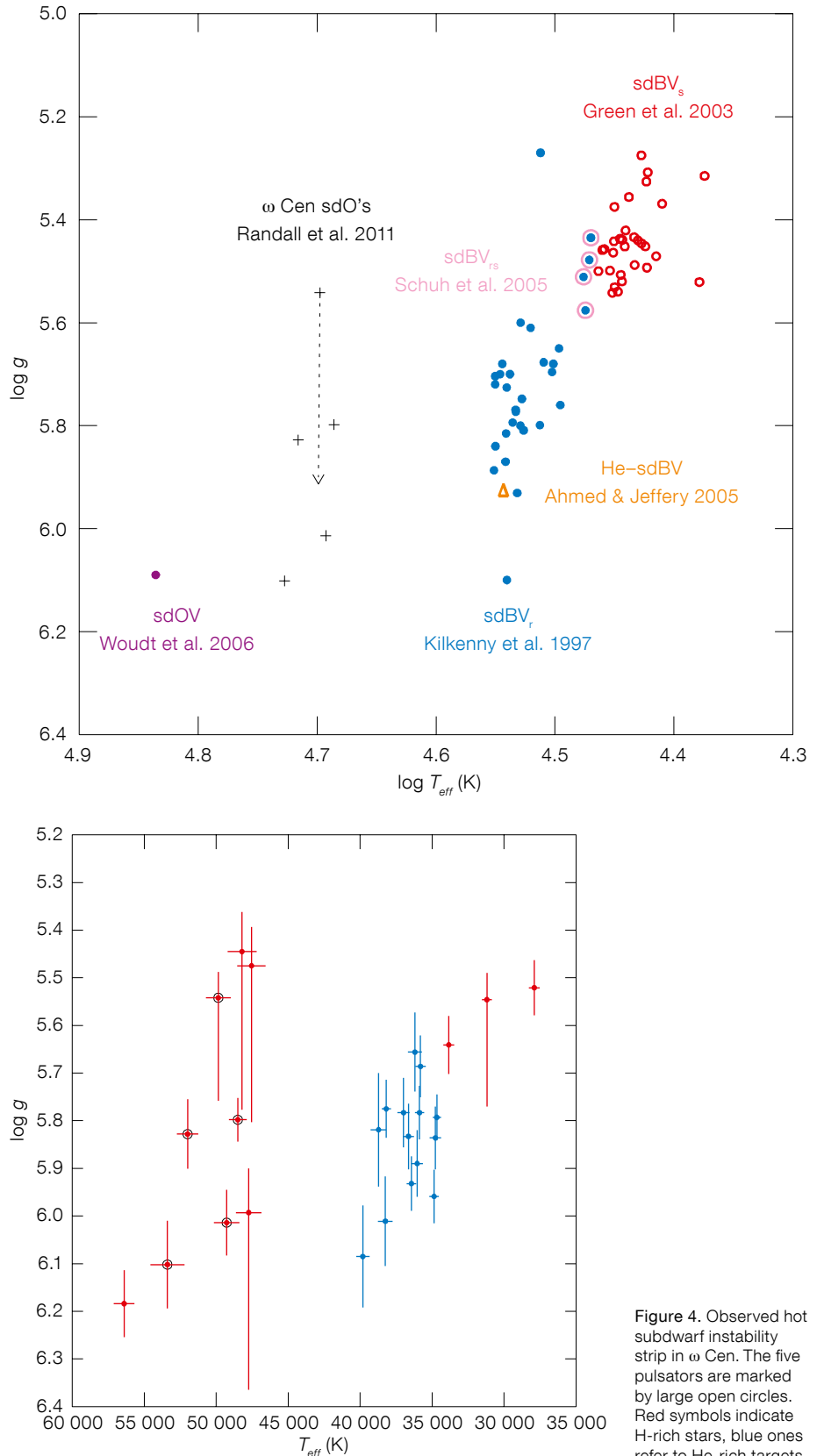
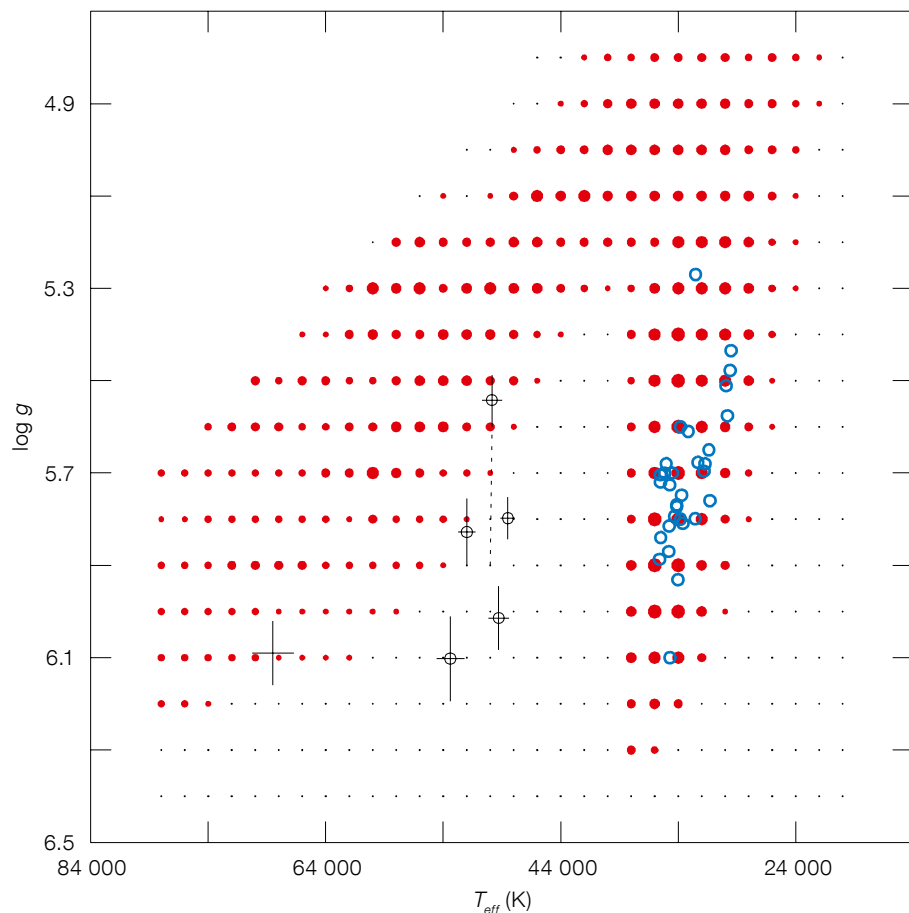


Figure 4. Observed hot subdwarf instability strip in  $\omega$  Cen. The five pulsators are marked by large open circles. Red symbols indicate H-rich stars, blue ones refer to He-rich targets.





**Figure 5.** Theoretical instability strip for rapid pressure-mode pulsations in hot subdwarfs. Each red point indicates a model where pulsations are driven. The blue circles show the location of observed sdBV<sub>r</sub> stars in the field, while the black cross represents the one sdO field pulsator known. The  $\omega$  Cen

pulsators are depicted as black open circles with error bars; the dotted extension to higher log  $g$  values for one of them indicates that the spectroscopic log  $g$  is likely underestimated due to contamination from nearby stars.

in a pure hydrogen envelope under the assumption that an equilibrium has been reached between radiative levitation and gravitational settling (Charpinet et al., 1996; 1997). The iron abundance profile as a function of stellar depth is then necessarily a function of log  $g$  and  $T_{\text{eff}}$ . Since the presence of an opacity bump associated with an overabundance of iron in the driving region allows pulsations to be excited, it follows that this will happen only for models with certain log  $g/T_{\text{eff}}$  combinations.

From our non-adiabatic oscillation calculations, we find that pressure-mode pulsations (corresponding to short periods up to a few hundred seconds) are indeed driven not only for sdB star mod-

els around 30 000 K, but also at higher temperatures above  $\sim 50$  000 K. This can be seen nicely in Figure 5, where we show the theoretical instability regions for the entire log  $g - T_{\text{eff}}$  space where hot subdwarfs are found.

Unfortunately, while the cooler instability strip matches the location of the sdBV<sub>r</sub> stars perfectly, the hotter instability region does not quite reach the  $\omega$  Cen pulsators, which lie beyond the predicted red edge. This mismatch may be partially due to the effective temperatures from our optical spectra being underestimated for these very hot stars, however the periods of the oscillations predicted are also significantly shorter than those observed. It is clear that the models need

to be improved, particularly with regards to other metals besides iron being included in the diffusion calculations. Nevertheless, we are confident that we have identified the basic driving mechanism in the  $\omega$  Cen pulsators to be the same opacity mechanism that is at work in the sdBV<sub>r</sub> stars.

### The plot thickens

Far from giving definite answers, the results of our survey have instead raised more questions. But that is the beauty of observational astronomy: you rarely find what you expect, and the deeper you look the more complicated the picture becomes, opening up new avenues of research. In this case, the unexpected discovery of a hitherto unknown type of pulsator in  $\omega$  Cen triggered an intense search for direct counterparts among the field population, which however came back negative (Johnson et al., 2014). On the other hand, a space-based search for rapid hot subdwarf pulsators in the globular cluster NGC 2808 (Brown et al., 2013) revealed six rapid pulsators with periods on timescales similar to the sdOV and sdBV<sub>r</sub> stars discussed here. Given the low quality of the available spectroscopy, it is completely unclear whether any of these pulsators correspond to the  $\omega$  Cen variables, or indeed any of the known field hot subdwarf pulsators. Further investigations and more detailed observations are clearly warranted.

### References

- Ahmad, A. & Jeffery, C. S. 2005, *A&A*, 437, 51
- Brown, T. M. et al. 2013, *ApJ*, 777, L22
- Castellani, V. et al. 2007, *ApJ*, 663, 1021
- Charpinet, S. et al. 1996, *ApJ*, 471, L103
- Charpinet, S., Fontaine, G. & Brassard, P. 1997, *ApJ*, 483, L123
- Fontaine, G. et al. 2012, *A&A*, 539, A12
- Green, E. M. et al. 2003, *ApJ*, 583, 31
- Johnson, C. et al. 2014, *ASP Conf. Ser.*, 481, 153
- Kilkenny, D. et al. 1997, *MNRAS*, 285, 640
- Randall, S. K. et al. 2011, *ApJ*, 737, 27
- Randall, S. K. et al. 2016, *A&A*, 589, 1
- Schuh, S. et al. 2005, *ASPC*, 334, 530
- Woudt, P. A. et al. 2006, *MNRAS*, 371, 149

# First Results from the XXL Survey and Associated Multi-wavelength Programmes

Christophe Adami<sup>1</sup>  
 Marguerite Pierre<sup>2</sup>  
 Nikola Baran<sup>3</sup>  
 Dominique Eckert<sup>4</sup>  
 Sotiria Fotopoulou<sup>4</sup>  
 Paul A. Giles<sup>5</sup>  
 Elias Koulouridis<sup>2</sup>  
 Chris Lidman<sup>6</sup>  
 Maggie Lieu<sup>7</sup>  
 Adam B. Mantz<sup>8</sup>  
 Florian Pacaud<sup>9</sup>  
 Emanuela Pompei<sup>10</sup>  
 Vernesa Smolčić<sup>3</sup>  
 Felicia Ziparo<sup>8</sup>  
 and the XXL Team<sup>11</sup>

<sup>1</sup> Aix Marseille Université, CNRS, LAM UMR 7326, Marseille, France

<sup>2</sup> Laboratoire AIM, CEA/DSM/IRFU/SAP, CEA Saclay, Gif-sur-Yvette, France

<sup>3</sup> Department of Physics, University of Zagreb, Croatia

<sup>4</sup> Department of Astronomy, University of Geneva, Versoix, Switzerland

<sup>5</sup> H. H. Wills Physics Laboratory, University of Bristol, United Kingdom

<sup>6</sup> Australian Astronomical Observatory, North Ryde, Australia

<sup>7</sup> School of Physics & Astronomy, University of Birmingham, United Kingdom

<sup>8</sup> Department of Astronomy and Astrophysics, University of Chicago, USA

<sup>9</sup> Argelander Institut für Astronomie, Universität Bonn, Germany

<sup>10</sup> ESO

<sup>11</sup> XXL Team: <http://irfu.cea.fr/xxl/members>

The XXL survey has mapped two extragalactic regions of 25 square degrees, using 10 ks XMM observations down to a point source sensitivity of  $\sim 5 \times 10^{-15}$  erg s<sup>-1</sup> cm<sup>-2</sup> in the 0.5–2 keV band. It is the largest XMM project approved to date (> 6 Ms in total). The two fields have been or will be observed by several ground- and space-based facilities from ultra-violet to radio wavelengths. Besides the imaging, the spectroscopic follow-up is of special interest and ESO has contributed through Large Programmes and dedicated allocations. As of December 2015,  $\sim 450$  new galaxy clusters are detected to  $z \sim 1.5$ –2, as well as more than 22 000 active galactic nuclei (AGN) to  $z \sim 4$ . The main goal of the project is to constrain the dark energy equation of state using clusters

of galaxies. This survey will have lasting legacy value for cluster scaling laws and studies of AGNs and the X-ray background. The first XXL scientific results are summarised.

## Introduction

The distribution of matter in the Universe reveals its history: small density perturbations present at the time of recombination (just after the Cosmic Microwave Background [CMB] was emitted) grew under the competing actions of gravity and expansion of spacetime. This led to the progressive formation of a remarkable network of filaments, sheets and voids that was first revealed from the galaxy distribution some 30 years ago and is now well rendered by numerical simulations. Basically as time proceeds, overdensities become denser and low density regions emptier as matter flows along the filaments. The rate at which structure forms and how it will ultimately develop is described by general relativity, depending on a set of cosmological parameters and on the nature of dark matter and dark energy (the latter being responsible for the acceleration of the expansion).

Tracking the evolution of cosmic structure in the quest for the cosmological parameters that describe the Universe is especially interesting, in particular to corroborate the cosmological constraints inferred from the CMB ( $z \sim 1000$ ) and from the matter distribution at much later times ( $z \sim 0$ –4), since they originate from very different physical processes. A traditional approach follows the distribution of galaxies in visible or infrared light. However galaxies account only for a few percent of the total matter content and are highly nonlinear objects, which makes establishing the connection with the initial density spectrum non-trivial. At the upper hierarchical level, one finds clusters of galaxies, the most massive objects in the Universe. They are located at the nodes of the cosmic web and are huge reservoirs of hot gas that fill the space between the galaxies. The gas has a temperature of a few tens of millions of degrees and emits in the X-ray.

The cosmological analysis of cluster surveys basically relies on number counts

( $dn/dz$  or  $dn/dM/dz$ ) and on the spatial analysis (3D correlation function). In order to establish these functions, it is necessary to have a good knowledge of: (i) the scaling relations that link the X-ray observables, like temperature and luminosity, to the mass; and (ii) the selection function, i.e., the probability of detecting a cluster of given mass as a function of redshift.

In this context, the XXL project (XXL Paper I) has undertaken a large survey of the X-ray sky with the European Space Agency XMM-Newton observatory. The primary goal of the XXL survey is to detect and confirm a few hundred clusters back to a time when the age of Universe was about half of its present value, i.e.,  $z \sim 1$ . From this data collection, we can infer the evolutionary properties and spatial distribution of the deepest potential wells of the Universe and, subsequently, test various cosmological scenarios. In addition, XXL will deliver several tens of thousands of active galactic nuclei (AGNs) out to a redshift of at least four, allowing statistical studies of the AGN population as a function of environment to be performed.

The XXL Survey is an XMM Very Large Programme that covers two extragalactic areas of 25 square degrees, located around (RA, Dec) of (2h 20m,  $-4.5^\circ$ ) and (23h 30m,  $-55^\circ$ ). Over 500 XMM XXL observations, typically of 10 ks each, were performed between 2011 and 2013. Two years after the completion of the X-ray observations, we have detected  $\sim 450$  clusters and 22 000 AGNs in the 0.5–2.0 keV energy band. The XXL survey samples the low end of the cluster mass function around  $z \sim 0.3$ –0.5. This group population is especially interesting, since it contains the building blocks of the local massive clusters. Moreover, it is sensitive to non-gravitational physics, like the energy input from AGNs, feedback from star formation or cooling processes. Such groups thus present useful environments in which to study the formation of cosmic structures and provide a unique input to test physical processes via numerical simulations. The XXL consortium gathers some 100 scientists including observers, theoreticians and simulators with a wide range of expertise encompassing the entire electromagnetic spectrum.



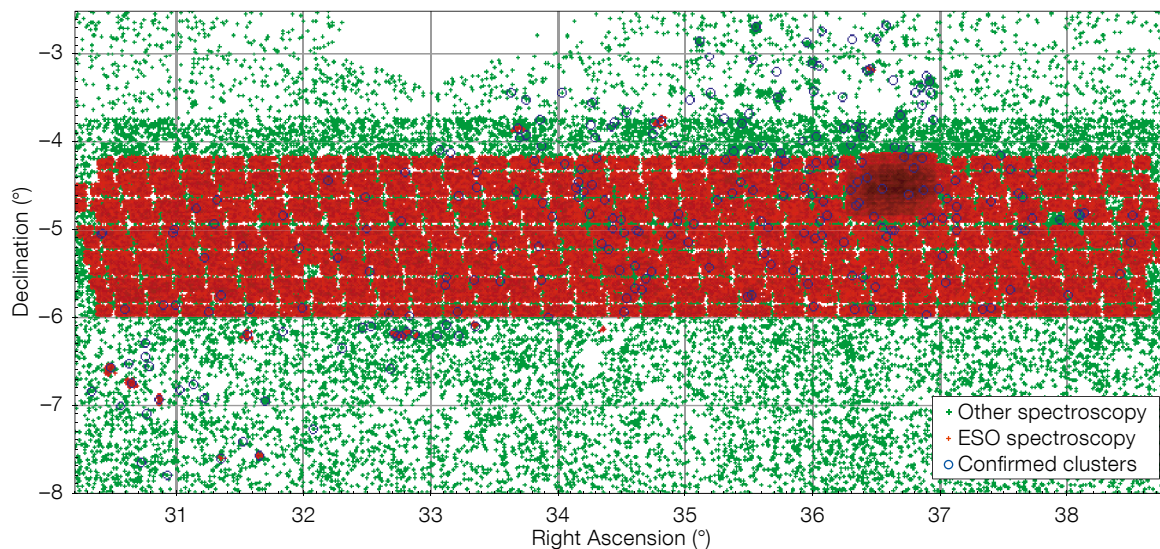


Figure 1. Sky distribution of the available spectroscopy and confirmed X-ray clusters of galaxies in the northern XXL field. The chessboard pattern of red points corresponds to the mosaic of VIMOS fields from the VIPERS survey (Guzzo et al., 2014), while the darker spot at RA = 36.5 degrees shows the deeper data from the VIMOS-VLT Deep Survey (VVDS; Le Fèvre et al., 2005). The isolated concentrations of red points are from the XXL ESO Large Programme (191.A-0268) and represent  $\sim 50\%$  of the redshifts inside all the confirmed clusters at  $z > 0.5$ .

### Associated multi-wavelength programmes and XXL samples

In order to characterise the properties of the detected clusters and AGNs, the XXL survey is accompanied by a comprehensive follow-up programme. Observations are coordinated with the largest ground-based and space observatories, from the X-ray to the radio (see, for example, XXL paper X for the  $K$ -band luminosity–weak-lensing mass relation for galaxy structures). Of these coordinated observations, the ESO Large Programme and principal investigator allocations (ESO 191.A-0268, 089.A-0666, and 60.A-9302), as well as galaxy surveys in the XXL fields, like the VIMOS Public Extragalactic Survey (VIPERS; for example, Guzzo et al., 2014) and the Galaxy And Mass Assembly survey (GAMA; for example, Driver et al., 2016), are of special relevance as they allow galaxy redshifts to be measured, hence accurately locating the galaxy clusters in 3D space (Figures 1 and 2). In the framework of the ESO Large Programme, we observed clusters out to a redshift of  $\sim 0.5$  at the New Technology Telescope (NTT) with the ESO Faint Object Spectrograph and Camera 2 (EFOSC2) and the more distant ones ( $0.5 < z < 1.2$ ) with the FOCal Reducer/low dispersion Spectrograph 2 (FOR2) instrument on the Very Large Telescope (VLT). An example from the latter is the detection of a  $z \sim 1.9$  cluster (see XXL Paper V).

Cluster redshifts constitute a critical input to cosmological analysis, allowing the computation of the cluster–cluster correlation function and further topological studies. Detailed investigations of the dynamics and galaxy properties of individual clusters are also undertaken at the William Herschel Telescope (WHT). The redshift measurement of the AGN is systematically performed with the AAOmega instrument on the Australian Astronomical Telescope (XXL XIV). Radio follow-up of the X-ray AGNs is undertaken with Giant Meterwave Radio Telescope (GMRT), the Jansky Very Large Array (VLA) and the Australia Telescope Compact Array (ATCA). In parallel, four numerical simulation programmes provide the necessary material to test *in situ* the various physical mechanisms that drive cluster and AGN evolution and their respective interactions. Simulations also allow accurate determination of the cluster selection function, which is an essential ingredient for the cosmological analysis.

In a first series of 13 articles published in the December 2015 *Astronomy & Astrophysics* special issue, plus one in *Publications of the Astronomical Society of Australia*, we released the catalogues of the brightest 100 clusters (XXL-100-GC) and 1000 AGNs (XXL-1000-AGN) as well as the reduced XMM observations. We present a number of scientific results for the, to date, little-explored low-mass range characterising the XXL cluster sample.

### Scaling relations

Scaling relations are key elements for parameterising cluster evolution and the XXL project aims at a self-consistent determination. We therefore investigated the luminosity–temperature (LT) relation of the XXL-100-GC sample (XXL III, see also XXL IV for the mass–temperature relation). The first step was to measure the cluster X-ray luminosity and temperature from the XMM survey data. The sample spans a wide range of redshift ( $0.05 < z < 1.05$ ), temperature ( $0.6 < kT < 7.0$  keV), and luminosity ( $9 \times 10^{41} < L < 5 \times 10^{43}$  erg s $^{-1}$ ) and is equivalent to a flux-limited sample ( $3 \times 10^{-14}$  erg s $^{-1}$  cm $^{-2}$ ).

Our methods to determine the LT relation fully take into account the selection effects of the survey. We measure the evolution of the LT relation internally using the broad redshift range of the sample and find a slope of the bolometric LT relation that is steeper than the self-similar expectation. Regarding evolution, our best fit is fully consistent with strong self-similar evolution where clusters scale self-similarly with both mass and redshift: clusters in the past would appear as scaled replicates of the local ones, as a function of mass. However, this result is marginally more significant than the weak self-similar evolution solution, where clusters scale with redshift alone. We further investigated the sensitivity of our results to the assumptions made in our fitting model, finding that the use of an external LT relation as

a low- $z$  baseline can have a profound effect on the measured evolution. The present calculations were performed assuming a given cosmology. The next step, involving the complete XXL sample, will be to implement the cosmological dependency of the luminosity in the determination of the evolution rate of the LT relation.

### Cosmological constraints

We further used the XXL-100-GC sample to infer preliminary cosmological constraints (XXL II). The measured luminosities and temperatures allowed us to model the predicted cluster number counts for the presently favoured set of cosmological parameters. The number density of clusters is found to be less than predicted by the Planck CMB cosmology, once the XXL selection effects are duly accounted for; this tension is similar to that found for the Planck Sunyaev–Zeldovich (S–Z) detected cluster sample, but pertains to a cluster mass range about one order of magnitude lower. However, the alternate Nine Year Wilkinson Microwave Anisotropy Probe (WMAP9) model is not perfect either and still overpredicts the number of faint clusters. Basic attempts to assess the cosmological leverage of the sample revealed that, even with the current subsample, the error budget is already dominated by uncertainties in the cluster mass calibration, which therefore will be one of the priorities of the XXL cluster science programme over the next few years. In particular, we are starting a collaboration with the Subaru Hyper-SuprimeCam team in order to obtain reliable lensing masses for most of the XXL clusters.

### Cluster baryon content

Beside counts and topology, another potential cosmological probe is the baryon fraction ( $f_{gas}$ ) in clusters (XXL XIII). This test assumes that  $f_{gas}$  is constant as a function of redshift for the high-mass clusters, because they are supposed to have retained all the material accreted since their formation epoch. Gas mass and total mass measurements do not scale in the same way as a function of cosmology; therefore, requiring that their ratio is constant ought to put con-

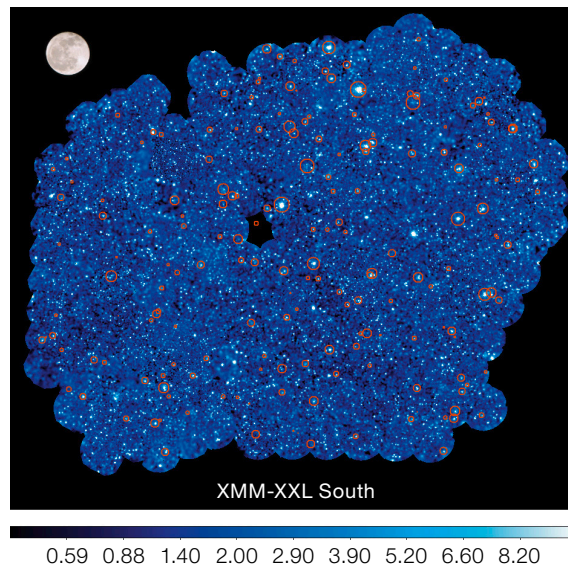
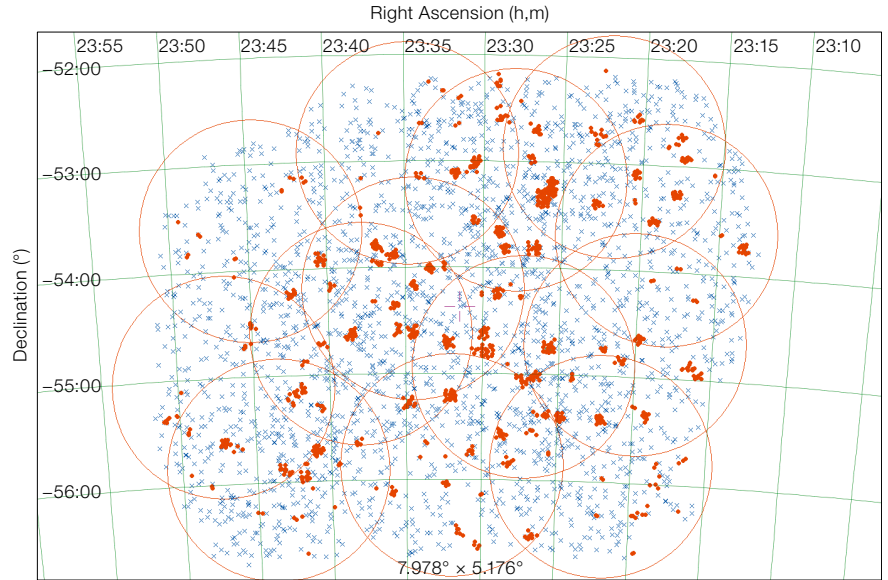


Figure 2. Upper: Spectroscopically confirmed AGNs (blue) and cluster galaxies (red) in the southern XXL field from the AAOmega follow-up (XXL Paper XIV). Left: Corresponding X-ray mosaic (units of colour bar are counts  $s^{-1} \text{ degree}^{-1}$ ). The 25-square-degree field is covered by some 220 XMM pointings. The XMM field of view has a size comparable to that of the Moon (30 arcminutes diameter, shown at the upper left). More than 12 000 AGNs have been detected in this image. The red circles show the clusters of galaxies.

straints on the cosmological parameters. We measured the number of baryons (X-ray gas and stars) in the XXL-100-GC sample. Halo masses were estimated from a mass–temperature relation that was directly calibrated using weak-lensing measurements (from the Canada France Hawaii Telescope Legacy Survey, CFHTLS) for a subset of XXL clusters. We find that the weak-lensing calibrated gas fraction of XXL-100-GC clusters is lower than was found in previous clusters using hydrostatic masses.

We compared our  $f_{gas}-M$  relation with the predictions of cosmological simulations using different gas physics. It was found

that our results favour extreme AGN feedback schemes in which a large fraction of the baryons are expelled from the potential well of dark matter halos. Such models are, however, in tension with X-ray-only proxies, such as the gas density and entropy profiles (Le Brun et al., 2014) and are not able to reproduce the relation between gas mass and temperature of XXL clusters.

Therefore, the results presented are challenging for current numerical simulations, and reconciling the observed gas fraction with the predictions would require that our weak-lensing masses be systematically overestimated. A mass



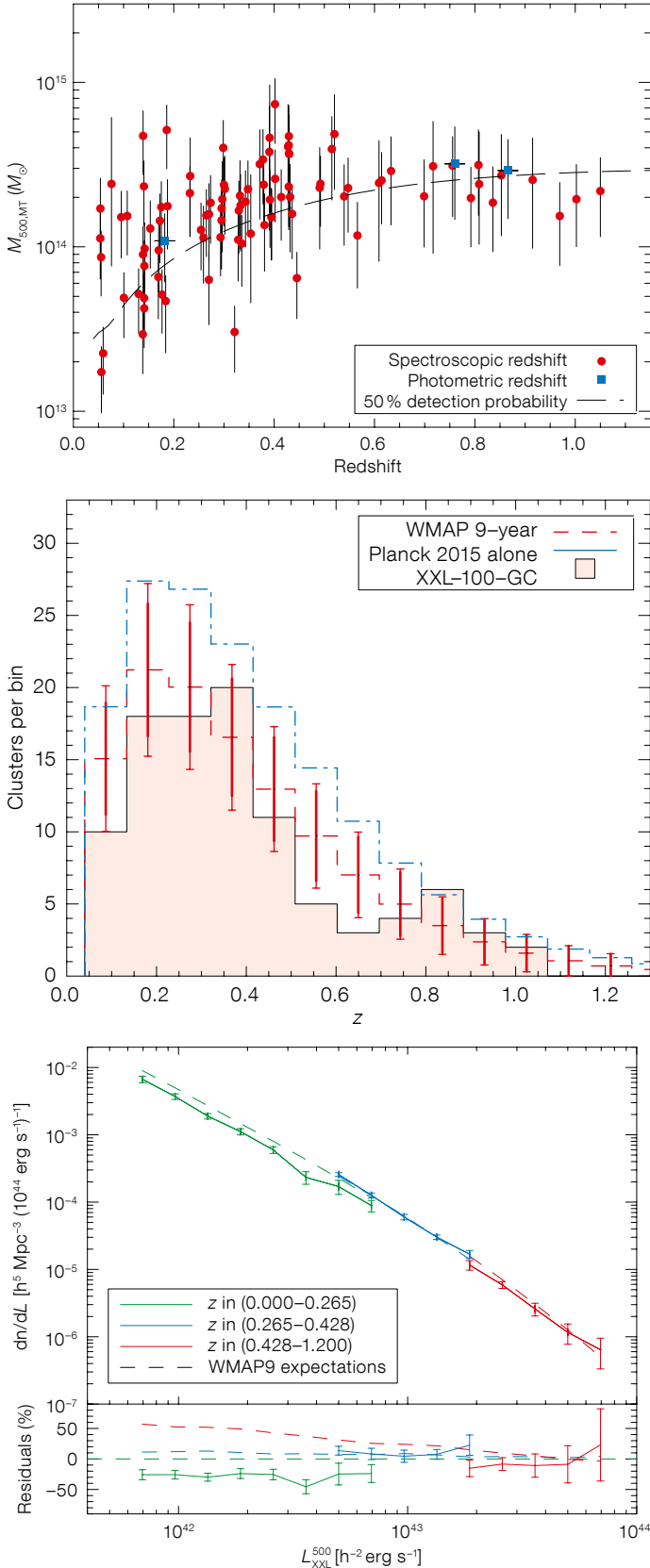


**Figure 3.** Upper: Distribution of the bright XXL cluster sample in the  $M_{500}$  vs. redshift plane. The dashed line shows the 50% completeness limit in the WMAP9 cosmology. Middle: Redshift distribution of the XXL-100-GC sample (filled histogram) compared with different model expectations (CMB measurements from WMAP + H0 + BAO presented in Hinshaw et al. [2013], and latest CMB measurements from the Planck satellite, but without additional constraints from Planck Collaboration 2015). Lower: Differential luminosity function of the bright XXL cluster sample in three redshift bins. The lower plot shows the residuals with respect to the low-redshift WMAP9 prediction (XXL Paper II).

bias  $1 - b = 0.58 \pm 0.04$ , which is required to reconcile Planck cluster counts with the primary CMB, would further exacerbate the tension between the baryon fraction and the cosmological value, challenging our understanding of cluster physics. Therefore, a satisfactory solution to the tension between CMB and cluster counts must also simultaneously explain the low baryon fraction measured for the XXL halos.

### Discovery of five superclusters

Given its depth and sky coverage, XXL is particularly suited to systematically unveiling the clustering of X-ray clusters and to identifying superstructures in a homogeneous X-ray sample down to the typical mass scale of a local massive cluster. Although a few isolated, very high redshift superclusters are known, our work is the first attempt to systematically unveil superstructures up to  $z \sim 0.5$  in a homogeneous X-ray sample. In this framework, we discovered five low-mass superclusters consisting of three to seven galaxy structures.

One of them is particularly interesting and is presented in more detail (XXL VII and Figure 4). It is composed of six clusters of galaxies and the structure is very compact with all the clusters residing in one XMM pointing. Our subsequent spectroscopic follow-up with WHT and NTT provided a median redshift of  $z \sim 0.43$ . An estimate of the X-ray mass and luminosity of this supercluster returns values of  $1.7 \times 10^{15} M_A$  and of  $1.68 \times 10^{44} \text{ erg s}^{-1}$ , respectively, and a total gas mass of  $M_{gas} = 9.3 \times 10^{13} M_A$ . Instead of having a massive central cluster with infalling filaments and smaller structures, it has almost two equal-sized objects, making it qualitatively different from the network around an already formed massive cluster. This supercluster is currently the most massive and most distant found in XXL. If we put together the relatively small crossing time, the common X-ray emission of three members, and the measured gas fraction and mass, we can speculate that we are observing an unrelaxed structure with an ongoing merging between at least three of the member clusters. If nothing else intervened to alter the system, and assuming that the estimated

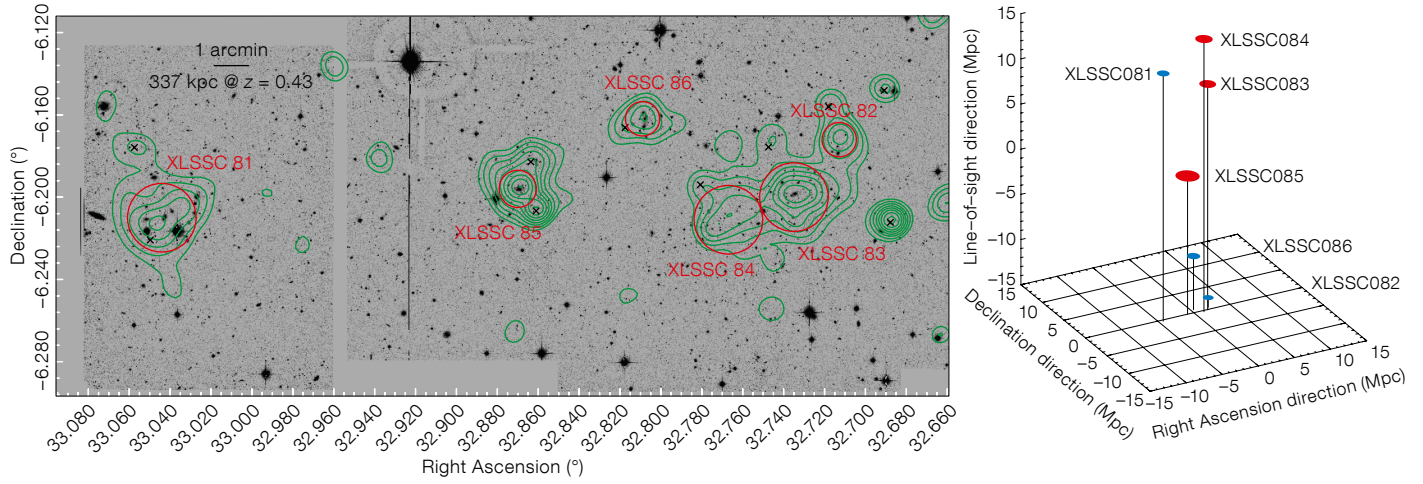
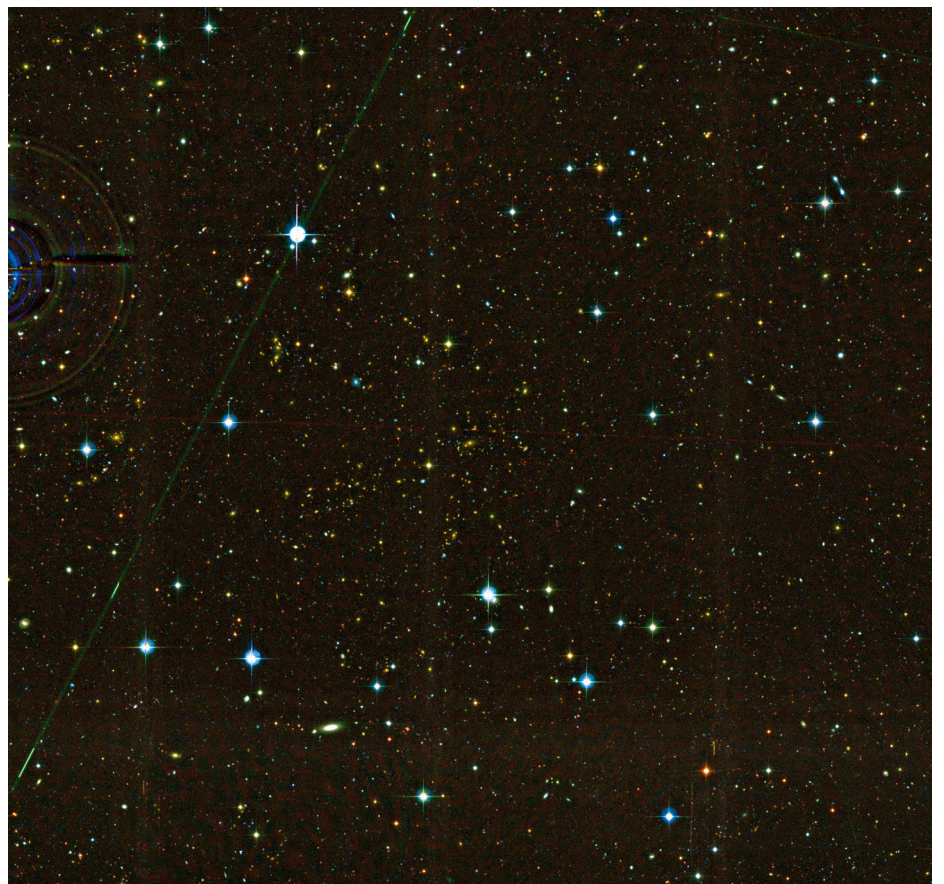


**Figure 4.** Top left: CFHTLS MegaCam mosaic image in the *i*-band with the XXL contours superimposed in green; X-ray clusters are red circles. The positions of the BCG in each cluster are shown and the black crosses highlight the point sources excluded from the X-ray analysis. Top right: Three-dimensional configuration of the  $z = 0.43$  supercluster (XXL Paper VII). Right: CFHTLS-wide colour  $u^r:r:z$ : image (8 by 8 arcminutes) of XLSS-C 82-83-84 inner complex.

crossing time is a good estimate of the merging time, it is likely that by the present time the supercluster would already have completely merged  $\sim 2$  Gyr before and resemble the most massive known clusters.

### First spectral characterisation of diffuse light in a cluster

Within a cluster, gravitational effects can lead to the removal of stars from their parent galaxies and subsequent dispersal into the intracluster medium (ICL). Gas hydrodynamical effects can additionally strip gas and dust from galaxies. The properties of the ICL can therefore help constrain the physical processes at work in clusters by serving as a fossil record of the interaction history. We detected in the XXL survey a very peculiar intermediate-mass cluster: XLSSC-116, with a very high level of such diffuse light, by applying a wavelet-based method to CFHT Megacam and Wide-field InfraRed Camera (WIRCAM) images (XXL VIII). The amount of diffuse light is equivalent to two brightest cluster galaxies (BCGs) in the *i*-band. To the best of our knowledge, this is the first detected cluster with such a large amount of diffuse light.



The source of the diffuse light was then spectroscopically characterised with ESO Multi-Unit Spectroscopic Explorer (MUSE) spectroscopic data (proposal 60.A-9302). MUSE data were also used to compute redshifts of 24 cluster galaxies and search for cluster substructures. The cluster consists of a main component with a velocity dispersion of the

order of  $600 \text{ km s}^{-1}$  and an infalling low-mass group with a velocity dispersion of  $170 \text{ km s}^{-1}$ . Part of the detected diffuse light has a very weak optical stellar component and apparently consists mainly of gas emission, while other diffuse light sources are clearly dominated by old stars. Furthermore, emission lines were detected in several places coinciding with



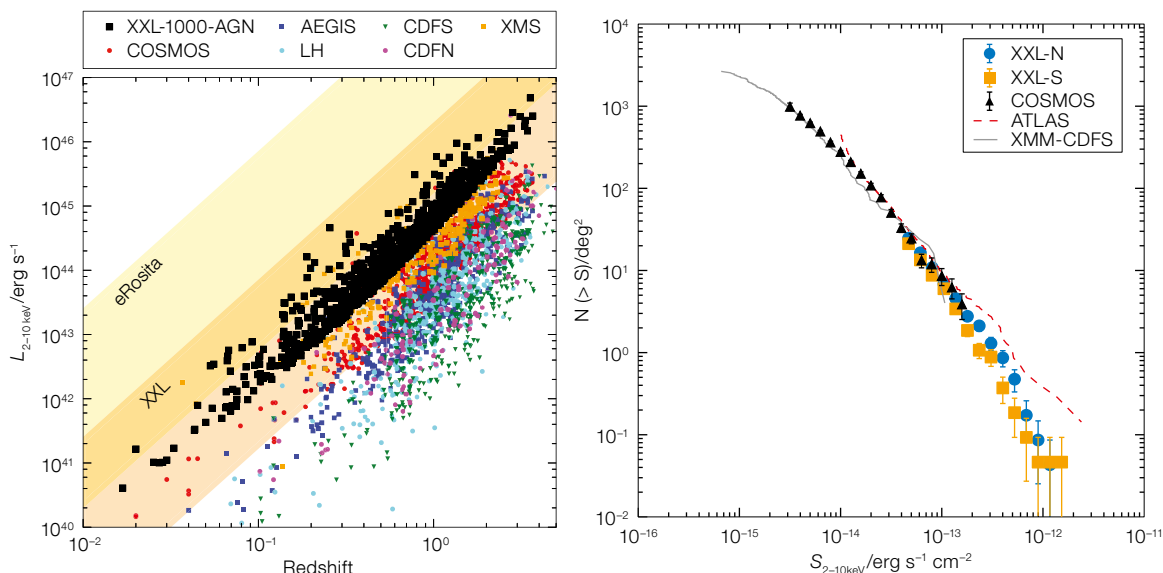


Figure 5. Left: Luminosity–redshift plane for different X-ray fields in the 2–10 keV energy band. Right:  $\log N$ – $\log S$  for the XXL-1000-AGN in the XXL-N field (blue circles) and in the XXL-S field (orange squares) as compared to other literature surveys (XXL Paper VI).

the diffuse light. Our spectral analysis shows that this emission likely originates from gas with a low-excitation parameter.

Globally, the stellar contribution to the ICL is about  $2.3 \times 10^9$  years old even though the ICL is not currently forming a large number of stars. On the other hand, the contribution of the gas emission to the ICL in the optical is much greater than the stellar contribution in some regions, but the gas density is likely too low to form stars. These observations favour ram-pressure stripping, turbulent viscous stripping, or supernovae winds as the origin of the large amount of intracluster light. Since the cluster appears not to be in a major merging phase, we conclude that ram-pressure stripping is the most plausible process that generates the observed ICL sources.

### AGNs in the XXL survey

X-ray extragalactic surveys are also ideal laboratories for the study of the evolution and clustering of AGN. Optimally, a combination of deep and wide surveys is necessary to create a complete picture of the population. Deep X-ray surveys provide the faint population at high redshift, while wide surveys provide the rare bright sources and the large-scale structure information. Nevertheless, very wide area surveys often lack the ancillary information available for modern deep surveys.

The XXL survey occupies the parameter space that lies between deep surveys and very wide area surveys, constituting a stepping stone between current deep fields and planned wide area surveys (Figure 5).

XXL-1000-AGN is our first point source catalogue. The sample is selected in the 2–10 keV energy band with the goal of providing an initial sizable sample useful for AGN studies (XXL Papers VI, XI, XII). The limiting flux is  $F_{2-10\text{keV}} = 4.8 \cdot 10^{-14} \text{ erg s}^{-1} \text{ cm}^{-2}$ . We use both public and proprietary datasets in the optical and near-infrared to identify the counterparts of the X-ray point-like sources by means of a likelihood ratio test, reaching 97.2% identification rate. Using multi-wavelength data from the far ultra-violet to the mid infrared, we derive the median spectral energy distribution of AGN as a function of X-ray absorption. We improve upon the photometric redshift determination for AGN by applying a Random Forest classification trained to identify, for each object, the optimal photometric redshift category (passive, star-forming, starburst, AGN, quasar). In addition, we assign a probability to each source that indicates whether it might be a star or an outlier. The photometric redshift accuracy is 0.095 for the full XMM-XXL with 28% catastrophic outliers estimated on a sample of 339 sources. We apply Bayesian analysis to model the X-ray spectra assuming a power-law model with the

presence of an absorbing medium, finding no trend of photon index or hydrogen column density with redshift and a fraction of 26% absorbed sources, consistent with the literature on bright sources.

The XXL-1000-AGN sample number counts extend the COSMOS  $\log N$ – $\log S$  to higher fluxes (Figure 5); they are fully consistent with the Euclidean expectation and agree with previous deep (Chandra Deep Field South [CDFS] and COSMOS) and wide (Herschel-ATLAS) XMM-Newton surveys. We constrain the intrinsic luminosity function of AGN in the 2–10 keV energy band where the unabsorbed X-ray flux is estimated from the X-ray spectral fit up to  $z = 3$ . An application of the friends-of-friends algorithm, at  $10 h^{-1}$  Mpc and  $20 h^{-1}$  Mpc percolation radii, shows significant structures with 2–3 members and identifies a supercluster-sized structure at redshift 0.14.

In future publications we will expand the analysis to the full XXL catalogue, containing an unprecedented number of  $\sim 10^4$  (X-ray) point-like 2–10 keV detected sources, and analysing the fully combined XMM pointings to reach maximum depth. A unique advantage of the XXL large statistical samples is the combined study of X-ray point-like sources and X-ray detected galaxy clusters, which will allow the study of AGN with respect to their environment and, *vice versa*, the study of the impact of AGN on clusters.

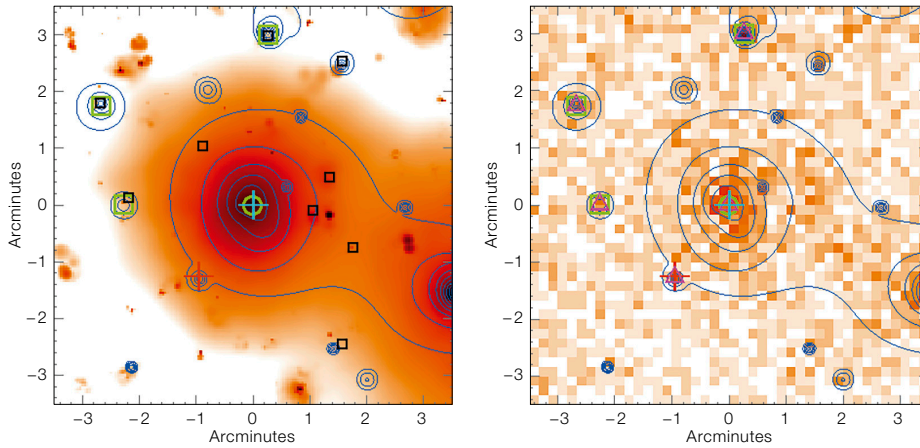


**Figure 6.** Left: Simulated X-ray emissivity map extracted from a 25 square degree by  $z = 0-3$  light cone (Overwhelmingly Large Simulations [OWLS], Le Brun et al., 2014). Right: Same portion of the virtual sky transformed into an XMM image by the XXL simulator. All XMM characteristics are taken into account: point spread function (and its variation with energy), quantum efficiency, various background components and vignetting.

### References

Clerc, N. et al. 2012, MNRAS, 423, 3561  
 Clerc, N. et al. 2012, MNRAS, 423, 3545  
 Driver, S. P. et al. 2016, MNRAS, 455, 3911  
 Hinshaw, G. et al. 2013, ApJS, 208, 19  
 Le Brun, V. et al. 2014, MNRAS, 441, 1270  
 Le Fèvre, O. et al. 2005, A&A, 439, 845  
 Guzzo, L. et al. 2014, A&A, 566, 108  
 Hinshaw, G. et al. 2013, ApJS, 208, 19  
 XXL Survey: I. Pierre, M. et al. 2016, A&A, 592, A1  
 XXL Survey: II. Pacaud, F. et al. 2016, A&A, 592, A2  
 XXL Survey: III. Giles, P. A. et al. 2016, A&A, 592, A3  
 XXL Survey: IV. Lieu, M. et al. 2016, A&A, 592, A4  
 XXL Survey: V. Mantz, A. B. et al. 2016, ApJ, 794, 157  
 XXL Survey: VI. Fotopoulou, S. et al. 2016, A&A, 592, A5  
 XXL Survey: VII. Pompei, E. et al. 2016, A&A, 592, A6  
 XXL Survey: VIII. Adami, C. et al. 2016, A&A, 592, A7  
 XXL Survey: IX. Baran, N. et al. 2016, A&A, 592, A8  
 XXL Survey: X. Ziparo, F. et al. 2016, A&A, 592, A9  
 XXL Survey: XI. Smolčić, V. et al. 2016, A&A, 592, A10  
 XXL Survey: XII. Koulouridis, E. et al. 2016, A&A, 592, A11  
 XXL Survey: XIII. Eckert, D. et al. 2016, A&A, 592, A12  
 XXL Survey XIV. Lidman, C. et al. 2016, PASA, 33, 1

### Prospects

The second phase of the XXL project is expected to end in 2018, with the publication of the complete cluster catalogue, including all data available from the multi-wavelength follow-up along with the selection functions. These will incorporate a thorough analysis of the impact of cluster shapes and AGN activity on the detection rates, which we will measure by means of  $N$ -body simulations performed under various physical hypotheses (Figure 6).

The final cosmological analysis of the full XXL cluster sample will involve a completely self-consistent treatment of the cluster evolution, selection function and cosmology. With some five times as many clusters (already some 450 clusters

have been identified), we expect to provide a useful and stand-alone set of cosmological constraints. In addition to the traditional study of the  $dn/dz$  and  $dn/dM/dz$  counts, we have developed a method based on the modelling of the X-ray observable parameter space, that globally by-passes the intermediate phase of the (cosmologically dependent) cluster mass determination (Clerc et al., 2012; Pierre et al., 2016). We will also release the XXL multi-wavelength AGN catalogue, that is some 22 000 objects. The dataset, including spectroscopic follow-up, has a unique legacy value for cosmological and extragalactic environmental studies and will constitute a calibration resource for future surveys, like eRosita (all-sky, but at significantly lower sensitivity and resolution) and Euclid.



Night-time observations with the New Technology Telescope at the La Silla Observatory.

Following two pages: VLT Survey Telescope (VST) composite  $u$ -,  $g$ - and  $i$ -band, large-field image (120 by 84 arcminutes) of the core of the nearby Fornax Galaxy Cluster. At a distance of about 19 Mpc, the Fornax cluster is a rich cluster (class 0) with more than 340 known members. The central brightest cluster galaxy, NGC 1399 can be seen to the north east, with the prominent barred spiral NGC 1365 to south west. See Release eso1612 for more details.











# The LEGA-C Survey: The Physics of Galaxies 7 Gyr Ago

Arjen van der Wel<sup>1</sup>  
 Kai Noeske<sup>1</sup>  
 Rachel Bezanson<sup>2</sup>  
 Camilla Pacifici<sup>3</sup>  
 Anna Gallazzi<sup>4</sup>  
 Marijn Franx<sup>5</sup>  
 Juan-Carlos Muñoz-Mateos<sup>6</sup>  
 Eric F. Bell<sup>7</sup>  
 Gabriel Brammer<sup>8</sup>  
 Stephane Charlot<sup>9</sup>  
 Priscilla Chauké<sup>1</sup>  
 Ivo Labbé<sup>5</sup>  
 Michael V. Maseda<sup>5</sup>  
 Adam Muzzin<sup>10</sup>  
 Hans-Walter Rix<sup>1</sup>  
 David Sobral<sup>11,5</sup>  
 Jesse van de Sande<sup>12</sup>  
 Pieter G. van Dokkum<sup>13</sup>  
 Vivienne Wild<sup>14</sup>  
 Chris Wolf<sup>15</sup>

<sup>1</sup> Max-Planck-Institut für Astronomie, Heidelberg, Germany

<sup>2</sup> Steward Observatory, University of Arizona, Tucson, USA

<sup>3</sup> Goddard Space Flight Center, Greenbelt, USA

<sup>4</sup> INAF–Osservatorio Astrofisico di Arcetri, Firenze, Italy

<sup>5</sup> Leiden Observatory, Leiden University, the Netherlands

<sup>6</sup> ESO

<sup>7</sup> Department of Astronomy, University of Michigan, Ann Arbor, USA

<sup>8</sup> Space Telescope Science Institute, Baltimore, USA

<sup>9</sup> Institut d'Astrophysique de Paris, France

<sup>10</sup> Institute of Astronomy, University of Cambridge, UK

<sup>11</sup> Department of Physics, Lancaster University, UK

<sup>12</sup> Sydney Institute for Astronomy, University of Sydney, Australia

<sup>13</sup> Department of Astronomy, Yale University, New Haven, USA

<sup>14</sup> School of Physics and Astronomy, University of St. Andrews, UK

<sup>15</sup> Research School of Astronomy and Astrophysics, Australian National University, Canberra, Australia

The LEGA-C (Large Early Galaxy Census) survey is made possible by the refurbishment of the Very Large Telescope Visible and Multi Object Spectrograph (VIMOS) instrument and the

implementation by ESO of a new generation of large spectroscopic surveys. The goal is to obtain high-quality continuum spectra of thousands of galaxies with redshifts up to  $z = 1$ , with which key physical parameters that were previously inaccessible can be measured. These include star formation histories and dynamical masses, which greatly improve our insight into how galaxies form and evolve. This article coincides with the first public data release of fully reduced and calibrated spectra.

Our knowledge of stellar populations tells us about the formation and evolution of galaxies. High-quality (continuum) spectroscopy of galaxies reveals the stellar absorption features that trace star formation histories and chemical content. Such data have been available for galaxies in the present-day Universe for some decades and have brought into clear focus the multi-variate correlations between stellar population properties and mass, structure, size, stellar velocity dispersion, nuclear activity and environment. This information has greatly illuminated the processes that drive star formation and the ongoing assembly of present-day galaxies.

The main limitation when examining present-day galaxies for the purpose of reconstructing their formation history is, however, that most of the star formation occurred in the distant past: the mean stellar ages of typical galaxies are typically well over 5 Gyr (Gallazzi et al., 2005) and it is difficult to resolve star formation histories from spectra: it is nearly impossible to distinguish stellar populations with ages of, for example, 5, 7 and 9 Gyr from integrated spectra. For this reason the community has put much effort into lookback studies, aimed at directly observing galaxies at earlier cosmic times.

On the one hand, redshift surveys, such as the VIMOS Very Deep Survey (VVDS; Le Fèvre et al., 2005) and the COSMOS spectroscopic survey (zCOSMOS; Lilly et al., 2008) have created large samples of galaxies with spectroscopic redshifts, tracing the evolution of the number density and the luminosity function of galaxies. On the other hand, photometric sur-

veys (for example, UltraVISTA; McCracken et al., 2013) have collected multi-wavelength datasets used to derive photometric redshifts, which have gradually improved to the point that spectroscopic redshift surveys are no longer needed for the purpose of quantifying galaxy evolution (with the exception of the effect of environment). In addition, the photometric surveys provide estimates of integrated galaxy properties such as stellar mass, star formation rate and restframe colours. Adding Hubble Space Telescope (HST) imaging to the mix enables us to reveal the internal structure of distant galaxies (for example, van der Wel et al., 2014a).

The results of these very significant efforts is that we now understand that the galaxy population at large lookback times is in many ways similar to the present-day galaxy population: mass, structure and star formation activity are correlated in the same manner (for example, Franx et al., 2008). At the same time, there are many differences: at higher redshift, star formation rates were much higher (Madau et al., 1996), morphologies less regular (for example, Conselice et al., 2008), and galaxies of the same stellar mass are smaller in size (for example, van der Wel et al., 2014b).

The main limitation of the lookback studies is the challenge of connecting progenitors and descendants: despite our exquisite knowledge of the evolution of the population of galaxies as an ensemble, the evolutionary history of individual galaxies has remained hidden from view. In our Universe, with hierarchical structure growth that is largely stochastic in nature, we should expect that galaxies that are similar today were probably very different in the past, and, analogously, galaxies that were similar in the past will be very different today.

To summarise, our current insight into galaxy evolution is limited by two factors: 1) the archaeological approach of obtaining spectroscopy of present-day galaxies lacks the power to reveal the bulk of star formation history, because galaxies are too old; 2) the lookback approach only reveals the evolution of the population, not of individual galaxies. The solution is both obvious and very challenging: to obtain high-quality spectroscopy of galaxies at

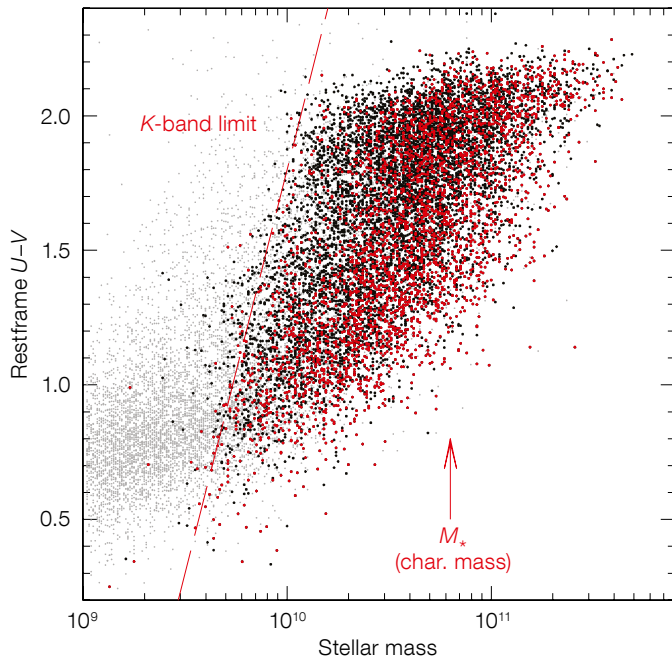


Figure 1. Rest-frame UV colour vs. stellar mass of the K-band selected primary galaxy sample of the LEGA-C survey at redshift  $0.6 < z < 1.0$ . Light grey points refer to the full UltraVISTA sample; black points: primary galaxy candidates; and red points: primary galaxies included in the LEGA-C survey.

large lookback times. This is the aim of the LEGA-C survey (van der Wel et al., 2016).

### The LEGA-C survey

The challenge lies in obtaining continuum spectra of sufficient resolution and depth for faint targets. The design of the LEGA-C survey is constrained by several practical factors:

- 1) the resolution should be at least  $R \sim 2000$  to distinguish individual features and constrain the kinematic properties of the targets;
- 2) the signal-to-noise ratio (S/N) should be at least 10 per resolution element, and preferably  $\sim 20$ ;
- 3) the maximum redshift is  $z \sim 1$ , otherwise targets become too faint and the diagnostic features shift into the near-infrared, where ground-based near-infrared spectrographs are still a factor  $\sim 100$  slower in survey speed for the purpose of continuum spectroscopy;
- 4) the sample size should be in the 1000s, otherwise the population is either undersampled or biased toward

particular types of galaxies, either of which would preclude the general goals of constraining the evolutionary history of galaxies in general.

Given these constraints, we started the LEGA-C survey in December 2014 with VIMOS in multi-object (MOS) mode. The survey is led and coordinated from the Max Planck Institute for Astronomy in Heidelberg, Germany, and has co-investigators across Europe and indeed the globe.

Upon completion, likely in 2018, we will have collected more than 3000 spectra of galaxies in the redshift range  $0.6 < z < 1.0$  in the COSMOS field, at Right Ascension 10 hr and Declination  $+2^\circ$ . The sample is selected based on K-band magnitude — in order to approximate a selection by stellar mass and avoid biases due to extinction — from the publicly available UltraVISTA catalogue by Muzzin et al. (2013). The selection is independent of any other parameter and the sample, shown in Figure 1, therefore spans the full range of galaxy properties in terms of morphology, star formation activity and dust attenuation across the galaxy population with stellar mass in excess of about  $10^{10} M_\odot$ . This primary sample is complemented by  $\sim 900$  fillers — lower-mass galaxies and higher-redshift galaxies. With the high-resolution red grating

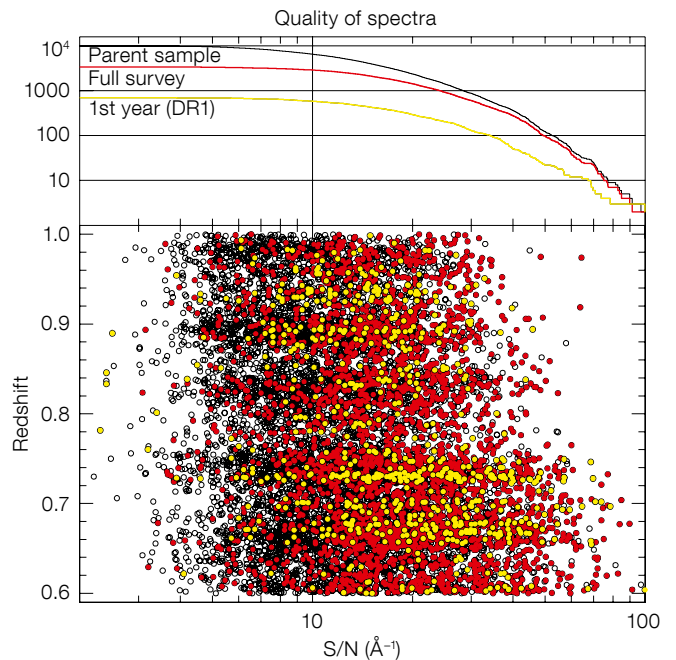


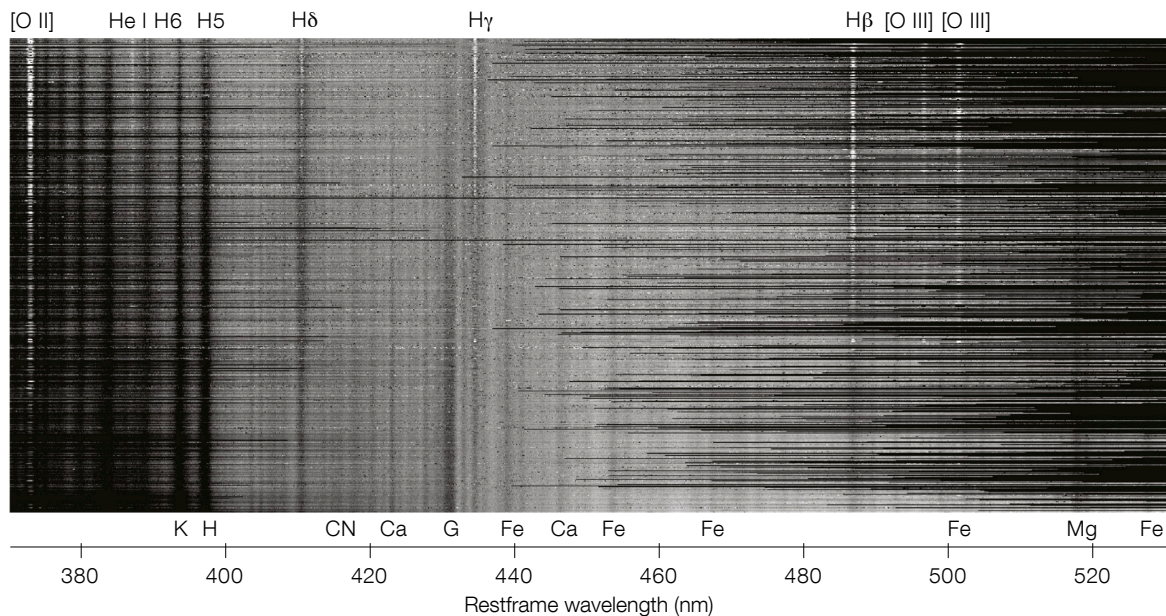
Figure 2. Redshift and signal-to-noise (S/N) distribution of the LEGA-C primary sample. The parent sample from which targets are selected is shown in black; the survey design includes objects shown in red; while the observed sample is shown in yellow/black.

(HR\_red) and integration times of 20 hours per target, the required resolution and S/N can be achieved. The typical wavelength range of 6300–8800 Å samples essential features such as the Balmer/4000 Å break, all Balmer lines except  $H\alpha$ , the G-band, and multiple Fe, Ca and Mg features.

VIMOS slits are assigned to the primary targets first, prioritised by apparent K-band magnitude as far as slit collisions permit. Then one or more blue stars for telluric absorption correction and several alignment stars are included in the slit mask design. The remaining slit real estate is used for fillers: higher-redshift objects with bright K-band magnitudes, fainter targets in the  $0.6 < z < 1.0$  redshift range, and other fainter sources, respectively. With slit lengths of  $\sim 10$  arcseconds, VIMOS can simultaneously observe  $\sim 130$  objects, bringing the on-sky survey execution time to 640 hours. In Visitor Mode 128 nights were allocated to achieve this goal, spread out over 200 actual nights (due to fractional-night scheduling). This allocation makes LEGA-C the



**Figure 3.** 1D extracted restframe spectra of 654 primary-sample galaxies observed in the first year of LEGA-C. Each row shows one spectrum, where the galaxies are sorted from high star formation activity (at the top) to low star formation activity (at the bottom).



most expensive extragalactic spectroscopic survey to date on an 8-metre-class telescope. The redshift and expected S/N distribution of the resulting primary galaxy sample is illustrated in Figure 2.

### The spectra

The data are reduced using a combination of the ESO pipeline and our own pipeline based on customised algorithms for sky subtraction, object extraction and co-addition. In Figure 3 we show extracted 1D spectra of 654 primary targets observed in the first year of observations. The galaxies are sorted by their specific star formation rate (star formation rate per unit stellar mass), with the most actively star-forming galaxies at the top. The high star formation rate galaxies show nebular emission lines, Balmer lines in absorption and emission, but also metal lines. The more passive systems show stronger metal features and across this sample up to 50 unique absorption features are readily visible, illustrating the superb depth of the spectra. Kinematic information is revealed thanks to the high spectral resolution: Ca and Fe features appear more Doppler broadened for the spectra near the bottom, as those galaxies are more massive.

Figures 4 and 5 show typical examples of 1D spectra in more detail. In Figure 4 we show ten galaxies ordered by their basic morphology as traced by the Sérsic index: galaxies with high Sérsic indices, that is, more concentrated light profiles usually associated with early-type morphologies, are at the top; galaxies with low Sérsic indices, that is, disc-like morphologies, are at the bottom. The correspondence with morphology is clearly seen in the HST image cut-outs from the COSMOS survey (Scoville et al., 2007). LEGA-C reveals that for the first time, beyond the present-day Universe, a clear correlation exists between morphology and spectral properties: early-type galaxy spectra are characterised by strong metal absorption line features and a lack of strong Balmer absorption and nebular emission lines; while for late-type galaxies this is reversed.

In Figure 5 we show five late-type galaxies ordered by inclination. Absorption lines are detected regardless of viewing angle. The example spectra illustrate a unique aspect of the LEGA-C survey: even the dustiest and the bluest galaxies show absorption line features with high fidelity, despite the challenges presented by the low surface brightness and bright, blue stellar populations with strong continuum features.

### Towards understanding the physics of galaxy formation

The high-quality spectra shown in Figures 3–5 allow us to measure with good accuracy and precision a large range of physical parameters that were previously inaccessible for galaxies at large lookback times. These parameters fall into two broad categories: stellar populations and kinematics. The basic stellar population measurements are mean stellar age and metallicity, and eventually a more general description of the star formation history. Now that LEGA-C has overcome the challenge of creating spectra of galaxies at significant lookback times, we actually have a clear advantage over present-day galaxy studies when it comes to reconstructing the full star formation history. At the redshifts studied, stars will typically be younger than 3 Gyr in essentially all LEGA-C galaxies, which is an age range over which different generations of stars can be resolved in age. This will inform us directly what the stellar masses of progenitors at  $z > 1$  must be. Our knowledge of those potential progenitors is very substantial indeed, such that we can, for the first time, follow the evolution of individual galaxies across a significant part of cosmic time, right into the epoch when star formation activity was highest in a cosmically average sense.

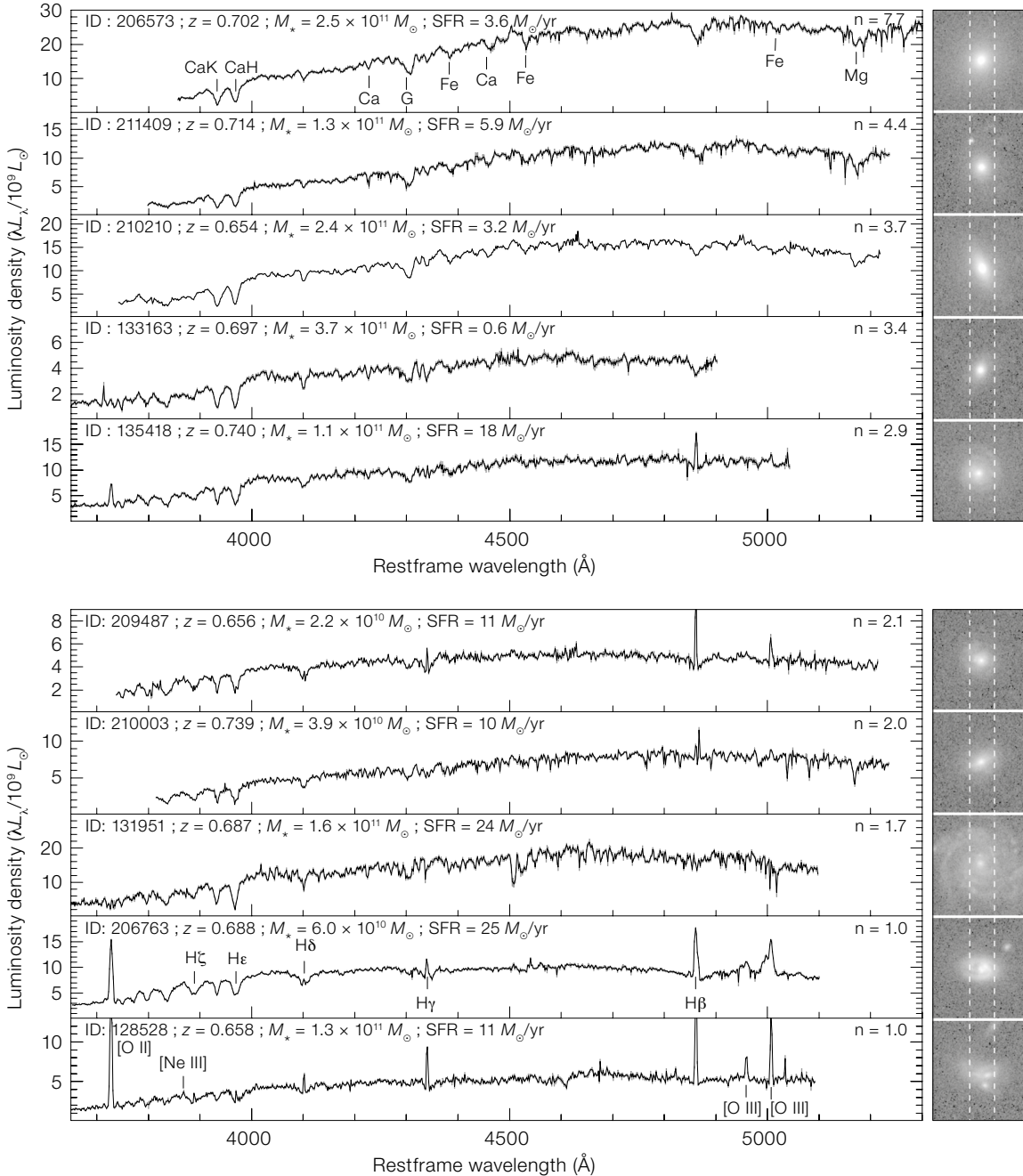


Figure 4. Spectra of ten typical LEGA-C targets ordered by morphology (using the Sérsic index). Flux density uncertainties are indicated in grey. HST image cut-outs are shown on the right. Labels (left) record object ID, redshift, stellar mass and star formation rate; with Sérsic index at right.

The primary kinematic measurement is the stellar velocity dispersion. Collisionless star particles are excellent tracers of the gravitational potential and thus the total mass, which opens new avenues of exploration. A practical application is to test whether the much-maligned stellar mass estimates are robust at large look-back times for all galaxy types. At these times velocity dispersions and central mass density are thought to be key fac-

tors in determining the star formation activity of a galaxy. Now that we have direct measurements for distant galaxies that support this notion (see Figure 6) we can ask the question of how some galaxies cease to form stars and evolve sedately afterward. Furthermore, the evolution of velocity dispersions in combination with other properties (for example, size) informs us about the rate of growth of passive galaxies through merg-

ing. A secondary kinematic measurement is the gas velocity dispersion. Gas motions are affected by numerous other forces besides gravity and, while gas kinematics is widely used as a tracer of mass, it remains to be tested how large are the uncertainties. A comparison between gas and stellar velocity dispersion now allows us to make this test.



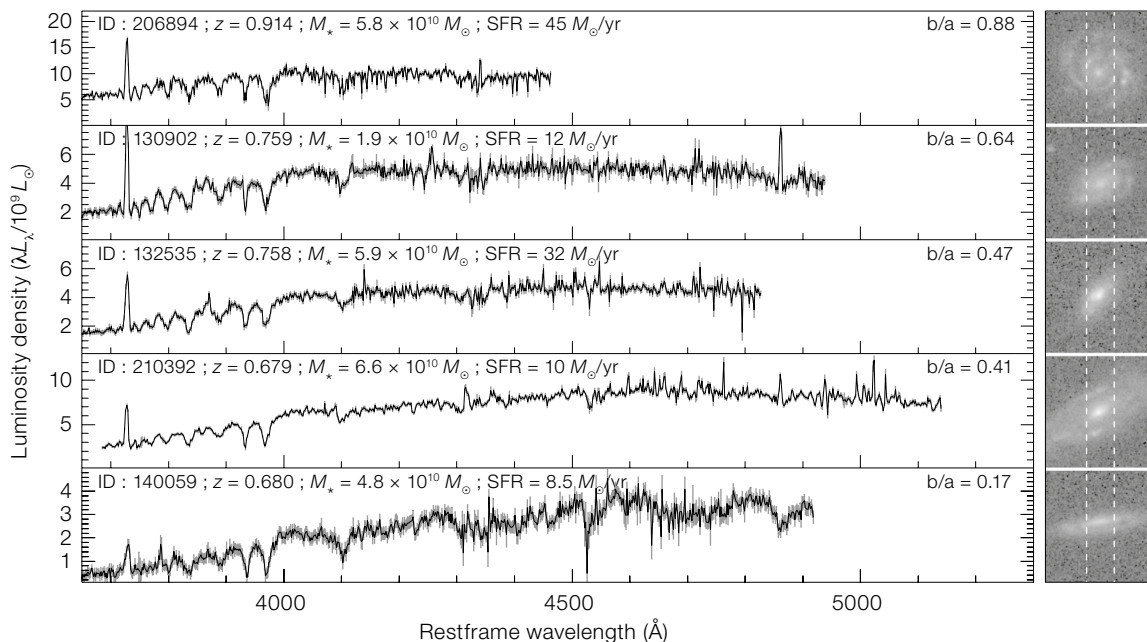


Figure 5. Spectra of five LEGA-C disc galaxies ordered by inclination (axis ratio  $b/a$ ). Details as Figure 4.

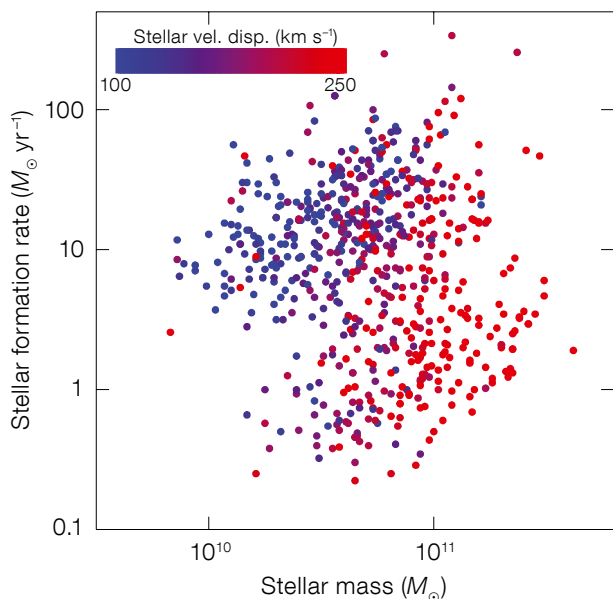


Figure 6. Star formation rate vs. stellar mass for the primary LEGA-C sample observed in the first year. The colour coding represents the stellar velocity dispersion.

Finally, despite the fact that the LEGA-C spectra are seeing limited, we have spatial information on both the stellar population characteristics and the kinematics. While the primary goal of the LEGA-C survey is to obtain integrated spectral properties, exploring this aspect will undoubtedly prove to be highly interesting. Stellar rotation curves and age gradients provide strong constraints on the physics of galaxy formation and the connection to the dark matter halo hosts.

### Timeline

At this point we have collected approximately 45 % of the dataset based on the first two years of observation. This article coincides with the first data release<sup>1</sup> that includes fully calibrated 1D and 2D spectra of the data taken in the first year: 925 galaxies (22 % of the full survey). Figure 2 shows the redshift and S/N distribution of the data obtained in the first year: as can be seen, LEGA-C is on schedule to

be completed by 2018 and, excitingly, the data quality is precisely as good as anticipated, confirming the competitiveness of VIMOS.

A second data release will follow by the end of 2016. This will double the sample and expand to higher-level data products in the form of derived physical parameters, such as velocity dispersions and line indices. There will be updated data releases in subsequent years. For more technical information on the sample selection, observations, data reduction and modelling techniques, please refer to the LEGA-C survey paper (van der Wel et al., 2016).

### References

Conselice, C. et al. 2011, MNRAS, 417, 2770  
 Franx, M. et al. 2008, ApJ, 688, 770  
 Gallazzi, A. et al. 2005, MNRAS, 362, 41  
 Le Fèvre, O. et al. 2005, A&A, 439, 845  
 Lilly, S. et al. 2007, ApJS, 172, 70  
 Madau, P. et al. 1996, MNRAS, 283, 1388  
 McCracken, H. J. et al. 2012, A&A, 544, 156  
 Scoville, N. J. et al. 2007, ApJS, 172, 1  
 van der Wel, A. et al. 2014a, ApJ, 792, 6L  
 van der Wel, A. et al. 2014b, ApJ, 788, 28  
 van der Wel, A. et al. 2016, ApJS, 223, 29

### Links

<sup>1</sup> Access to Phase 3 LEGA-C data: [http://archive.eso.org/wdb/wdb/adp/phase3\\_spectral/form](http://archive.eso.org/wdb/wdb/adp/phase3_spectral/form)

# ALMACAL: Exploiting ALMA Calibrator Scans to Carry Out a Deep and Wide (Sub)millimetre Survey, Free of Cosmic Variance

Iván Oteo<sup>1,2</sup>  
 Martin Zwaan<sup>2</sup>  
 Rob Ivison<sup>2,1</sup>  
 Ian Smail<sup>3,4</sup>  
 Andrew Biggs<sup>2</sup>

<sup>1</sup> Institute for Astronomy, University of Edinburgh, United Kingdom

<sup>2</sup> ESO

<sup>3</sup> Centre for Extragalactic Astronomy, Department of Physics, Durham University, United Kingdom

<sup>4</sup> Institute for Computational Cosmology, Department of Physics, Durham University, United Kingdom

We present the latest results from ALMACAL, a novel, wide and deep (sub-)millimetre survey that exploits ALMA calibration data that comes for free during science observations. Combining compatible data acquired during multiple visits to many ALMA calibrators, sufficiently low noise levels can be reached to detect faint dusty star-forming galaxies (DSFGs). As of April 2016, we have analysed data for more than 240 calibrators, reaching noise levels as low as  $\sim 10 \mu\text{Jy beam}^{-1}$ , at sub-arcsecond spatial resolution. We have found 15 DSFGs, some less luminous than the sources detected by the deepest far-infrared surveys. Future analyses will deliver larger samples, free of cosmic variance, with redshifts determined via detection of multiple (sub-)millimetre lines, and dust emission imaged at milliarcsecond spatial resolution. The combination of area and depth reached by ALMACAL is unlikely to be surpassed by any other ALMA (sub-)millimetre survey.

A fraction of the restframe ultra-violet light emitted by star-forming galaxies (SFGs) is internally absorbed by dust and re-emitted at far-infrared wavelengths (Lutz et al., 2014). Detecting dust emission using far-infrared surveys is then essential to determine accurate star formation rates (SFR) and levels of dust attenuation for SFGs and, therefore, to understand the star formation history of the Universe. Indeed, this has been one of the main goals of many surveys carried out with past and current far-infrared/

submillimetre facilities (for example, Spitzer, Herschel, James Clark Maxwell Telescope or the Atacama Pathfinder EXplorer). However, due to their limited sensitivity, the detection of dust emission has been restricted to the most extreme sources at each redshift, hindering broader studies of galaxy formation and evolution.

Currently, the Atacama Large Millimeter/submillimeter Array (ALMA) is the only facility able to surpass these limits and select galaxies more than ten times fainter, which are responsible for much of the SFR density at redshift  $z > 1$  and the main contributors to the extragalactic background light — the integrated unresolved emission from extragalactic sources. Furthermore, this faint far-infrared population might be the link between the far-infrared-bright galaxies extensively studied in the past — submillimetre galaxies or SMGs — and the less extreme SFGs selected in optical/near-infrared surveys (and typically represented by Ly $\alpha$  emitters or Lyman-break galaxies) for which far-infrared detections are found for only  $\sim 5\%$  of the total population (Oteo et al., 2013).

## ALMACAL: A wide and deep (sub-)millimetre survey

Using ALMA calibration observations, we are carrying out a novel, wide and deep (sub-)millimetre survey: ALMACAL (Oteo et al., 2016). Every ALMA science project includes calibration observations of very bright, compact sources to set the flux density scale, to measure the bandpass response, and to calibrate the amplitude and phase of the visibilities of the science targets (Fomalont et al., 2014). Observations of such calibrators are essential and represent a significant fraction of each observing block (OB). Each calibrator will typically be observed several times, often many times, on different dates, in several different ALMA bands, as part of one or several ALMA science projects. Therefore, by combining compatible data for a high number of calibrators, it is possible to reach sensitivities and areas that allow the detection of dusty star-forming galaxies.

There are several, key advantages of using ALMA calibrators to search for and analyse high-redshift DSFGs. First, the sensitivities that can be reached after combining compatible data for different calibrators allow us to detect DSFGs fainter than those detected previously with the ESA Herschel satellite or other submillimetre, ground-based single dish observations. This opens a window to study dust emission in normal SFGs, with the data coming for free. Perhaps more importantly, a number of calibrators will be observed at extremely high spatial resolution, if this is amongst the requirements of the science project within which they are observed. The simultaneous presence in the map of one or more DSFGs and a bright ALMA calibrator lends itself perfectly to self-calibration (for example, Pearson & Readhead, 1984), which permits near-perfect imaging, even with the longest available interferometric baselines and highest frequencies. This advantage enables us to analyse the morphological properties in exquisite detail for any DSFG that is fortuitously located in a calibrator field.

The fact that each calibrator is often observed in several different ALMA frequency bands allows us to ensure that the faint detections are genuine with high confidence. Furthermore, such multi-band data allows the study of the spectral indices of DSFGs at matched spatial resolution, and determination of their redshifts via detections of (sub-)millimetre spectral lines (for example, Weiss et al., 2009). Furthermore, the number counts obtained for the selected galaxies, and the properties derived for those galaxies, come from sparse sampling of the astronomical sky and are thus relatively free of cosmic variance. ALMACAL is not however restricted to the detection of continuum sources. Several additional science goals include: blind searches for emission-line galaxies in the ALMACAL cubes to constrain the CO and [C II] luminosity functions (Decarli et al., 2014; Popping et al., 2016) and the cosmic H<sub>2</sub> mass density, to compare with models (for example, Lagos et al., 2011); studies of the physical mechanisms involved in the emission of powerful jets from quasars; and searches for common interstellar species in the lines of sight towards bright quasars (for example, Muller et al., 2014).



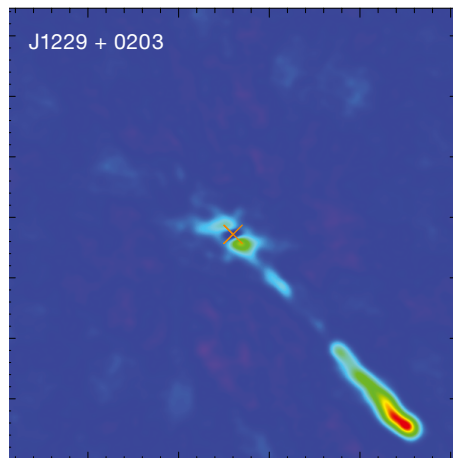
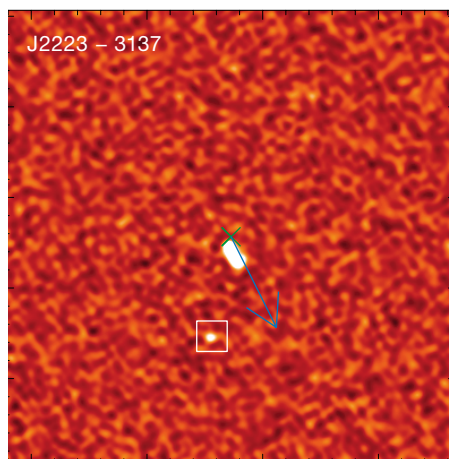
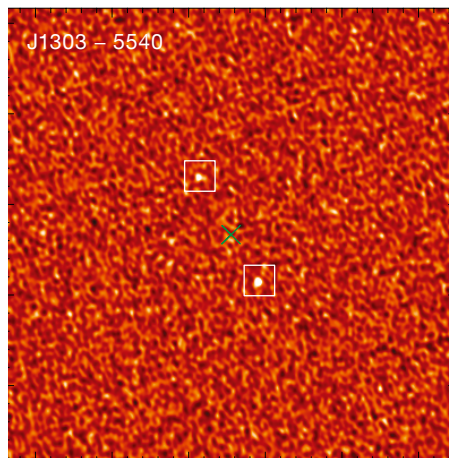


Figure 1. ALMA Band 6 (1.2 mm) image of the spectacular jet emanating from the calibrator J1229+0203. The multi-frequency observations provided by ALMACAL enable the nature of these jets to be studied in exquisite detail.

### Source selection

We have extracted from the ALMA archive all calibration data between the beginning of ALMA Cycle 2 and April 2016. No restriction on ALMA bands was applied, since different bands are useful for different science cases. First, the data for each calibrator in each OB are calibrated, following standard procedures. Then, for each observation, the calibrator is subtracted from the data in the Fourier  $uv$  plane using a point-source model, and the visibilities and clean maps are visually inspected, discarding all those datasets which show evidence of poor calibration. Next, all data for each calibrator in each band are combined after re-scaling the visibility weights. In order to detect DSFGs via their dust emission, we focus the source extraction on ALMA Band 6 (B6, 1.2 mm) and Band 7 (B7, 870  $\mu\text{m}$ ). Imaging in Bands 3 and 4 are used to identify jets emanating from the calibrators, which are quasars. Some jets are very obvious once the central bright calibrator is subtracted from the maps (one of the most spectacular cases found so far is shown in Figure 1). However, others may appear as unresolved “blobs” and are easily confused with DSFGs. Whenever possible, we compute the B3 or B4 to B6 or B7 flux density ratios for the B6-/B7-detected sources.



Ratios higher than unity indicate jets, while lower ratios, or a lack of detection in B3 and/or B4, are compatible with the far-infrared spectral energy distribution of a high-redshift DSFG. At the present phase of the survey, where data for more than 240 calibrators have been analysed, we have found 15 robust ALMACAL DSFGs (see Figure 2 for a small selection). Their far-infrared spectral indices (B7 to B6 flux density ratios) are compatible with them being at  $z \sim 2-3$ .

### The importance of ALMACAL DSFGs

The discovery of a population of DSFGs with flux densities 5–10 times fainter than the faintest SMGs from the SCUBA2 survey (Koprowski et al., 2015) allows us to study the sub-mJy population that might overlap with normal SFGs, such as Ly $\alpha$  emitters, star-forming galaxies selected by their  $BzK$  colours ( $sBzK$ ), or Lyman-break galaxies, which all lack

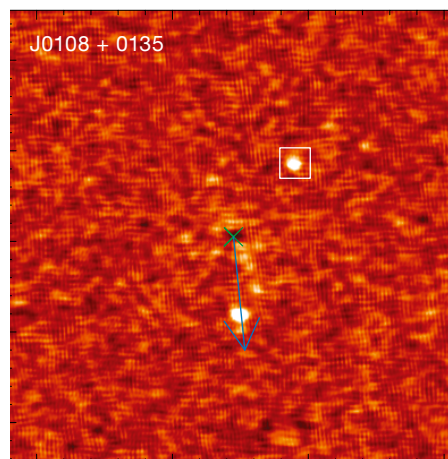
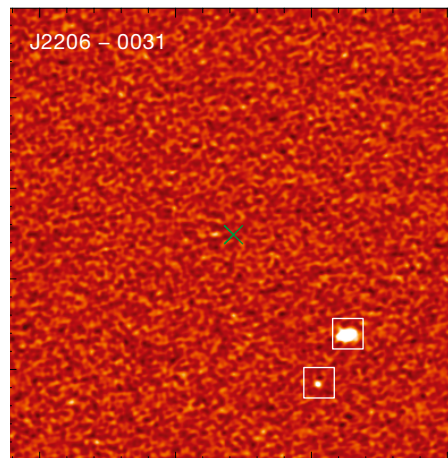
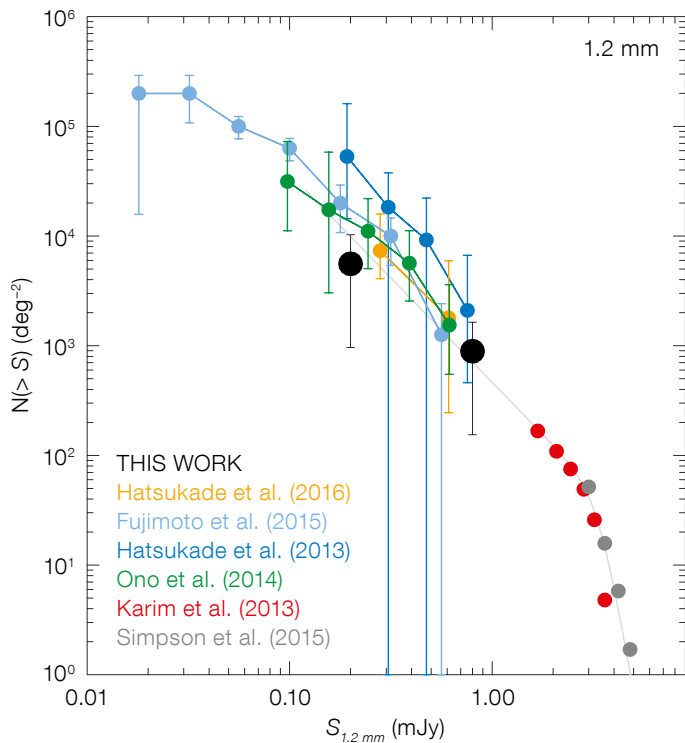


Figure 2. ALMA images (Band 6, 1.2 mm) of four calibrator fields in each of which at least one DSFG has been detected. Jets emanating from calibrators (identified via 3 mm imaging) are represented by the blue arrows, while DSFGs are indicated by white open squares. The calibrators, which have been subtracted in the  $uv$  plane using point-source models, are located in the centre of the images (green crosses).

dust emission detections in 95 % of cases. Uniquely detecting dust emission and measuring the total SFR of normal SFGs, without the uncertainties of ultraviolet-based dust correction factors, is feasible without having to rely on analysis via stacking (B  thermin et al., 2012). Additionally, faint ALMACAL DSFGs are among the very few high-redshift populations, alongside bright and extreme SMGs and gravitationally amplified systems (where interpretation is complicated by lens modelling), for which superb high-resolution imaging will be available from self-calibration by the bright calibrator in the centre of the map.



**Figure 3.** Cumulative number counts of DSGFs derived from ALMACAL at 1.2 mm, along with previous results (Hatsukade et al. 2013; Karim et al. 2013; Ono et al. 2014; Fujimoto et al. 2015; Simpson et al. 2015). Number counts derived in previous works have been converted to 1.2 mm by using the average far-infrared spectral energy distribution of SMGs at  $z \sim 2.3$  (Swinbank et al., 2014). The grey curve is the fit obtained in Simpson et al. (2015), extrapolated toward the flux densities covered in the present ALMACAL phase.

## The future

ALMACAL is continuously in progress, adding more and more calibration data on a daily basis. We will keep gathering and combining observations while ALMA keeps observing. This will likely result in the largest ALMA (sub-)millimetre map down to a depth of several  $\mu\text{Jy}$ , a unique dataset to study the nature of the faint submillimetre population. Apart from compiling more and more calibrator data, future work includes the characterisation of the ALMACAL detected sources via multi-wavelength observations to determine their redshift (for the sources without multiple millimetre line detections), stellar mass or obscuration. This step is needed to explore the relation between ALMACAL DSGFs and the normal SFG population typically represented by Ly $\alpha$  emitters, Lyman-break galaxies or sBzK galaxies selected in ultra-violet/optical/near-infrared-based surveys.

## References

- B ethermin, M. et al. 2011, *A&A*, 529, 4  
 Cai, Z.-Y. et al. 2013, *ApJ*, 768, 21  
 Casey, C. M. et al. 2014, *PhR*, 541, 45  
 da Cunha, E. et al. 2013, *ApJ*, 765, 9D  
 Decarli, R. et al. 2014, *ApJ*, 782, 78  
 Fomalont, E. et al. 2014, *The Messenger*, 155, 19  
 Fujimoto, S. et al. 2016, *ApJS*, 222, 1  
 Hatsukade, B. et al. 2013, *ApJL*, 769, L27  
 Hatsukade, B. et al. 2016, *PASJ*, 34  
 Karim, A. et al. 2013, *MNRAS*, 432, 2  
 Lagos, C. del P. et al. 2011, *MNRAS*, 418, 1649  
 Muller, S. et al. 2014, *A&A*, 566, 112  
 Ono, Y. et al. 2014, *ApJ*, 795, 5  
 Oteo, I. et al. 2013, *A&A*, 554, 3  
 Oteo, I. et al. 2016, *ApJ*, 822, 36  
 Pearson, T. J. & Readhead, A. C. S. 1984, *ARA&A*, 22, 97  
 Popping, G. et al. 2016, arXiv:1602.02761P  
 Simpson, J. M. et al. 2015, *ApJ*, 807, 128  
 Smail, I., Ivison, R. & Blain, A. W. 1997, *ApJ*, 490, L5  
 Swinbank, A. M. et al. 2014, *MNRAS*, 438, 1267  
 Weiss, A. et al. 2009, *ApJ*, 705, 45

## The (sub-)millimetre number counts

The cumulative number counts (i.e., the number of galaxies above a given flux density) is an observable that any credible model of galaxy formation and evolution must match. Most recent models can reproduce the bright end of the number counts ( $S_{1.2\text{ mm}} > 1\text{ mJy}$ ), but there are disagreements at fainter flux density levels. For example, model predictions based on the redshift evolution of the mass function of SFGs (B ethermin et al., 2011) give a number density of sources about five times lower than those based on the spectral energy distribution of the galaxies (da Cunha et al., 2013) and about 2.5 times smaller than predictions based on epoch-dependent luminosity functions (Cai et al., 2013). Therefore, firmer constraints on the faint end of the (sub-)millimetre number counts are needed to discriminate between the plausible models. At present, ALMACAL has derived number counts down to  $S_{1.2\text{ mm}} \sim 0.2\text{ mJy}$ , resolving about 50% of the extragalactic background light, and those counts are found to be lower than previously reported (Figure 3).

One of the main differences between ALMACAL and previous work is the source extraction technique. Whilst in ALMACAL only sources detected at  $> 5\sigma$  are included in the sample, other works employ significantly lower thresholds to compensate for the lower area and/or sensitivity and boost the number of sources. This leads to contamination by spurious detections. Although statistical corrections are normally applied, these are not always accurate. Recently, Hatsukade et al. (2016) also obtained slightly lower number counts, considering only  $> 5\sigma$  detections. One of the unique aspects of ALMACAL is that most of the galaxies are observed in multiple bands, so we can be confident that all ALMACAL DSGFs are real. Furthermore, and very importantly, since ALMA calibrators are distributed over the whole southern and equatorial sky, the ALMACAL (sub-)millimetre number counts are relatively free from cosmic variance. The apparent flattening we observe in the (sub-)millimetre number counts towards low flux densities has strong implications for our understanding of the dust emission from (and attenuation in) SFGs. ALMACAL will be the key to a fuller understanding.





Installation of the star-roof for the ESO Supernova Planetarium & Visitor Centre on 12 April 2016. The roof consists of glass panels set in a metal framework with representations of some southern constellations.



# Light Phenomena over the ESO Observatories III: Zodiacal Light

Petr Horálek<sup>1</sup>  
Lars Lindberg Christensen<sup>1</sup>  
David Nesvorný<sup>2</sup>  
Rebecca Davies<sup>1</sup>

<sup>1</sup> ESO

<sup>2</sup> Dept. of Space Studies, Southwest  
Research Institute, Boulder, USA

The zodiacal light is often seen at the ESO observatories in the hours after sunset and before sunrise. The origin of the zodiacal light is described and recent research briefly summarised. Some fine images of the zodiacal light from Paranal and La Silla, including the full extent of the night sky are presented.

On a moonless night from Paranal Observatory in the Atacama Desert in Chile, it is possible to see several different large-scale sky phenomena in addition to the faint light from the Milky Way. These include atmospheric phenomena, such as airglow — natural radiation arising in the Earth's atmosphere (Christensen et al., 2016) — and occasional flashes called sprites that can appear over the Andes and are connected with electrical storms (Horálek et al., 2016). Another light phenomenon that can be seen on every moonless night at a very dark site is the zodiacal light (Figure 1). Most evident in the hours after dusk or before dawn, zodiacal light appears as a faint, diffuse column of light in the sky, just above the horizon and extending towards the zenith (Figure 2).

Even after the brightest part of the zodiacal light is below the horizon, faint traces of it are still present. During the night it takes the shape of an extremely faint wispy bridge that brightens again in the early morning, before sunrise. Figures 3 and 4 show sophisticated panorama images of the zodiacal light from sunset to sunrise, clearly demonstrating its full extent across the sky.

## The nature of the zodiacal light

The origin of the zodiacal light is to be found in the inner Solar System. Infrared observations from the Infrared Astronom-



Figure 1. (Above) Column of zodiacal light (right) photographed from the platform at Paranal Observatory. The bright source within the zodiacal light cone is Venus.

Figure 2. (Below) The zodiacal light photographed soon after sunset from La Silla Observatory.



ical Satellite (IRAS<sup>1</sup>; Low et al., 1984) and Cosmic Background Explorer (COBE<sup>2</sup>; Reach et al., 1995) revealed emission from small grains composed of dust and ice surrounding the Sun. Most of the observed particles have sizes in the range 1 to 100  $\mu\text{m}$ . The Poynting–Robertson effect (Guess, 1962) forces particles

inward through the absorption of solar radiation and isotropic emission, reducing their angular momentum, while the dominant force for micrometre-sized particles is the solar radiation pressure that accelerates them away from the Sun. The zodiacal dust hence needs to be constantly replenished. This replenishment is



primarily served by crumbling icy comets, but also by colliding asteroids and possibly interstellar dust (Rowan-Robinson & May, 2013). The zodiacal light itself is sunlight that is forward-scattered from these particles in the direction of Earth.

Recent studies show that over 85 % of the cometary material in the zodiacal cloud comes from dust from comets in the Jupiter family (Nesvorný et al., 2010; Schulz et al., 2015). These are short-

period comets, with orbital periods less than 20 years, that take their name from the fact that their current orbits are determined primarily by the gravitational influence of Jupiter. The Jupiter family of comets contains 67P/Churyumov–Gerasimenko, now extremely well known as a result of the *in situ* research carried out by ESA’s *Rosetta* satellite in August 2014. The *Philae* probe landed on the nucleus of this comet in November 2014.

The dust grains that give rise to zodiacal light are distributed in a disc in the plane of the ecliptic (Nesvorný et al., 2003). When viewed from Earth, this disc appears as a band across the sky passing through the constellations of the zodiac, hence the name zodiacal light. As the scattering of sunlight is most effective at smaller angular distances from the Sun, the band of light along the ecliptic gets fainter and narrower further away from the Sun (Figure 3). Along the ecliptic, at the point in the sky opposite the Sun (the antisolar point), coherent backscattering from dust particles further out in the Solar System beyond the Earth’s orbit leads to the oval patch of

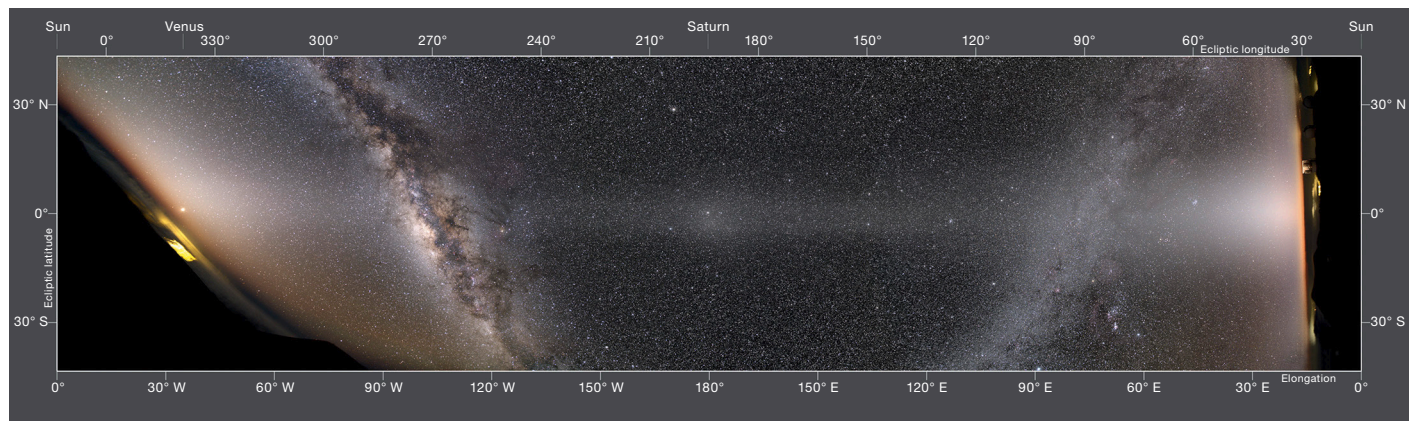
light known as the Gegenschein (Figures 3, 4 and 5). The name was given by the German explorer Alexander von Humboldt (1769–1859).

Observations of the zodiacal light

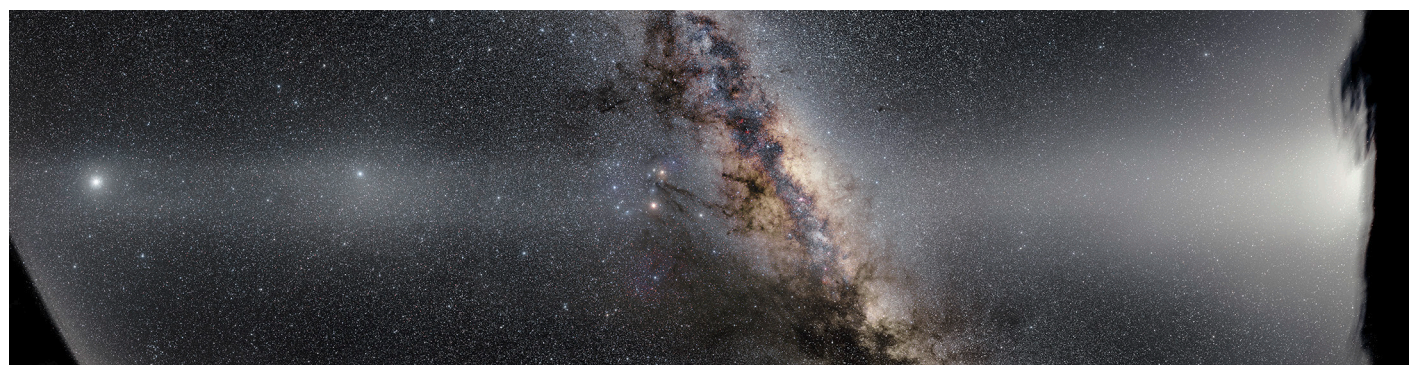
The zodiacal light was first investigated in the late 1600s, by the Italian astronomer Giovanni Cassini and the Swiss mathematician Nicolas Fatio de Duillier. Of course, back in the 17th century there was very little light pollution, so it was relatively easy to observe this phenomenon, even from cities. Observations of zodiacal light in more recent times have mostly focused on particular structures of the zodiacal cloud. Interesting zodiacal dust bands were discovered by IRAS in 1984 (Low et al., 1984; Dermott et al., 1984). They are produced by collisions of asteroids in the Main Belt between Mars and Jupiter within the last few million years (Nesvorný et al., 2003). Hints of these dust bands are noticeable on the full-night panoramic imaging of the zodiacal light taken by commercial cameras after post-processing, including colour

Figure 3. (Upper) All-night 360-degree panorama of the zodiacal light from Mauna Kea in April 2011, showing the structure of the zodiacal light almost in its entirety. On the left and right, the columns of light are visible after dusk (right) and before dawn (left) respectively, brighter closer to the Sun (which is under the left and right horizons). In the middle of the band, the Gegenschein appears at the antisolar point.

Figure 4. (Lower) 270-degree panorama of the zodiacal light, photographed from La Silla in April 2016, showing almost the full structure. On the right, the column of light is visible before dawn, brighter closer to the Sun (which is below the right horizon). To the left, the Gegenschein appears at the antisolar point. Unique hints of substructure are visible around the Gegenschein. Extensive image processing was performed by Petr Horálek and Miroslav Druckmüller to enhance the structures.



Miroslav Druckmüller & Shadia Habbal



ESO/P. Horálek & M. Druckmüller

Figure 5. Image of the Gegenschein obtained in October 2007 above Paranal Observatory.

correction of the background (see Figures 3 and 4).

Subsequent observations with IRAS and more sensitive photometric observations from NASA's STEREO satellites<sup>3</sup> have revealed a circumsolar dust concentration in a ring along the orbit of Venus. This was expected and is caused by the influence of the planet's gravitational resonance on the particles (Dermott et al., 1994; Jones et al., 2013). A brightening of the zodiacal cloud by ~ 10% near the apex of the Earth's orbital motion has also been found (Dermott et al., 1994).

Recent observations of nearby stars have demonstrated that the Solar System may not be the only one to exhibit zodiacal light. Data from the Very Large Telescope Interferometer have revealed that other planetary systems are also surrounded by interplanetary dust leading to zodiacal light, but much brighter than in the Solar System (for example, Lebreton et al., 2013; Marion et al., 2014; Ertel et al., 2015).

#### Acknowledgements

The contribution of David Nesvorný was supported by the Southwest Research Institute. We are grateful to Prof. Milošlav Druckmüller (Inst. of Mathematics,



Y. Beletsky/ESO

Brno University of Technology, Czech Republic) for significant support of the image processing of Figure 4, and to Bob Fosbury for illuminating discussions.

#### References

- Christensen, L. L., Noll, S. & Horálek, P. 2016, *The Messenger*, 163, 38  
 Dermott, S. F. et al. 1994, *Nature*, 369, 719  
 Dermott, S. F. et al. 1984, *Nature*, 312, 505  
 Ertel, S. et al. 2015, *The Messenger*, 159, 24  
 Guess, A. W. 1962, *AJ*, 135, 855  
 Horálek, P. et al. 2016, *The Messenger*, 163, 41  
 Jones, M. H., Bewsher, D. & Brown, D. S. 2013, *Science*, 342, 960  
 Lebreton, J. et al. 2013, *A&A*, 555, A146

- Low, F. J. et al. 1984, *AJ*, 278, L15  
 Marion, L. et al. 2014, *A&A*, 570, A127  
 Nesvorný, D. et al. 2003, *ApJ*, 591, 486  
 Nesvorný, D. et al. 2010, *ApJ*, 713, 816  
 Reach, W. T. et al. 1995, *Nature*, 374, 521  
 Rowan-Robinson, M. & May, B. 2013, *MNRAS*, 429, 2894  
 Schulz, R. et al. 2015, *Nature*, 515, 216

#### Links

- <sup>1</sup> IRAS: <http://irsa.ipac.caltech.edu/Missions/iras.html>  
<sup>2</sup> COBE satellite: <http://lambda.gsfc.nasa.gov/product/cobe/>  
<sup>3</sup> NASA STEREO satellites: <http://stereo.gsfc.nasa.gov/mission/mission.shtml>

## The First NEON School in La Silla

Michel Dennefeld<sup>1</sup>  
 Claudio Melo<sup>2</sup>  
 Fernando Selman<sup>2</sup>

<sup>1</sup> Institut d'Astrophysique de Paris, CNRS, and Université P. et M. Curie, Paris, France

<sup>2</sup> ESO

The NEON Observing Schools have long provided PhD students with practical experience in the preparation, execution and reduction of astronomical observations, primarily at northern observatories. The NEON School was held in Chile for the first time, with observations being conducted at La Silla. The school was attended by 20 students, all from South America, and observations were

performed with two telescopes, including the New Technology Telescope. A brief description of the school is presented and the observing projects and their results are described.

After many years of discussions and preparations, the NEON Observing School could finally take place at La Silla



for the first time, from 22 February to 4 March 2016, with joint sponsorship from ESO and OPTICON<sup>1</sup> and strong support from the ESO Director General, the Director for Science and the Heads of the Office for Science.

As is well known by now, the NEON Schools are intended to provide PhD students with practical training on how to prepare and execute an observing programme. The schools have taken place in several active observatories, comprising the Network of European Observatories in the North (NEON; including Asiago, Calar Alto, Haute-Provence and La Palma), with which ESO is also associated. Devoting a small fraction of the time at 4- and 2-metre-class telescopes to training purposes can thus be regarded as a useful investment for the overall efficiency of all the facilities, developing the observing skills of the next generation of astronomers.

The format of the schools is similar: beginning with writing a proposal followed by the preparation of observations (instrument set-up, calibrations, etc.) and the observations themselves, then completing the data reduction and finally presenting the results. Work is carried out in small groups of four students, with each group under the supervision of an experienced tutor, who also provides the science project to be executed. This kind of training is much needed, as instruments are getting more and more complex, and many observatories (and ESO not least...) offer a large fraction of their observing time at the large telescopes in Service Mode, so that practical experience can be lacking for many young astronomers.

### The La Silla school

So, how did it work in La Silla? Thanks to a generous allocation from the Director's Discretionary Time, the New Technology Telescope (NTT) was made available for three nights for the school, close to full Moon. As the operations there are quite similar to the Very large Telescope (VLT), with an operator for the telescope, the same set of observing preparation tools and operations principles (observing blocks to prepare, pipelines for reduction, etc.), this provided an excellent

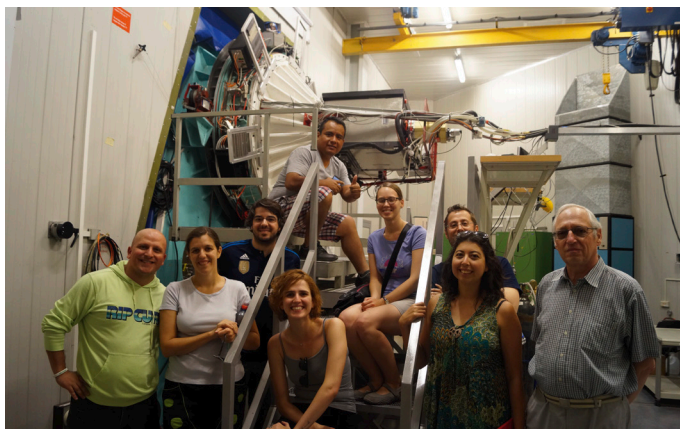


Figure 1. Two of the student project groups around the EFOSC2 Nasmyth focus of the NTT during the NEON School at La Silla.

training for future use of larger (VLT) facilities. But it is still a bit too “automatic” to understand all the details needed to operate less advanced facilities. Thus, since according to the local Chileans, NTT also means *No Tocar al Telescopio* (“Do not touch the telescope”), we also used the Danish 1.54-metre telescope, made available during Czech time thanks to Petr Pravec and with the support of Jan Janik (Mazaryk University), who came over specially to support our run. The various science programmes used, as far as possible, a combination of both telescopes and instruments.

The observations were prepared in Santiago, prefaced by a set of lectures on fundamental observing techniques, instrument and detector properties and data reduction. The full programme of the school can be found on the dedicated website<sup>2</sup>. The tutors leading the observations in groups were all current, or former, ESO staff in Chile, and thus perfectly aware of all the requirements and instrument performance.

### Group projects

The group led by Amelia Bayo (University of Valparaiso) and Koraljka Muzic (ESO, and University of Diego Portales) studied the widest binary stars in young stellar groups from the Search for Associations Containing Young stars (SACY) sample, to find out whether or not they belonged to the same group. The H $\alpha$  and Li I 6708 Å lines were used as age indicators and observed with the ESO Faint Object Spectrograph and Camera (EFOSC), and the K I + Na I lines were observed

with Son of ISAAC (SOFI). This approach allowed four out of the eight stars observed to be confirmed as young stars of the same age.

The group led by Fernando Selman and Evelyn Johnston (ESO) tried to disentangle the counter-rotating discs in the lenticular galaxy IC 719. Long-slit spectroscopy with EFOSC for velocities, and *B*, *V*, *R*, H $\beta$  photometry with the Danish 1.54-metre (the H $\alpha$  filter had inexplicably disappeared...) revealed the different structures, and that more than one stellar component (identified through Lick indices) was present from the radial velocities. Evidence was also found for a young stellar population. This is clearly a case where a full 3D map with the Multi-Unit Spectroscopic Explorer (MUSE) would reveal the full power of this technique.

The group led by Giacomo Beccari (ESO) tried to find protoplanetary discs around young stars, from ultra-violet, H $\alpha$  or infrared excesses. Multi-band photometry of candidate regions in Carina was done at the Danish 1.54-metre telescope. As H $\alpha$  imaging was not possible, Brackett  $\gamma$  imaging was done instead with SOFI at the NTT. Finally, six new disc candidates were identified, whose confirmation is pending with spectroscopy.

Linda Schmidtobreick (ESO) observed a candidate cataclysmic variable detected in the Sloan Digital Sky Survey (SDSS) with her group, in order to measure/confirm its orbital period both by photometry, and by radial velocity measurements. Long series of imaging (with the Danish 1.54-metre telescope) and spectroscopy (with EFOSC at the NTT) data were thus



Figure 2. All NEON School students and tutors pose in the dome of the ESO 3.6-metre telescope for a group portrait.

obtained, the expected periods being about 80 minutes. The students, after being confronted by all sorts of drifting and aliasing problems, could finally show that the real period was in fact closer to 3–4 hours for one target, and 6–7 hours for the other, but longer series of data are still needed to confirm these values. Another, unknown, variable star was also found in one of the fields, the nature of which remains to be clarified.

Finally, Bruno Dias (ESO) conducted an ambitious, and difficult (at least for beginners) multi-object spectroscopy programme at the NTT with his group, to determine the nature of the globular cluster NGC 3201: whether it is a member of the Milky Way or an absorbed dwarf galaxy. This first required pre-imaging, then preparation of the masks, and finally observing during the last night of the run. After all the hard work, those students presented superb results, showing a trend of Fe abundance versus heliocentric velocity (demonstrating that the selected stars did indeed belong to the cluster). The CH versus CN indices showed that two different abundance groups were present, but both belonging to the Milky Way.

In addition to their main tasks, two of the groups were triggered to observe a Target of Opportunity (a situation that many observers have to face nowadays), led by Michel Dennefeld (IAP, Paris). The targets were provided by the European Space Agency's Gaia satellite, which has very recently started to provide dozens of alerts per day. One of them, Gaia16agf,

proved to be a young Type Ia supernova, caught about one week before maximum, while the other, Gaia16afz, was classified as a dwarf nova in eruption. Both results were immediately published as *Astronomer's Telegrams*, Nos. 8754 and 8766, respectively. Many of the other results from the student groups will also lead to publications, but over a slightly longer timescale.

### Back to Santiago

The last days in Santiago were mainly devoted to data reduction, before the scientific results were presented on the last day of the school. In addition, lectures on other topics of great interest for the future were presented: on the Atacama Large Millimeter/submillimeter Array (ALMA), on adaptive optics, the European Extremely Large Telescope, etc. There were also lively discussions about career prospects, how to make a good presentation or how to write a good telescope observing proposal.

Overall, the 20 students, all from South America, selected from over 140 applicants in total, were very enthusiastic, worked hard during the two weeks, both in Santiago and on the mountain, and presented excellent results at the end. The groups of four were very dynamic, covering a wide range of levels (from first year PhD to postdoc) and origins, although the majority came from those countries with a larger astronomical population, namely Argentina, Brazil and Chile, and with a good gender balance. The ambiance was very friendly, as it should be for a summer school, favoured by nice weather and excellent environment at the ESO premises in Santiago

and La Silla, including nice lunches in the ESO gardens in Vitacura.

### Prospects

One may wonder about the motivation to organise such a school at La Silla, as it is not especially intended for European students, who have ample opportunities to attend the regular NEON Schools in Europe, except for those students doing their PhDs in Chile. In fact, there is a high demand, as shown by the huge number of applications, and it is in ESO's interests (and the European community at large) to ensure the most efficient use of its facilities, which are open to everybody, since the allocation of observing time is based on scientific merit only. In addition, the operation of all the facilities in Chile requires a large number of dedicated and skilled astronomers and engineers, who have to be trained somewhere. In this sense, such a school also reinforces the European links with the local communities and emphasises the various job opportunities for the future. The success of the present event is already generating suggestions for future similar schools, a point well taken at ESO, and enthusiastically supported by the ESO tutors. It is a revival of past successes as the first observing school was organised jointly by ESO and Centre national de la recherche scientifique (CNRS) at the Haute-Provence Observatory in 1988 (Chalabaev & D'Odorico, 1988).

### Acknowledgements

This NEON School would not have been so successful without the efficient support of many people: Paulina Jiron and María Eugenia Gómez (Office for Science in Vitacura); Ivo Saviane, Javier Duk and the whole La Silla Logistics Team; Esteban Osorio and the IT team in Santiago, and many others, all of whom we warmly thank.

### References

Chalabaev, A. & D'Odorico, S. 1988, *The Messenger*, 53, 11

### Links

- <sup>1</sup> OPTICON: <http://www.astro-opticon.org>
- <sup>2</sup> School website: [http://www.eso.org/sci/meetings/2016/lasilla\\_school2016.html](http://www.eso.org/sci/meetings/2016/lasilla_school2016.html)



Report on the

## ESO Data Simulation Workshop

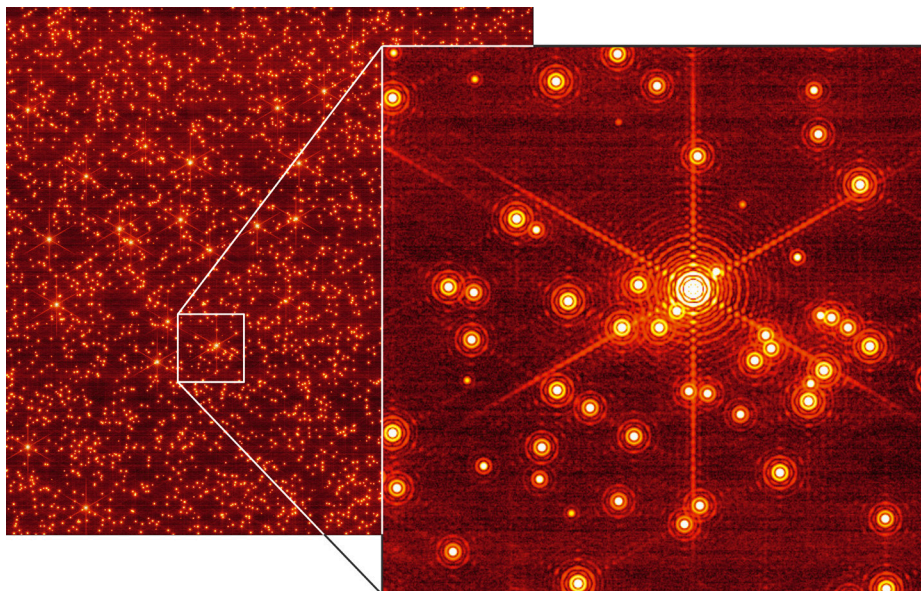
held at ESO Headquarters, Garching, Germany, 14–15 April 2016

Pascal Ballester<sup>1</sup><sup>1</sup> ESO

The role of simulated data is increasing rapidly across all phases of instrumentation projects, from design to scientific exploitation. The many commonalities among ESO instruments, their reduction software and archival products, makes it especially worthwhile to exchange knowledge between their instrument teams. The data simulation workshop was the first of its kind to bring together the ESO instrument simulator community and a brief overview of the workshop is presented. The participants expressed strong interest in continuing to exchange knowledge in this area.

End-to-end detector array simulations of observation and calibration data are applied in many phases of instrument projects, from the assessment of instrument performance, optimisation of instrument design, validation of science cases, preparation of the exposure-time calculators and observing tools to evaluation and testing of data reduction algorithms, optimisation of observing and calibration strategies, as well as for the design of physical-model driven calibrations.

The purpose of the data simulation workshop was to provide a forum for specialists from the instrument consortia and from ESO engineering departments, to exchange information, methods, and experience about their respective simulation approaches and results. Around 50 participants from about ten different institutes and ESO attended, and a video-conference connection allowed participants at four other institutes, in Marseilles, Oxford, Groningen and Innsbruck, to contribute to the workshop. The workshop was structured over two half days, with 11 talks and two lively discussion sessions. On Thursday evening, dinner at an Indian restaurant in Garching provided a relaxed setting for continuing discussions.



Kieran Leschinski/Univ. Vienna

### Workshop themes

The first half-day included talks by the instrument consortia, presenting the intended usage, status and current results of their simulation projects. The projects represented included the European Extremely Large Telescope (E-ELT) instruments HARMONI (first light integral field spectrograph), MICADO (first light adaptive optics imager) and METIS (first light mid-infrared imager and spectrograph), as well as the spectroscopy survey facilities 4MOST (4-metre Multi-Object Spectroscopic Telescope) and MOONS (Multi-Object Optical and Near-infrared Spectrograph). While some projects are already completed, like the Virtual MOONS simulation (Li Causi et al., 2014), a number of first results were shown for the MICADO (Leschinski et al., 2016) and METIS (Schmalz et al., 2012) instruments; see Figures 1 and 2 respectively. Many teams are building upon the experience acquired in previous simulation projects: for instance the Multi-Unit Spectroscopic Explorer (MUSE) instrument numerical model (Jarno, 2012) is being used in the development of HARMONI.

Time was also reserved for discussion sessions. During the first day, the topics of discussion covered configuration control of the projects, sharing of common models and data, and the validation of models. The first topic of discussion was

Figure 1. A simulated MICADO observation of a  $\sim 2000 M_{\odot}$  open cluster in the Large Magellanic Cloud produced with SimCADO. The left image shows the raw readout from the central H4RG infrared detector chip in the MICADO detector array. The SimCADO package simulates all aspects of the optical train including the atmosphere, telescope optics, various adaptive optics correction modes and the MICADO optical design as well as the detector characteristics.

the integration of simulations within and between the projects, in terms of change and configuration control. Shared repositories of simulation results for the common parts, such as telescope wavefront errors or adaptive optics simulations, were also discussed. Since all the simulation projects presented make use of sky radiance and transmission data from the Austrian in-kind sky radiance model (Noll et al., 2012), a programmatic interface to the model, as a complement to the web application<sup>1</sup> *Skycalc*, was addressed. The validation of the simulations was also a topic of interest. Different approaches like cross-instrument modelling were proposed. The respective advantages of faster, but simpler simulations versus advanced models based on Fourier optics were also discussed.

During the second day, presentations were provided by ESO engineers on aspects of E-ELT modelling, including telescope wavefront errors, telescope vibrations, and adaptive optics modelling

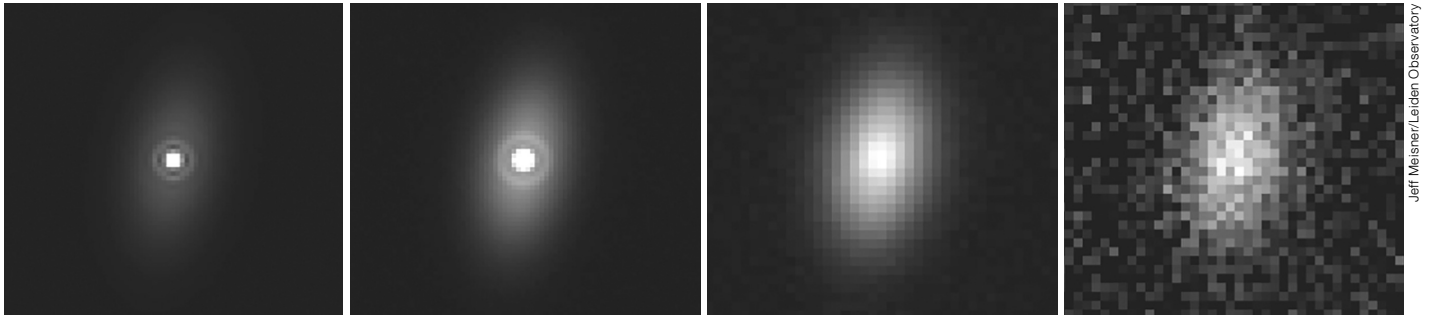
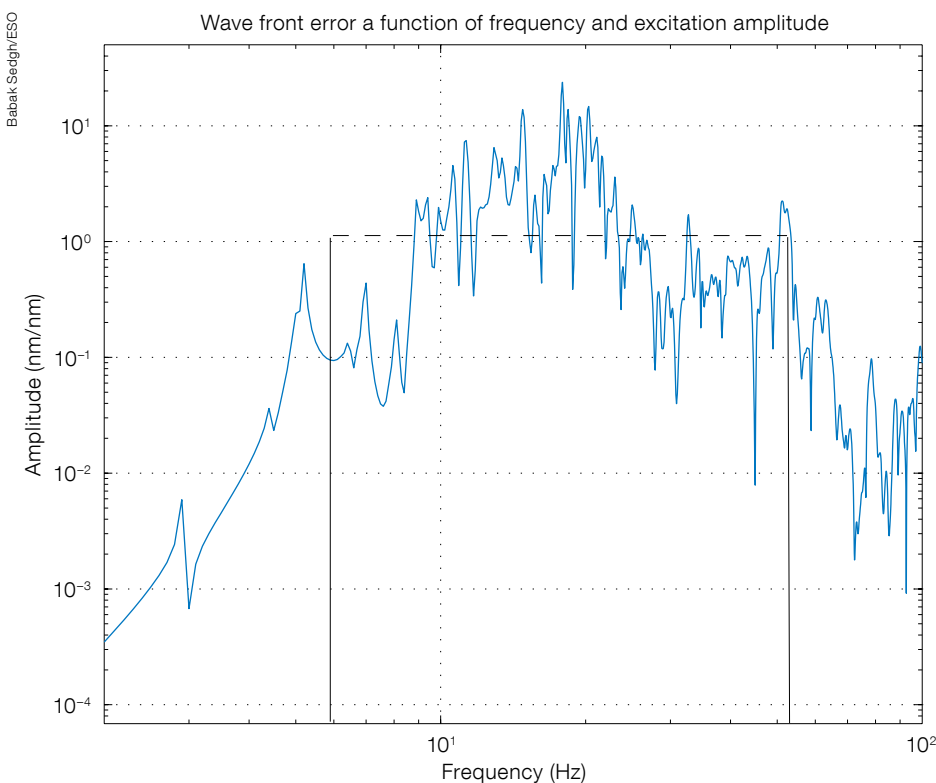


**Figure 2.** Using a model of a star surrounded by cooler circumstellar material, the METIS simulator predicts detector images using four different camera filters (from left to right) *L*-band (3.8  $\mu\text{m}$ ), *M*-band (5  $\mu\text{m}$ ), *N*-band (10.7  $\mu\text{m}$ ), and *Q*-band (17.7  $\mu\text{m}$ ). At shorter wavelengths the hotter star dominates; at longer wavelengths the nebulous component is brighter and the instrument sensitivity decreases.

and point spread function simulation. The main philosophy for modelling and simulation of the E-ELT was discussed and presented. The project deliberately avoids complex end-to-end modelling. Instead, aspects of the temporal and

**Figure 3.** Sensitivity response of the amplitude of the wavefront error (WFE) with the vibration frequency from the telescope pier.



spatial frequencies for the dynamics and control loops and the perturbations acting on the telescope are explored. The analysis and simulation environments are split into three different simulation toolkits: 1) active optics and phasing toolkit; 2) telescope dynamical and control toolkit; 3) adaptive optics toolkit (Octopus). This approach provides more flexibility to adjust the models to dedicated purposes and also reduces the computational effort. A model-based vibration sensitivity analysis and budgeting using the dynamical and control toolkit was presented (Figure 3).

A session on physical-model driven calibration presented results obtained in the

area of data quality control and science reduction for the Cryogenic Infra-Red Echelle Spectrometer (CRIRES), the Ultra-violet Visible Echelle Spectrograph (UVES) and the X-shooter instruments (Bristow, 2010). The Austrian in-kind sky radiance model, used by all ongoing instrument simulation projects, was also presented, and a specific discussion on modelling of infrared detectors concluded the workshop.

The slides of all talks are provided on the workshop web page<sup>2</sup>. The workshop was a very fertile platform for the exchange of practical and theoretical information among the participants. The participants expressed their interest in a continuation of this type of meeting and further sharing of paper references, methods and tools useful for data simulations.

#### Acknowledgements

Special thanks go to Martine Peltzer for help with organising the meeting and to the ESO IT team for their efficient support.

#### References

- Bristow, P. et al. 2010, Proc. SPIE, 7735, 271
- Jarno, A. et al. 2012, Proc. SPIE, 8449, 84490A
- Leschinski, K. et al. 2016, Proc. ASP Conf. Ser. ADASS XXV, in press
- Li Causi, G. et al. 2014, Proc. SPIE, 9147, 64-1
- Noll, S. et al. 2012, A&A, 543, A92
- Schmalzl, E. et al. 2012, Proc. SPIE, 8449, 1P

#### Links

- <sup>1</sup> Skycalc web interface to the Austrian in-kind sky radiance model: <https://www.eso.org/observing/etc/skycalc/>
- <sup>2</sup> Workshop programme, list of participants and presentations: <http://www.eso.org/sci/meetings/2016/simu2016.html>



# Retirement of Lothar Noethe

Jason Spyromilio<sup>1</sup>  
Ronald Holzlöhner<sup>1</sup>

<sup>1</sup> ESO

Lothar Noethe retired in April after 33 years at ESO. An appreciation of his contributions is presented, in particular his pioneering work in active optics and his role in the commissioning of the NTT and VLT.

Lothar Noethe joined ESO in January 1983 to work in the Telescope Group led by Ray Wilson. Lothar had studied physics at Bochum University and theoretical physics at Liverpool University and worked for Siemens. In this period Ray was developing active optics and a thin (19 mm) 1-metre test mirror with 78 actuators was the experimental testbed (Noethe et al., 1986; Madsen, 2012, p. 121).

## Active optics

Controlling the shape of telescope mirrors and their relative position has been a challenge for telescope builders since the earliest times. Passive control (for example, by mechanical astatic supports and Serrurier trusses), as well as semi-active operations (for example, by pneumatic or vacuum mirror supports) had been in use at telescopes for many years before the advent of what we now call active optics. The breakthrough for active optics was to build a system that would operate in closed loop on short enough timescales that the engineering of the telescope could be simplified, making for cheaper and better telescopes. Active optics, in contrast to adaptive optics, corrects the fine alignment and optical figure of a telescope under temperature and gravity vector variations, typically on a timescale of minutes (Noethe, 2002). The enabling technology was the digital detectors that could be used to sense the wavefront; the enabling thinking was the partnership between Ray Wilson and Lothar Noethe.

In today's environment it is difficult to contemplate an era when digital imaging was at the cutting edge of telescope technology. A charge-coupled device

(CCD) was first deployed at La Silla on the Danish 1.54-metre telescope in 1982. The CCDs were tiny, had poor quantum efficiency and high readout noise. Computing resources were limited and efficiency in the algorithms was paramount. The New Technology Telescope (NTT) project was audaciously launched at approximately the same time. It is worth noting that as late as the early 1990s there were highly respectable voices in the field who held that the thin meniscus mirror would never be able to deliver images of the same quality as stiffer mirrors. Lothar's keen mathematical mind excelled in this environment and he solved the problem of quickly processing the data from the wavefront sensors into mirror positioning and shaping commands.

While optical engineers had long worked in Zernike space when dealing with aberrations, Lothar revolutionised the field by shifting the control of the optics to natural modes. These, in effect, are the mechanical modes in which the mirror bends most naturally, whose deformations are significantly simpler to realise and require less force and therefore are easier to control. As Ray commented, this "is one of the great contributions of Lothar Noethe" (Wilson, 2003). The shift in thinking that this brought about is profound, not only in the control of the optics and the cost of the mirror cell and actuators through the use of lightweight substrates, but also, very critically, in the polishing requirements for the mirrors.

## NTT to VLT

Lothar was a key player in the commissioning of the NTT, and later for the Very Large Telescope (VLT), and present for all first stars (the first time the telescope sees a star). Lothar's work was critical in making it appear to the outside world that a smooth and elegant transition from the assembly of the telescopes to their first lights was taking place. Without Lothar it would have been neither smooth nor elegant, but there was also an element of luck involved. The initial success of the NTT, with the spectacular appearance of astronomical images with an image quality of 0.33 arcseconds during the commissioning night of 22–23 March 1989 (Wilson, 1989), was astounding; a

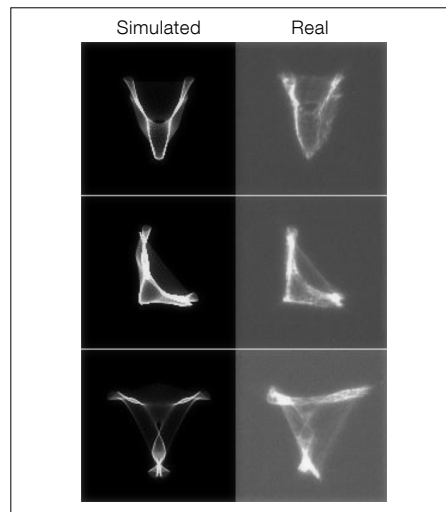


Figure 1. Simulated and real letters "written" in the sky, produced by creating aberrations with the VLT active primary mirror.

value difficult to believe at the time. This was of course more than a year before the launch of the Hubble Space Telescope. As observations with the Differential Image Motion Monitor (DIMM) showed, this was a night with exceptionally good seeing (Sarazin, 1989). But not much later, long-term atmospheric variations substantially increased the mean seeing at La Silla for a period of several years — the great success of the NTT first light would have had less impact under less favourable seeing conditions.

Lothar continued as a pioneer of active optics, which was also the foundation for the primary mirror of the Very Large Telescope (VLT). First star for Unit Telescope 1 (UT1) was achieved three weeks prior to the official first light (25 May 1998). Using just the guide probe wavefront sensor Lothar, supported by Stephane Guisard and Roberto Abuter, was able to work with the active optics system to give the commissioning team the confidence to communicate within ESO that the telescope was likely to work. Semi-cryptic public releases of information advised those in the know that all was going well. Some first stars were truly ugly and Lothar would compute manually the commands to transform stars that were 30 arcseconds in size and stretched out like strings of beads, into small roundish images that the active optics could deal with.

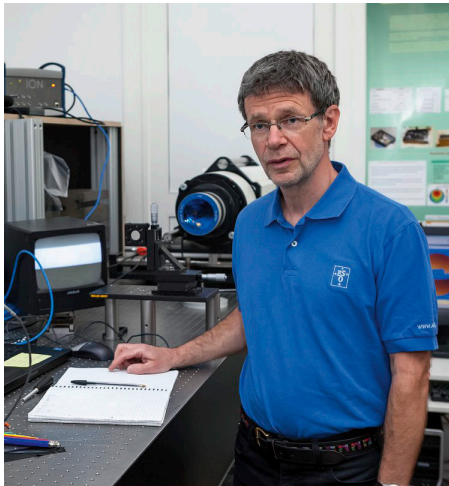


Figure 2. Lothar Noethe pictured in one of the optics laboratories at ESO Headquarters. The apparatus behind Lothar is a laser tracker, capable of measuring distances on the micrometre level.

A couple of anecdotes deserve recalling. After the first few million active optics corrections on UT1 (a couple of months into the commissioning of the telescope) the logging system that is an integral part of the VLT operational system could be used to provide beautiful statistics of the various aberrations. By this stage the telescope was providing exquisite imaging down to 0.26 arcseconds in the visible. The statistics were sent to Lothar as a recognition of his excellent work. Lothar immediately reacted, noting that the standard deviation of the focus term was too high and that something was not quite right. Some probing by him in the software resulted in a change in sign in the force setting for the outer ring of actuators for the primary mirror, and the almost perfect image quality became that little bit better.

One standard test of a telescope's performance is to make it write using starlight, by moving the telescope in particular patterns on the sky while exposing the detector. The NTT was made to write its own name. On the VLT Lothar decided that he could beat this: he created a mathematical description of the aberrations, converted them to forces on the primary mirror and movements of the secondary mirror as needed so that the stars would have the shapes of the letters V, L and T (see Figure 1). This was a strong demonstration that active optics had not only arrived, but was firmly under control.

## New envelopes

After the commissioning of all the VLT UT's and the beginning of discussions about the next step to larger telescopes, Lothar became involved with control of segmented mirrors. In 2002, he went to the University of California at Irvine for six months to work with Gary Chanan and developed a long and fruitful collaboration on the challenges of active optics with segmented telescopes. Lothar also obtained a *Habilitation* (German higher degree) in 2001 at the Berlin Technische Universität, again on active optics. He was appointed head of the Optical Systems Department in 2003. When ESO embarked on the E-ELT project, Lothar was critical in pushing for novel systems engineering solutions (Karban et al., 2008) and for ESO to maintain its position as an innovation centre for telescopes. Lothar also had a clear vision for the needs of complex projects to be managed through requirements and structured thinking and contributed towards the adoption of a proper systems engineering culture at ESO.

Most recently Lothar looked at applying closed-loop active optics to wide-field telescopes. The correction procedure is more demanding in a wide-field telescope because of the tight alignment tolerances in fast optics. The field dependence of aberrations in misaligned wide-field systems also places tighter constraints on various system degrees of freedom than is the case with more conventional, narrow field-of-view telescopes, such as the VLT. On account of the higher sensitivity to aberrations and the large field of view, the science images can be used to derive the aberrations. This realisation laid the foundation for a novel method of active correction.

In the two wide-field telescopes operated by ESO, namely the 4-metre Visible Infrared Survey Telescope for Astronomy (VISTA) and the 2.6-metre VLT Survey Telescope (VST), curvature wavefront sensors are employed for the active optics control, in contrast to the more commonly used Shack–Hartmann (in the case of the NTT and VLT) or pyramid wavefront sensors. In a generalisation of curvature wavefront sensing, Lothar initiated an active optics control method based on an analytical model of small

point spread function aberrations across the science image. The scheme has been implemented in *Mathematica* and successfully operated with OmegaCAM on the VST during several technical nights in 2015 (Holzlöhner et al., 2014). Development is still required to simplify the processing before this can become a standard technique for improving the image quality of the VST.

Lothar has advised many projects outside ESO and has selflessly supported the work of many junior engineers to advance the field. As Ray put it in his article (Wilson, 2003), “[Lothar’s] application for the ESO job was one of the greatest pieces of good fortune in our whole active optics development”. Telescope design and operation, and ground-based observational astronomy in general, have been profoundly affected by Lothar’s work.

## Retirement

Lothar retired at the end of April 2016 and a farewell lunch for the Optics Department was held on 29 April 2015 at ESO Headquarters (he had asked not to have a large farewell party organised). Besides excelling in optical engineering, Lothar has always been active in various sports, in particular table tennis, which he plays several times a week and coaches young players at the local sports club. Never ceasing to be curious and eager to learn, he has now enrolled in an advanced algebra course at the Technische Universität München. We wish him a very “active” retirement and look forward to more contributions in the field of telescope optics.

## Acknowledgements

We gratefully thank Dietrich Baade and Katjuscha Lockhart for comments.

## References

- Holzlohner, R. et al. 2014, SPIE, 9151, 2I
- Karban, R. et al. 2008, Proc. SPIE, 7017, #11
- Madsen, C. 2012, *The Jewel on the Mountaintop*, (London: Wiley-VCH)
- Noethe, L. et al. 1986, SPIE, 628, 285N
- Noethe, L. 2002, Progress in Optics, 43, 1
- Sarazin, M. 1989, The Messenger, 56, 8
- Wilson, R. 1989, The Messenger, 56, 1
- Wilson, R. 2003, The Messenger, 113, 2



## Fellows at ESO

### Katharina Immer

I do not exactly know when I started to be interested in astronomy. For as long as I can remember, I have watched the night sky and the beautiful coloured images of astronomical objects from the Hubble Space Telescope and other telescopes. When I was a teenager, I got a little reflecting telescope with which I observed stars and the Moon.

In high school, I was particularly interested in physics and mathematics and thus it was a natural step to decide to study physics at the University of Bonn. Since I already knew at that time that I wanted to be an astrophysicist at the end of my studies, I chose astronomy as my minor subject. The introduction to Galactic astronomy, as well as lectures about microquasars and the interstellar medium, were particularly interesting. During my studies, I had several opportunities to visit the 100-metre radio telescope in Effelsberg. Standing in front of this huge telescope was very impressive. Since this telescope operates in the radio wavelength regime, it can even observe through heavy clouds and rain.

In 2008, I started my Diploma thesis at the Max Planck Institute for Radio Astronomy (MPIfR) in Bonn, one of the hubs of radio astronomy in Germany. I worked with Karl Menten on Very Large Array (VLA) observations of the dust ridge clouds in the Galactic Centre in the search for H II regions and thus ongoing star formation in these clouds. Since we did not find any radio sources in the clouds, we could exclude the existence of stars with spectral types earlier than B0.5. I also worked on data from the infrared spectrograph onboard the Spitzer Space Telescope with Frederic Schuller. From the slope of the spectra and the detected emission lines, we sorted the observed sources into young stellar objects and late-type evolved stars. By the end, we could derive a star formation rate for the Galactic Centre.

For my PhD, I decided to stay in Karl Menten's group in Bonn. In 2010, I went for a year to the Harvard-Smithsonian Center for Astrophysics (CfA) in Cambridge, Massachusetts, as a predoctoral



Katharina Immer

fellow to work with Mark Reid on VLA observations of DR21 and Submillimeter Array observations of W33. In addition, I am part of the Bar and Spiral Structure Legacy Survey, led by Mark Reid, which determines the trigonometric parallaxes of star-forming regions in the Milky Way. That year was one of the best of my life, learning a lot about interferometry, submillimetre and radio observations, as well as high-mass star formation, meeting some of my closest collaborators and friends, as well as my boyfriend, travelling along the East coast of the US and having a wonderful time.

After I moved back to Bonn, I became one of the visiting observers for the Atacama Pathfinder Experiment (APEX) telescope in Chile. During my time at the MPIfR, I went to APEX for four runs. Here, I learned how to observe with a single dish telescope and gained insights into all kinds of science projects that were conducted with this telescope. The experience that I gained helped me to improve my observing proposals significantly.

After finishing my PhD in 2013 and a short-term postdoc at the MPIfR, I started at ESO in Chile in 2014. I decided to come to ESO because I liked the duty and science combination of the fellowship. Since I wanted to stay in contact with APEX, but also get to know the Atacama Large Millimeter/submillimeter Array (ALMA), I chose the commissioning and Science Verification of the Band 5

receivers at both APEX and ALMA as my duties. This is a very interesting project, giving me insights into the workings of a new instrument and the different problems and quirks that come with it at the beginning. The Science Verification of these receivers brought me into contact with cutting-edge science in very different astronomical fields, from star formation to evolved stars to extragalactic projects, and I learnt a lot about many topics outside of my own field. I am now also involved in the ongoing commissioning and Science Verification for the Band 9 receiver at APEX.

For my science, I am still mostly focused on high-mass star formation, trying to understand the chemical evolution of the molecular clouds during the star formation process as well as the kinematics in the clouds. While I have started several projects with colleagues within the star formation group, the multi-science environment at ESO also sparked new ideas and collaborations outside of my field of expertise, which is both challenging but rewarding.

I am looking forward to continuing with research on high-mass star formation and the work with submillimetre and radio telescopes of this and future generations like APEX, ALMA, the Jansky Very Large Array (VLA), or the Square Kilometer Array (SKA), during my remaining time at ESO as well as in future positions during my career.



Evelyn Johnston

### Evelyn Johnston

I was always interested in science as a child, but growing up in Belfast in Northern Ireland, with the light pollution and regular wet and cloudy weather, meant that I was lucky to see any stars at night. But when we went on holiday and found clear, dark skies, I would often be amazed at the number of stars that would appear. I loved trying to identify new constellations, looking at the planets through binoculars, and wondering what else was out there that I couldn't see. As early as nursery school, my favourite song was "Twinkle twinkle little star", although it was only later, when a teacher told us that the Sun is a star, that I started to really wonder about the Universe.

I never really considered astronomy as a potential career until I started university, but I did know as a teenager that I wanted to go to university and become a scientist. At college I met very enthusiastic physics and maths teachers who picked up on my interest and helped me widen my knowledge beyond simply what I needed to know to pass my exams. Maybe it helped that, during those years, I skipped classes to watch two partial solar eclipses with my teachers, and ended up explaining what was happening to the crowds of interested students who joined us.

I moved to Sheffield in England to do a degree in Physics and Astronomy. During those years, my interest in astronomy

grew, and for my Masters year I was lucky enough to be offered the chance to carry out my research project while working as a student support astronomer at the Isaac Newton Telescope (INT) in La Palma. This position gave me my first opportunity to experience life as an astronomer at an observatory, and while the job was hard, I thoroughly enjoyed the experience. The INT is a rather hands-on telescope, where visitors have to do everything themselves, including refilling the cryostats, pointing the telescope, opening and closing the dome, etc. As a result, it gave me a real feel for how astronomical observations are really carried out, the preparation that has to go into planning the night, and a true appreciation of the work by the whole observatory team to build and maintain the precision of such impressive machinery.

My experience in La Palma convinced me to do a PhD in astronomy, so I returned to the UK for my PhD at the University of Nottingham on how the star formation in spiral galaxies shuts off to transform them into lenticulars. I quickly became interested in understanding the star formation histories within different components, such as bulges and discs, and the role those structures play in the evolution of the galaxy as a whole. As part of my PhD, I developed a technique to apply bulge–disc decomposition to long-slit spectra along the major axis of a galaxy in order to separate the spectra of these two components. From their independent spectra, I was able to study

their individual stellar populations and star formation histories.

I found that the lenticular galaxies in the Virgo and Fornax clusters experienced a final episode of star formation within the bulge region once the discs had already started fading. These young stellar populations within the bulge region suggest that at some point during the transformation, small amounts of gas were funnelled into the inner regions of the galaxy, where the gas eventually became dense enough to trigger a final episode of star formation. I am now working to further develop my spectroscopic bulge–disc decomposition technique to apply it to integral field unit (IFU) datacubes to make full use of the spectral and spatial information. I hope to be able to determine whether this final central episode of star formation activity occurs throughout the bulge or only at the centre of the disc, and which processes are most likely to trigger it and the dependence on environment.

During my PhD I only had one opportunity to go observing, since all the data I needed had already been collected. During that time, I found that I missed the observing side of astronomy and wanted the opportunity to experience a new culture again. So, after my PhD, I moved to ESO in Chile, and now have duties on Unit Telescopes 1 and 4, particularly working with the Multi-Unit Spectroscopic Explorer (MUSE). Carrying out observations with IFU spectrographs, such as SINFONI, KMOS and MUSE, helps me better understand the limitations of my own plans with such data. I am enjoying contributing to the running of such a large observatory and learning more about the instrumentation at Paranal from the various specialists I work with there. I also love learning my way around the southern skies when I get a few free minutes to stargaze, and I hope that by the end of my fellowship, my Spanish will be good enough to talk people through the constellations at local outreach events.

### Wolfgang Kerzendorf

I have always been fascinated with science. As a kid in elementary school I was very interested in biology. From experiments with growing tadpoles to



catching various critters in the Mediterranean Sea, I always wanted to know how things work and live. Astronomy was also an early passion of mine. I remember that I was fascinated by the planetarium at the Deutsches Museum in Munich. This must have inspired my parents to Xerox a star map (laser printers didn't exist then) to A3 format at the local library. I cut self-adhesive phosphorescent tape to the different sizes of "stars", representing the different "magnitudes", and this would illuminate my bedroom at night.

During high school I started to become more interested in physics. In particular, I remember one project where our physics teacher built air-pressure powered rockets with plastic soda bottles and we would try to gauge how high things flew. In the later years of high school, I became very interested in computing and helped to set up the computer labs. My *Facharbeit* (end of high school thesis) was a Java program that would calculate and visualise the electric field of a radiating dipole (created with the help of a Professor of Physics in Würzburg).

Despite my strong interest in computing, I wanted to study physics and selected a university in Germany that did active research in astrophysics. Thus, I started studying physics at Heidelberg University in the autumn 2002. My first serious contact with astronomy came with my advanced laboratory course in physics that involved obtaining photometry of a globular cluster and subsequently fitting isochrones. My lab partner and I were one of the few who were actually able to obtain the required photometry on a cold December night. After many nights configuring my computer to run Linux and installing IRAF (a difficult endeavour even in 2004), we were finally able to obtain the photometry with DAOPhot and fitted an isochrone. Despite the rather difficult and arduous nature of this lab, I was excited: finding out the age and distance of a star cluster was definitely a highlight of my undergraduate studies.

After two and a half years of study, I started to be interested in doing a semester abroad. My tutor Rainer Wehrse had his colleague Mike Bessel visiting him and he encouraged me to meet him.



Wolfgang Kerzendorf

Mike suggested contacting a young professor named Brian Schmidt at his home institute, Mount Stromlo Observatory. Brian was very enthusiastic about my applying for a summer scholarship and working with him over three months at the end of 2005. I departed for Australia in December 2005, not knowing that would be the start of a ten-year journey outside Germany.

As my first task, Brian instructed me to work on a tool that would help the observing astronomers at the 2.3-metre telescope in Siding Spring Observatory select the right instrument set-up when a new gamma-ray burst (GRB) alert triggered a Target of Opportunity observation. With my training in physics, I also started attending astronomy courses for the first time and learned about the rather strange units that are commonplace in astrophysics.

After three months, I was still excited about working in astronomy and decided to extend my stay for a further three months. During this time, the then PhD student Anna Frebel told me about an opportunity to switch from a Masters in physics to a PhD in astrophysics at Mt Stromlo Observatory. With the help of Brian, Rainer Wehrse and Penny Sackett (then director of Mt Stromlo Observatory), I applied for a PhD at the Australian National University (the parent university of Mt Stromlo). I started this PhD in February 2007 with Brian as my primary supervisor on Type Ia supernovae.

My main research task was to find surviving companion stars of these objects in ancient supernova remnants. Over the course of my PhD I tried and failed to locate these companions in three different ancient remnants (SN 1006, SN 1572 and SN 1604), thus contributing to an important result — Type Ia supernovae likely work differently than described in current astronomy text books.

For my second project, I tried to automatically fit the spectrum of Type Ia supernovae with a sophisticated radiative transfer code. This technique would allow us to reconstruct the structure of a supernova by analysing subsequent spectra. This meant optimising a function in a high-dimensional and complex search space. After some initial failures using the techniques I was taught in my physics classes, I started working with a friend of mine in computational neurobiology who taught me several nature-inspired optimisation algorithms that are ideally suited for such problems, but rarely used in astrophysics. This collaboration introduced me to the power of interdisciplinary work, that to this day is one the core themes of my research.

After finishing my PhD in the middle of 2011, I started as a postdoc working with Marten van Kerkwijk at the University of Toronto. Marten was not simply a boss, but a mentor who guided my independent research. During this time, I started working on my own radiative transfer code for Type Ia supernovae (having used

someone else's during my PhD). This was the start of the TARDIS collaboration<sup>1</sup> that I am now leading. TARDIS is built to be a modular code that allows us to experiment with different physical approximations, built on modern software development techniques and uniting researchers with very different backgrounds (computer science and statistics), to work on an astrophysical problem. Part of this success was through a programme called the Google Summer of Code that allowed me to recruit smart and enthusiastic undergraduates from

several fields of study to work with us for three months.

At the beginning of 2014, I heard the great news that I had been selected for an ESO Fellowship. This would not only allow me to build on my current research, but also start close collaborations with the supernova researchers at ESO. I started my fellowship at the end of 2014 and was very quickly introduced to my duties: testing new algorithms to obtain better results in data processing and analysis.

Now almost one and a half years into my fellowship, I have expanded on my research of analysing Type Ia supernova spectra with several results to be published soon. The ESO Fellowship is an exciting step forward for me in my career and I'm keen to see what the second half of it will bring.

[Links](#)

<sup>1</sup> TARDIS spectrum synthesis code: <http://tardis.readthedocs.org>

## Personnel Movements

### Arrivals (1 April–30 June 2016)

Europe	
Bhardwaj, Anupam (IN)	Student
Cheffot, Anne-Laure (FR)	Student
Palla, Federica (IT)	Assistant to the Data Reduction Manager
Puglisi, Annagrazia (IT)	Student

Chile	
Acuña, Andrea (CL)	Executive Bilingual Secretary
Bartlett, Elizabeth (UK)	Fellow
Iglesias, Daniela (CL)	Student
Pérez Sánchez, Andrés Felipe (CO)	Fellow
Sbordone, Luca (IT)	Operation Staff Astronomer

### Departures (1 April–30 June 2016)

Europe	
Grunhut, Jason Harley (CA)	Instrument Scientist
Karabal, Muhammet Emin (TR)	Student
Noethe, Lothar (DE)	Head of the Optical Engineering Department

Chile	
Acuña, Margarita (CL)	Administrative Technician
Gonzalez, Oscar (CL)	Fellow
Marsset, Michaël (FR)	Student
Muzic, Koraljka (HR)	Fellow
Rodríguez, Paula Valentina (CL)	Team Leader Public Outreach Vitacura

Image on page 59: Artist's rendering of the design of the telescope and dome of the European Extremely Large Telescope (E-ELT). The ACe Consortium, consisting of Astaldi, Cimolai and the nominated sub-contractor EIE Group, signed a contract with ESO for the construction of the dome and telescope structure on 25 May 2016. See Release eso1617 for more information.





ESO

European Organisation  
for Astronomical  
Research in the  
Southern Hemisphere



## ESO Fellowship Programme 2016/2017

The European Organisation for Astronomical Research in the Southern Hemisphere awards several postdoctoral fellowships each year. The goal of these fellowships is to offer outstanding early-career scientists the opportunity to further develop their independent research programmes. ESO Fellows return to the scientific community with the insights and experience gained from working at one of the world's foremost observatories.

ESO is the leading intergovernmental astronomy organisation in Europe. Its approximately 110 staff astronomers, 40 fellows and 40 PhD students conduct frontline research in fields ranging from exoplanets to cosmology, offering one of the most vibrant and stimulating scientific settings anywhere in the world.

Fellowships are available both at ESO's Headquarters in Garching near Munich, Germany, and at ESO's astronomy centre in Santiago, Chile.

ESO Headquarters is situated in one of the most active research centres in Europe, boasting one of the highest concentrations of astronomers. ESO's offices are adjacent to the Max Planck Institutes for Astrophysics and for Extraterrestrial Physics and close to the observatory of Munich's Ludwig-Maximilian University. Additionally, ESO participates in the Excellence Cluster Universe at the Garching campus, which brings together nearly 200 scientists to explore the origin and structure of the Universe. Consequently, ESO Fellows in Garching have many opportunities to interact and collaborate with astronomers at neighbouring institutes.

In Chile, fellows have the opportunity to collaborate with the rapidly growing Chilean astronomical community as well as with astronomers at other international observatories located in Chile. The ALMA building next to ESO's Santiago offices and the many astronomers and fellows working on the ALMA project further enhance the stimulating scientific environment available to ESO Chile Fellows.

At both sites, ESO Fellows are expected to actively participate in ESO's scientific life, for instance, by proposing and getting involved in the organisation of scientific workshops, co-supervising PhD students, coordinating thematic research groups, joining scientific committees, organising seminars, etc.

The fellowships in Garching start with an initial contract of one year followed by a two-year extension (three years total). In addition to developing their independent research programmes, ESO Garching Fellows will be expected to engage in some functional work, for up to 25% of their time, related to, for example, instrumentation, the VLT/I, ALMA, APEX, E-ELT, science operations support either in Garching or at one of ESO's observatories in Chile, software development, or public outreach. This provides the fellows with the opportunity to get involved with ESO projects or operations, and to gather valuable insights and experience not available in any other setting.

The fellowships in Chile are granted for one year initially, with annual extensions for three additional years (four years total). During the first three years, the fellows are assigned to one of the science operations groups of Paranal, ALMA or APEX, where they will contribute to the operations at a level of 80 nights per year. For ALMA fellows a fraction of their duties can alternatively be spent on data processing, participation in the ALMA review process as technical experts, software testing and optimisation and extension of the array capabilities.

During the fourth year of Chile fellowships several options are provided. The fellow may choose to spend the fourth year either at ESO's astronomy centre in Santiago, or at ESO Headquarters in Garching or at any astronomy/astrophysics institute in an ESO Member State. There are no functional duties during the fourth year, except when the fourth year is spent at ESO Chile, where fellows are expected to carry out functional work for up to 25% of their time. Under certain conditions, the fellow may also be hosted by a Chilean institution where she/he will be eligible to apply for time on all telescopes in Chile through competition for Chilean observing time.

The programme is open to applicants who will have achieved their PhD in astronomy, physics or a related discipline before 1 November 2017. Early-career scientists from all astrophysical fields are welcome to apply. While scientific excellence is the primary selection criterion for all fellowships, candidates should also explain (in their motivation letter) how ESO's facilities and their work at ESO would facilitate their scientific development.

We offer an attractive remuneration package including a competitive salary and allowances (tax-free), comprehensive social benefits, and we provide financial support for relocating families.

If you are interested in enhancing your early career through an ESO Fellowship, then please apply by completing the web application form available at: <http://jobs.eso.org>

Please include the following documents in your application:

- a cover/motivation letter;
- a curriculum vitae with a list of publications;
- a proposed research plan (maximum of two pages);
- a brief outline of your technical/observational experience (maximum of one page);
- the names and contact details of three persons familiar with your scientific work and willing to provide a recommendation letter. Referees will be automatically invited to submit a recommendation letter. However, applicants are strongly advised to trigger these invitations (using the web application form) well in advance of the application deadline.

The closing date for applications is 15 October 2016. Review of the application documents, including the recommendation letters, will begin immediately. Incomplete or late applications will not be considered.

Candidates will be notified of the results of the selection process between December 2016 and February 2017. Fellowships will begin in the second half of 2017.

### Further information

For more information about the fellowship programme and ESO's astronomical research activities, please see: <http://www.eso.org/sci/activities/FeSt-overview/ESOfellowship.html>

Details on the application procedure and the working conditions are explained in the FAQ's.

For a list of current ESO staff and fellows, and their research interests please see: <http://www.eso.org/sci/activities/personnel.html>

Details of the Terms of Service for fellows including details of remuneration are available at: <http://www.eso.org/public/jobs/conditions/fellows/>

### For any additional questions please contact:

**For Garching:** Eric Emsellem, Tel. +49 89 3200 6914,  
email: [eric.emsellem@eso.org](mailto:eric.emsellem@eso.org)

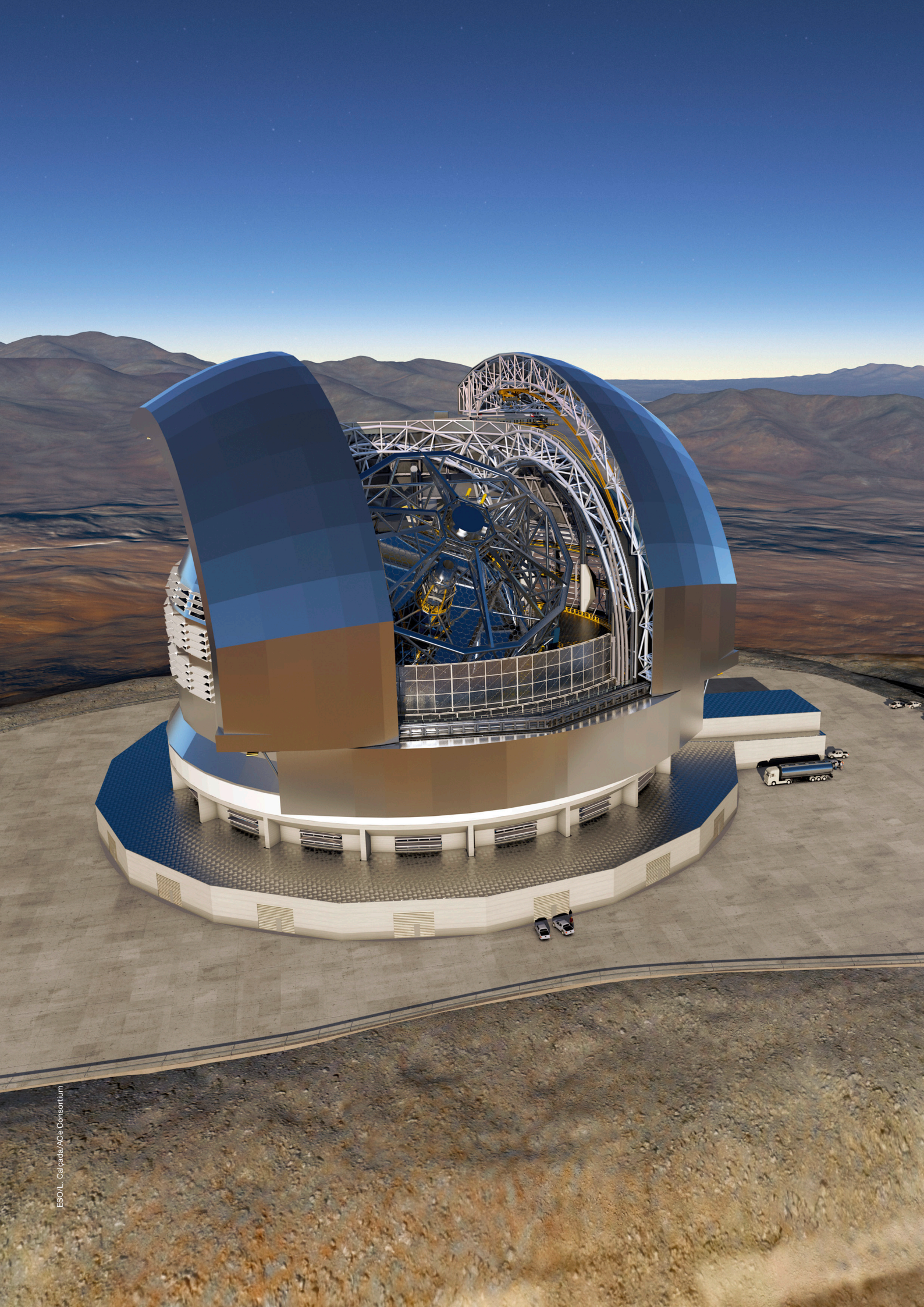
**For Chile:** Claudio De Figueiredo Melo, Tel. +56 2 463 3032,  
email: [cmelo@eso.org](mailto:cmelo@eso.org)

Although recruitment preference will be given to nationals of ESO Member States (members are: Austria, Belgium, Brazil, the Czech Republic, Denmark, Finland, France, Germany, Italy, the Netherlands, Poland, Portugal, Spain, Sweden, Switzerland and United Kingdom) no nationality is in principle excluded.

The post is equally open to suitably qualified female and male applicants.









ESO, the European Southern Observatory, is the foremost intergovernmental astronomy organisation in Europe. It is supported by 16 countries: Austria, Belgium, Brazil, the Czech Republic, Denmark, France, Finland, Germany, Italy, the Netherlands, Poland, Portugal, Spain, Sweden, Switzerland and the United Kingdom. ESO's programme is focused on the design, construction and operation of powerful ground-based observing facilities. ESO operates three observatories in Chile: at La Silla, at Paranal, site of the Very Large Telescope, and at Llano de Chajnantor. ESO is the European partner in the Atacama Large Millimeter/sub-millimeter Array (ALMA). Currently ESO is engaged in the construction of the European Extremely Large Telescope.

The Messenger is published, in hard-copy and electronic form, four times a year: in March, June, September and December. ESO produces and distributes a wide variety of media connected to its activities. For further information, including postal subscription to The Messenger, contact the ESO education and Public Outreach Department at:

ESO Headquarters  
Karl-Schwarzschild-Straße 2  
85748 Garching bei München, Germany  
Phone +49 89 320 06-0  
information@eso.org

The Messenger:  
Editor: Jeremy R. Walsh;  
Design, Production: Jutta Boxheimer;  
Layout, Typesetting: Mafalda Martins;  
Graphics: Joanna Law.  
www.eso.org/messenger/

Printed by FIBO Druck und  
Verlags GmbH, Fichtenstraße 8,  
82061 Neuried, Germany

Unless otherwise indicated, all images in The Messenger are courtesy of ESO, except authored contributions which are courtesy of the respective authors.

© ESO 2016  
ISSN 0722-6691

## Contents

### Telescopes and Instrumentation

Arsenault R. et al. – Adaptive Optics Facility Status Report: When First Light Is Produced Rather Than Captured	2
Fourniol N. et al. – A Fruitful Collaboration between ESO and the Max Planck Computing and Data Facility	8
Martayan C. et al. – Solar Activity-driven Variability of Instrumental Data Quality	10
Asmus D. et al. – Science Verification for the VISIR Upgrade	14

### Astronomical Science

Kamann S. et al. – A Stellar Census in NGC 6397 with MUSE	18
Randall S. K. et al. – Pulsating Hot Subdwarfs in Omega Centauri	23
Adami C. et al. – First Results from the XXL Survey and Associated Multi-wavelength Programmes	27
van der Wel A. et al. – The LEGA-C Survey: The Physics of Galaxies 7 Gyr Ago	36
Oteo I. et al. – ALMACAL: Exploiting ALMA Calibrator Scans to Carry Out a Deep and Wide (Sub)millimetre Survey, Free of Cosmic Variance	41

### Astronomical News

Horálek P. et al. – Light Phenomena over the ESO Observatories III: Zodiacal Light	45
Dennefeld M. et al. – The First NEON School in La Silla	47
Ballester P. – ESO Data Simulation Workshop	50
Spyromilio J., Holzlöhner R. – Retirement of Lothar Noethe	52
Fellows at ESO – K. Immer, E. Johnston, W. Kerzendorf	54
Personnel Movements	57
ESO Fellowship Programme 2016/2017	58

Front cover: First light for the 4Laser Guide Star System (4LGSF) at the Very Large Telescope occurred on 26 April 2016. The image shows the four 22 watt Raman laser beams (at the frequency of the Na D<sub>2</sub> line 5896 Å) propagated from Unit Telescope 4 into the sky in the plane of the Milky Way. The 4LGSF is an integral part of the Adaptive Optics Facility (AOF) that is being gradually commissioned. Further details can be found in the article by Arsenault et al. (p. 2) and in Release eso1613. Credit: ESO/F. Kamphues

